Investigation of Thermoluminescence Properties of Silicon Quantum Dots and $Ca_3Y_2(Si_30_9)_2 : x\ Ce^{3+}$ Nanophosphor

By

Nebiyu Gemechu

SUBMITTED TO OFFICE OF GRADUATE PROGRAMS IN PARTIAL FULFILLMENT OF THE
REQUIREMENTS FOR THE DEGREE OF
DOCTOR OF PHILOSOPHY
AT
ADDIS ABABA UNIVERSITY
DEPARTMENT OF PHYSICS
JUNE 2017

© Copyright by Nebiyu Gemechu, 2017

ADDIS ABABA UNIVERSITY
DEPARTMENT OF
PHYSICS

The undersigned hereby certify that they have read and recommend to the College of Natural and Computational Sciences for acceptance a thesis entitled "**Investigation of Thermoluminescence Properties of Silicon Quantum Dots and** $Ca_3Y_2(Si_30_9)_2 : x\ Ce^{3+}$ **Nanophosphor**" by **Nebiyu Gemechu** in partial fulfillment of the requirements for the degree of **Doctor of Philosophy**.

Dated: June 2017

External Examiner: _____
Dr. Genene Tessema

Research Supervisor: _____
Dr. Teshome Senbeta, and Dr. Belayneh Mesfin

Examing Committee: _____
Dr. Genene Tessema

_____
Dr. Tesgera Bedassa, Dr. Tilahun Tesfaye

ADDIS ABABA UNIVERSITY

Date: **June 2017**

Author: **Nebiyu Gemechu**

Title: **Investigation of Thermoluminescence Properties of Silicon Quantum Dots and $Ca_3Y_2(Si_30_9)_2 : x\ Ce^{3+}$ Nanophosphor**

Department: **Physics**

Degree: **Ph.D.** Convocation: **June** Year: **2017**

Permission is herewith granted to Addis Ababa University to circulate and to have copied for non-commercial purposes, at its discretion, the above title upon the request of individuals or institutions.

Signature of Author

THE AUTHOR RESERVES OTHER PUBLICATION RIGHTS, AND NEITHER THE THESIS NOR EXTENSIVE EXTRACTS FROM IT MAY BE PRINTED OR OTHERWISE REPRODUCED WITHOUT THE AUTHOR'S WRITTEN PERMISSION.

THE AUTHOR ATTESTS THAT PERMISSION HAS BEEN OBTAINED FOR THE USE OF ANY COPYRIGHTED MATERIAL APPEARING IN THIS THESIS (OTHER THAN BRIEF EXCERPTS REQUIRING ONLY PROPER ACKNOWLEDGEMENT IN SCHOLARLY WRITING) AND THAT ALL SUCH USE IS CLEARLY ACKNOWLEDGED.

This thesis is dedicated to my family

Table of Contents

Table of Contents **v**

List of Tables **viii**

List of Figures **ix**

Abstract **xiv**

Acknowledgements **xvi**

1 Introduction **1**
1.1 Background 1
1.2 Statement of the Problem 6
1.3 Objectives of the Study 7
1.4 Thesis Layout 8

2 Theoretical Background on Thermoluminescence **10**
2.1 The Concept of Luminescence 10
2.2 Types of Luminescence 14
2.2.1 Photoluminescence 14
2.2.2 Electroluminescence 15
2.2.3 Thermoluminescence 15
2.2.4 Cathodoluminescence 16
2.2.5 Chemiluminescence 17
2.2.6 Bioluminescence 18
2.2.7 Triboluminescence 18
2.2.8 Radioluminescence (Scintillation) 18
2.2.9 Ionoluminescence 19
2.3 Characteristic Luminescence 20

2.4 Defect Centers and Mechanism of Thermoluminescence 21
2.4.1 Transitions involving delocalized bands 23
2.4.2 Transitions not involving delocalized bands 25
2.5 Applications of Thermoluminescence 27
2.5.1 Defect analysis in solids 27
2.5.2 Radiation dosimetry 28
2.6 Models of Thermoluminescence 29
2.6.1 Randall and Wilkins model 32
2.6.2 Garlick and Gibson model 36
2.7 Order of Kinetics 41
2.7.1 First and second order kinetics 41
2.7.2 General order kinetics 42
2.7.3 Mixed order kinetics 43

3 Analysis of Thermoluminescence Glow Curves and Characterization Techniques 45
3.1 Introduction 45
3.2 Methods of Analysis 47
3.2.1 Heuristic method (First approximation of E) 47
3.2.2 Initial rise method 48
3.2.3 The whole TL glow curve method 51
3.2.4 Methods of analysis based on the various heating rates 53
3.2.5 Method of analysis based on the shape of the glow curve . . . 54
3.2.6 Isothermal decay method 58
3.2.7 Curve fitting method 60
3.3 General Precautions in Glow Curve Analysis 61
3.4 Characterization Techniques 61
3.4.1 X-ray diffraction (XRD) 61
3.4.2 Photoluminescence spectroscopy (PL) 64
3.4.3 Ultra-violet visible (UV-VIS) spectroscopy 65
3.4.4 Thermoluminescence (TL) spectroscopy 67

4 Thermoluminescence from Silicon Quantum Dots in Two Traps-One Recombination Center Model 70
4.1 Introduction 70
4.2 Statement of the Problem 74
4.3 Electron Rate Equations 76
4.4 First Order Kinetics 77
4.5 Second Order and a Case Beyond Second Order Kinetics 79

4.6 Conclusion 82

5 Thermoluminescence Properties of UV-irradiated $Ca_3Y_2(Si_3O_9)_2$ Nanophosphor 84

5.1 Introduction 84
5.2 Experimental Details 86
5.2.1 Solution combustion method of synthesizing nanophosphor . . 86
5.2.2 Characterization techniques 88
5.3 Results and Discussion 88
5.3.1 XRD analysis 88
5.3.2 Thermoluminescence analysis 89
5.4 Optical Properties 99
5.5 Conclusion 101

6 Synthesis and Luminescence Properties of $Ca_3Y_2(Si_30_9)_2 : x\ Ce^{3+}$ Nanophosphor 102

6.1 Introduction 102
6.2 Optical Transitions in Ce^{3+} 104
6.3 Experimental Details 105
6.4 Results and Discussion 106
6.4.1 XRD analysis 106
6.4.2 Photoluminescence properties 108
6.4.3 Thermoluminescence properties 113
6.5 Conclusion 117

7 Summary 118

7.1 Summary 118
7.2 Limitation of the Study 119
7.3 Recommendation for Future Work 119

Bibliography 121

List of Tables

3.1 The values of the parameters T_0 and K for different input values of β/s [79]. 47

4.1 Approximate size dependence of radiative recombination rate A_r of the quantum dots [103]. D is the diameter of the dots. 80

5.1 FWHM, crystallite size and strain of the synthesized $Ca_3Y_2(Si_3O_9)_2$ host material. 89

5.2 μ, E, and s of the glow peaks 1, 2, and 3 of $Ca_3Y_2(Si_30_9)_2$ host material. 91

5.3 The first 15 data points for comparison of the experimental data and theoretical result. 94

6.1 Strain developed in the synthesized $Ca_3Y_2(Si_30_9)_2 : x\ Ce^{3+}$ samples. . 108

6.2 Shape factor, activation energy and frequency factor of the glow peaks corresponding to different UV exposure times (t). T_1, T_M, and T_2 are measured in ^oC. 114

List of Figures

2.1 The types of luminescence based on the characteristic time t for the emission of light to take place [1]. 11

2.2 Energy level diagram illustrating (1) excitation, (2) emission, (3) falling to metastable state, and (4) depopulation of the metastable state. . . 12

2.3 Common electronic transitions in crystalline semiconductors and insulators: (a) ionization; (b) and (e) electron and hole trapping respectively; (c) and (f) electron and hole release; (d) and (g) indirect recombination; (h) direct recombination. Electrons are represented by solid circles and electron transitions by solid arrows. Holes are represented by open circles and hole transitions by open arrows [1]. 24

2.4 Electron transitions in a semiconductors or insulators not involving the delocalized bands [1]. 25

2.5 Two level model for thermoluminescence. Allowed transitions: (1) ionization; (2), (5), trapping; (3) thermal release (detrapping); (4) radiative recombination and emission of light. 30

2.6 Profile of trapped electron population n. Calculations are carried out using the Randall- Wilkins model. Input parameters used are $E = 0.4\ eV$, $s = 10^{12}\ s^{-1}$, $\beta = 1\ ^0C\ s^{-1}$. The initial value of n is $10^{15}\ cm^{-3}$. 34

2.7 TL intensity versus temperature in Randall- Wilkins model with the same input paramaters as in Fig. 2.6. 35

2.8 Profile of probability p of excitation as a function of T during heating Randall- Wilkins model. The same input parameters as in Fig. 2.6 are used. This increment in p for all T is, however, ideal. 36
2.9 Change in temperature T_M of glow peak maximum with change in E. The values of other parameters are the same as in Fig. 2.6. 37
2.10 First order (1) and second order (2) peaks with $E = 0.5\ eV$, $s = 10^{12}\ s^{-1}$, $n_0 = N = 10^{15}\ cm^{-3}$. 38
2.11 First order (1) and second order (2) peaks with $E = 0.5\ eV$, $s = 10^{12}\ s^{-1}$, $n_0 = 10^{15}\ cm^{-3}$, $N = 2 \times 10^{15}\ cm^{-3}$, $\beta = 1\ ^0C\ s^{-1}$. 39
2.12 Second order peaks with (1) $n_0/N = 1$, (2) $n_0/N = 0.5$, and (3) $n_0/N = 0.1$. In addition, $E = 0.5\ eV$, $s = 10^{12}\ s^{-1}$ and $\beta = 1\ ^0C\ s^{-1}$ for all the peaks. 40

3.1 The initial rise part of TL glow curve. 49
3.2 The graphical method proposed by Ilich. 50
3.3 Calculation of the area $n(T)$ in the whole glow peak measurement method. 52
3.4 The change in temperature T_M of maximum intensity with heating rate. 54
3.5 The geometrical shape parameters ω, τ and δ. 55
3.6 The relation between kinetic order b and geometrical shape factors μ and γ [28]. 57
3.7 Schematic diagram of x-ray diffraction. The incident angle, θ, is defined between the x-ray source and the sample. The diffracted angle, 2θ, is defined between the incident beam and the detector angle. 62
3.8 Two incident x-rays entering a crystal with interplanar spacing d. . . 63
3.9 A schematic diagram showing the main elements for measuring PL spectra [99]. 64

3.10 (a) An experimental arrangement used to measure direct reflectance spectra, (b) A schematic drawing of an integrating sphere for measuring diffuse reflectance spectra. As indicated in (a), I_0 is the incident intensity minus the reflection losses I_R at the surface [99]. 66
3.11 A schematic diagram of typical TL experiment [100]. 69

4.1 IMTS model for TL. Allowed transitions: (1) ionization; (2), 4, (6), trapping; (3) thermal release (detrapping); (5) radiative recombination and emission of light. 73
4.2 Three level model for thermoluminescence. Allowed transitions: (1) ionization; (2), (4) and (7) trapping; (3) and (5) thermal release; (6) radiative recombination and emission of light. 75
4.3 The normalized concentration of electrons $n_1(T)$ and $n_2(T)$ in the first trap ($E_1 = 0.65\ eV$) and second one ($E_2 = 0.8\ eV$) versus the temperature T (in ^0C) for first order kinetics with the following values of parameters: $n_1(0) = n_2(0) = 10^{15}\ cm^{-3},\ \beta = 1\ ^0C/s,\ s_1 = s_2 = 10^8\ s^{-1}$. 78
4.4 The intensity of TL in arbitrary units versus temperature T for first order kinetics with the same parameters as in Fig. 4.3. 79
4.5 Variation of concentration of electrons $n_1(T)$ in the shallower trap ($E_1 = 0.65\ eV$) for general order kinetics. 80
4.6 Variation of concentration of electrons $n_2(T)$ in the deeper trap ($E_2 = 0.8\ eV$) for general order kinetics. 81
4.7 Variation of TL intensity I versus temperature for general order kinetics. 82

5.1 (a) XRD pattern of the synthesized $Ca_3Y_2(Si_30_9)_2$ sample, and (b) FWHM with the corresponding crystallite size. 89
5.2 (a) TL glow peak for heating rate of $1\ ^0C/s$ and UV dose of 5 minutes, and (b) deconvoluted glow curve of $Ca_3Y_2(Si_30_9)_2$ host material. . . . 90

5.3 Graphs of (a) the sample quickly heated at 2 $^oC/s$ to 58 ^oC, and (b) its phosphorescence decay curve. 91
5.4 Experimental data and the theoretically fitted graph using Kitis et al equation. 92
5.5 Four level model for thermoluminescence. Allowed transitions: (1) ionization; (2), (4), (6) and (9) trapping; (3), (5) and (7) thermal release; (8) radiative recombination and emission of light. 95
5.6 Numerically simulated glow curve using the experimentally determined TL kinetic parameters. 96
5.7 Numerically simulated curves for variation of concentration of electrons in the three identified traps of $Ca_3Y_2(Si_30_9)_2$ host material using the experimentally determined TL kinetic parameters. 97
5.8 Numerically simulated glow curve for general values of $n_{10},\ n_{20},\ n_{30},$ and N. 98
5.9 Numerically simulated curves for variation of concentration of electrons in the three identified traps of $Ca_3Y_2(Si_30_9)_2$ host material for general values of $n_{10},\ n_{20},\ n_{30}$, and N. 99
5.10 Graphs of (a) Reflectance as a function of wavelength, (b) $[F(R)\ h\nu]^{\frac{1}{n}}$ versus energy $h\nu$ for indirect allowed transition (n=2), and (c) $[F(R)\ h\nu]^{\frac{1}{n}}$ versus energy $h\nu$ for direct allowed transition ($n = 1/2$) of the prepared sample. 100

6.1 Unit cell of $Ca_3Y_2(Si_30_9)_2$ [111]. Ca and Y randomly occupy the same three sites of 6-, 7 and 8- fold coordination symmetries. 104
6.2 XRD pattern of the synthesized $Ca_3Y_2(Si_30_9)_2 : x\ Ce^{3+}$ samples. . . 106
6.3 The variation of the dominant diffraction peak around $2\theta = 29\ ^0$ with the concentration x. The values are normalized with respect to the highest diffraction peak at $x = 0.08$. 107

6.4 (a) Room temperature PL emission spectra of $Ca_3Y_2(Si_30_9)_2 : x\ Ce^{3+}$. The inset shows the PL excitation of the host material at emission of 432 nm and its PL emission at excitation of 365 nm, and (b) CIE chromaticity coordinates. 109
6.5 The graph of $\log(I/x)$ versus $\log(x)$ of Ce^{3+} for $Ca_3Y_2(Si_30_9)_2 : x\ Ce^{3+}$.111
6.6 Graph of Reflectance as a function of wavelength. 112
6.7 (a) TL glow curves for different UV exposure time, and (b) the variation of TL maxima with UV dose. 113
6.8 The TL glow curves of $Ca_3Y_2(Si_30_9)_2 : x\ Ce^{3+}$. 115
6.9 TL fading of $Ca_3Y_2(Si_30_9)_2$ host material, and (b) the variation of TL peak maxima with storage time. 116

Abstract

Analytical, numerical and experimental results of thermoluminescence (TL) from nanomaterials are studied and correlated. In particular, theoretical investigation of TL from silicon quantum dots in the presence of multiple trap states is compared to the TL properties of $Ca_3Y_2(Si_30_9)_2 : x\ Ce^{3+}$ nanophosphor of average crystallite size 28 nm synthesized by solution combustion technique. The TL properties of the silicon quantum dots of diameters in the range of 2-8 nm are investigated in the model of two active electron traps and one recombination center. The rate equations corresponding to the active electron traps which are, in general, located at different trap depths below the edge of the conduction band are written. The assumption of negligible retrapping results in the analytically solvable rate equations, whereas, the consideration of the retrapping terms complicates the rate equations requiring numerical solutions. The TL measurements of $Ca_3Y_2(Si_30_9)_2 : x\ Ce^{3+}$ nanophosphor are measured and analyzed. Samples are heated from 0 to 400 ^oC for different UV doses. Measurements of TL fading are done after keeping the sample for different storage times before heating. Peak shape and initial rise methods are employed to evaluate the different TL kinetic parameters such as activation energy (E), the frequency factor (s) and the order of kinetics (b). Moreover, the experimental data is fitted in the analytical solution of TL glow curves obeying general order kinetics using Kitis et al equation. The optical band gap of the synthesized sample (not doped) is estimated from Kubelka-Munk (K-M) function for both direct and indirect allowed transitions.

The TL intensity of the silicon quantum dots increases with a decrease in the dot

size, indicating that quantum confinement effect enhances the radiative recombination rate. For the TL kinetic parameters used in the theoretical approach, the number of peak maxima of the glow curve corresponding to a given quantum dot is the same as the number of active electron traps taken in to account. For first order kinetics, the simulated variation in the concentration of electrons in all the traps decreases with temperature, whereas, it considerably increases with temperature in the deeper traps for general order kinetics due to retrapping. This result bridges the experimental gap where the TL glow curves are generated and the variation of concentration of electrons in traps remain unknown.

Analysis of the glow curve deconvolution shows that the TL glow curves of $Ca_3Y_2-(Si_30_9)_2$ host material ($x = 0$) can be well fitted by three constituent peaks which obey general order kinetics; indicating the presence of three active electron trap levels. The TL intensity of the synthesized phosphor (not doped) increases for all the UV doses applied up to 50 minutes. Simulation of the TL glow curve of this material is performed by using the rate equations corresponding to the determined active electron trap levels and employing the evaluated TL kinetic parameters. This glow curve is broad and much similar to the experimentally obtained glow curve. The isothermal decay analysis of this host material shows that it suffers from fast phosphorescence decay. Moreover, the incorporation of Ce^{3+} into the host material resulted in a broad TL glow curves over a wide temperature range.

The photoluminescence (PL) emission spectra of the doped samples ($x = 0$, 0.01, 0.02, 0.04, 0.08 and 0.16) monitored at excitation wavelength of 365 nm show a broad band extending from about 350 to 600 nm and this band can be ascribed to the allowed $[Xe]5d^1$-$[Xe]4f^1$ transition of Ce^{3+}. Moreover, the PL intensity increases up to critical concentration of $x = 0.08$ and then decreases. The reflectance spectra of the doped samples show a red shift in their optical band gap compared to the host.

Acknowledgements

Thank you God for Your guidance and blessings! My acknowledgement goes to following persons and institutions.

- My supervisor the late Professor Vadim Nickolaevich Mal'nev for his most valuable insight, invaluable suggestions, comments, scientific advice, scholarly remarks, respect and understanding right until his passage.
- Dr. Teshome Senbeta and Dr. Belayneh Mesfin who took the responsibility of advisement after the passing away of Professor Vadim Nickolaevich Mal'nev for the work to be successfully accomplished. This thesis would not have been finalized without their unreserved efforts.
- Dr. Tesgera Bedassa, Dr. Lemi Demeyu and Prof. Gholap for their useful comments during my seminar work.
- Department of Physics of Addis Ababa University for its financial support.
- Professor F. B. Dejene from University of the Free State, and Dr. K. T. Roro from Counsel for Scientific and Industrial Research, South Africa, for collaboration.
- All staff members in the Department of Physics of Addis Ababa University. In particular, I am thankful to Dr. Deribe Hirpo and Dr. Kenate Nemera for their encouragement.
- W/ro Tsilat for her continuous unchanging treatment at Department of Physics.
- Mizan Tepi University for sponsoring my study.

- All friends and colleagues, particularly, Leta Tesfaye, Sioma Debela, and Abdulhayi Mohammed for useful discussions we had together.
- My wife, parents, brothers and sisters for their love, patience, encouragement and continuous support.

Nebiyu Gemechu

June 2017

Chapter 1

Introduction

1.1 Background

The connection between phosphorescence and radiation was the subject of extensive examination in the late nineteenth century and the study of radiation-induced thermoluminescence (TL) received a boost in early 20th century [1]. The phenomenon of TL has been extensively studied by many investigators [2, 3, 4, 5, 6, 7]. The understanding of the mechanism of occurrence of thermally stimulated emission is the important field of fundamental research. Many researchers have suggested their views for TL mechanism for pure and impurity activated materials. With expanding knowledge of solid state physics, it is a topic of research to know the latest plausible mechanism of TL. However, the present research on TL has explored vast application potential of it in various fields [1, 7]. The advances and development in the instrumentation; and better understanding of TL have helped researchers solve their problems in many fields.

Fields like dosimetry for radiation protection and dating of ancient potteries, ceramics, bricks, and geological sediments involves the wide application of TL and

contributed a lot to the present day progress on research of this field [1, 7]. TL has grown basically as an applied branch of science. It was routinely used to measure UV component of sunlight from the early stage of rocket flights [8, 9, 10]. With the use of different filters including some opaque ones with phosphor packets on board, the rocket produced the direct evidence of the existence of high energy UV components and x-rays in the solar spectrum at high altitudes.

The post-world war II period saw a sudden increase in the source of ionizing radiations due to the various applications of nuclear energy in military and civil applications. Therefore, a simple, reliable, and cheap method for measuring these radiations is necessary. In late 1940s, scientists began a search for a better device for use in radiation monitoring in military as well as civilian activities. A radiophotoluminescence glass dosimeter was first to be developed and it is known that more than a million units of this device were made and used in military [11, 12]. This was soon followed by the development of TL phosphors for dosimetry. The TL phosphors used in the present day dosimetry such as LiF and $CaF_2 : Mn$ were discovered and extensively studied in early 1950s [13, 14]. Varieties of TL phosphors are now being produced in large scale commercially and are being used throughout the world in radiation protection and medical radiation dosimetry. Apart from radiation dosimetry, in which luminescence technique has become indispensible, it has been established as an important technique in archeological and geological dating [15, 16].

The search for better and more efficient phosphors for such practical applications is still underway and requires more effort from researchers in the field. Studying the TL properties of a given phosphor powder for related practical applications requires the understanding of the dependence of the TL on host structure, presence of impurities

(defects) and their position in the host structure, synthesis method and on various other experimental parameters such as heating rate and exposure time to ionizing radiation (radiation dose). These factors or parameters control the TL characteristics of a phosphor.

Selection of a suitable host material is very important and can lead to improved luminescence properties of a material in general and enhanced TL characteristics in particular. A chemically stable and durable host material having thermal stability for high temperature processes is required and it has been reported that oxide based phosphors satisfy these properties [17]. Moreover, doping induced controlling or chemical modification of the host matrix composition influences the host chemical environment and hence the luminescence properties of a given phosphor.

Defects or surface states generated by introduction of dopants into the host material influence the band gap and induces oxygen vacancies that form electron-trap centers. These trap centers have the advantage of delaying the decay of charge carriers, enhancing the visible light absorption property and decreasing the electron hole recombination rate [18]. Careful control of dopant concentration can also modify the luminescence properties of the rare earth elements. Moreover, the luminescence properties of materials are also strongly associated with geometrical factors such as shape, dimensionality, size, etc. Crystalline, spherical shaped, uniform size particles with narrow size distribution with well defined morphologies can reduce light scattering and produce fine luminescence properties [19].

The luminescence properties of materials are in general improved following miniaturization to nanoscale [20]. The development of nanoscience and nanotechnology

so far has been possible by the success in the production of nanomaterials which involve control of size, shape and structure of the materials. During the last few years, nanoparticles of insulator materials have been produced in large quantities by the use of physical and chemical techniques. The significant improvements in the preparation of nanomaterials such as long after glow phosphors has been due to the discovery of new synthesis techniques such as sol-gel and combustion.

Heating rate β is an important parameter for the determination of the various kinetic parameters of TL glow curves. In literature it has been reported that the glow peak height decreases [21] or increases [22, 23, 24] with increasing heating rate. In addition, it plays a critical role in deciding the time required to record the TL glow curves because thousands of dosimeters have to be processed in a short time when personnel monitoring is carried out using TL dosimeters. This is also important because higher heating rate records the glow curves faster, which forms the basis of TL dosimetry in large scale personnel monitoring. Moreover, the fact that a good dosimeter should not exhibit thermal quenching can be verified by investigating the TL response with increase in heating rates.

Radiation dose plays a crucial role in the filling of the traps constituting a TL material and the TL response of a given sample to a known dose depends on the number of the traps filled by the given dose. A simple way to estimate the number of the filled traps is to assume the filling rate to be directly proportional to the dose and also directly proportional to the vacancies in the traps [25]. The dose at which all of the traps get filled up depends solely on the fraction of vacant traps which are filled up per unit dose. The TL intensity of most phosphor materials increases with increasing radiation dose up to a certain level and then decreases. This decrease of the

TL signal can be attributed to the stronger competition with non-radiative centers at higher doses [26].

Various theoretical approaches have also been made in analysis of TL glow curves [6, 27, 28]. The continuous advancement in numerical methods has greatly helped various researchers in solving the complex TL kinetic equations (rate equations) which can not be solved analytically. The complexity of the rate equations increase with the number of traps considered. Accordingly, there are different models of TL depending on the number of traps involved and whether these traps are active or not.

In this thesis theoretical investigation of TL properties of silicon quantum dots and experimental study of TL phenomena in $Ca_3Y_2(Si_3O_9)_2$ nanophosphor powder is carried out. In particular, the TL properties of silicon quantum dots are investigated in the model of two active electron traps and one recombination center. In order to check that experimentally investigated TL from nanomaterials show similar results to the theoretical ones, the TL properties of $Ca_3Y_2(Si_3O_9)_2 : x\ Ce^{3+}$ nanophosphor synthesized using solution combustion technique are investigated for $x = 0,\ 0.01,\ 0.02,\ 0.04$ and 0.08. The structure and phase purity of the synthesized phosphor are studied by x-ray diffraction (XRD) using Bruker D8 advance x-ray diffractometer. The TL measurements of $Ca_3Y_2(Si_30_9)_2 : x\ Ce^{3+}$ nanophosphor are taken using TL reader type TL1009I offered by Nucleonix systems Pvt. Ltd., India, interfaced to computer. Moreover, its reflectance spectra are measured using ultra-violet visible (UV-VIS) spectrometer and the PL properties are investigated using Cary Eclipse fluorescence spectrometer. Finally, for possible applications in the white light emission, the values of the chromaticity coordinates of the phosphor are estimated from the 1931 Commission Internationale de l'Eclairage (CIE) system.

1.2 Statement of the Problem

The absorption of radiation increases the level of TL observed from a specimen by filling the localized energy levels with trapped electrons. The absorption of heat from the environment, on the other hand, tends to reduce the numbers of trapped electrons by detrapping process. Thus, the intensity of the TL is a competition between trap filling by radiation and trap emptying by thermal excitation. At a given temperature of irradiation, many materials display an intensity of TL which is proportional to the amount of radiation absorbed, and this leads to the fact that TL may be used as a means of radiation dosimetry. Moreover, TL has various important applications in different fields as discussed above. In addition, more should be done on how the TL characteristics of a material is directly related to the materials solid state properties and how these properties are being utilized in the diverse fields mentioned above.

Developing inorganic phosphor materials that can be effectively and efficiently used in various applications is highly important at present time. Investigating the TL properties of a material is crucial in the development of more efficient materials though many challenges are being faced during manufacturing and processing of these materials. Therefore, there should be a mechanism to overcome these challenges and enhance the TL properties of a phosphor. This includes selection of a suitable host material with high chemical durability and thermal and chemical stability.

Making TL more efficient for practical use without deviating from reality should also be given more attention in theoretical approaches. For this matter, three cases are taken in to consideration. Firstly, nanostructures, where there is more efficient TL behavior because of quantum confinement effect, are taken in to account. Secondly, multiple active electron trap levels are considered because of the fact that real

semiconductors involve several number of impurities or defect levels beneath the edge of the conduction band which act as localized energy levels. These localized energy levels are therefore a potential electron or hole traps. Thirdly, the free electron in the conduction band may be trapped several times before recombination with trapped hole. Thus, the rate equations governing the TL kinetics which takes into account the aforementioned three cases are then written. In general, these rate equations can not be solved analytically. Therefore, consideration of numerical approaches is important in this case. In this work, the numerical solutions and the simulated results of TL in the existence of multiple active electron trap levels are generated using Mathematica 8. Moreover, the TL properties of $Ca_3Y_2(Si_3O_9)_2 : x\ Ce^{3+}$ nanophosphor is investigated for possible applications in dosimetry.

1.3 Objectives of the Study

The following are the objectives of the study.

- To study the TL properties of silicon quantum dots in the model of two active electron traps and one recombination center using analytical and numerical solutions of the electron rate equations governing the TL phenomena. Analytical solution of the rate equations are achieved by assuming negligible retrapping, whereas, the consideration of retrapping complicates the rate equations and hence numerical approaches are employed.

- To investigate that, for a given TL kinetic parameters, experimentally investigated TL from nanomaterials show results which are similar to the theoretical

ones . For this purpose, $Ca_3Y_2(Si_3O_9)_2$ nanophosphor is synthesized using solution combustion technique and its TL properties are studied. The estimated number of active electron traps (defects) as well as the TL kinetic parameters such as the trap depth (E), the frequency factor (s) and the order of kinetics (b) of this host material are then determined from TL glow curves. Using the determined number of active electron trap levels and the evaluated TL kinetic parameters, the rate equations governing the TL process in the synthesized nanophosphor are written by considering the effect of retrapping.

- To study the effect of incorporation of Ce^{3+} impurity on the TL properties of $Ca_3Y_2(Si_3O_9)_2$ host material. In order to investigate this effect, the TL glow curves of $Ca_3Y_2(Si_3O_9)_2 : x\ Ce^{3+}$ are generated for various values of the molar concentration x. The results are then discussed in detail.

- To study the possibility of using $Ca_3Y_2(Si_3O_9)_2$ host material for dosimetric applications. For this purpose, the TL response of this material is analyzed for different UV doses.

1.4 Thesis Layout

Chapter 2 deals with the theoretical background on luminescence in general and thermoluminescence in particular. The concepts, applications, and different models of thermoluminescence are discussed in this chapter. The various methods of analysis of thermoluminescence glow curves and the different characterization techniques used in this work are explained in Chapter 3. The main results of the study are discussed in Chapters 4, 5, and 6. Theoretical study of TL from silicon quantum dots

in two traps-one recombination center model is studied in Chapter 4. In addition, TL properties of UV-irradiated $Ca_3Y_2(Si_3O_9)_2$ nanophosphor are discussed in Chapter 5. Chapter 6 explains synthesis of $Ca_3Y_2(Si_3O_9)_2 : x\ Ce^{3+}$ nanophosphor for various molar concentration x as well as its TL and PL properties. Finally, summary, limitation of the study and recommendation for future work are presented in Chapter 7.

Chapter 2

Theoretical Background on Thermoluminescence

2.1 The Concept of Luminescence

Luminescence is the emission of light by a material as a consequence of absorption of energy [1, 28, 29]. A material that emits light is called luminescent material. More precisely, luminescence is produced by the selective excitation of the atomic or molecular energy levels. The atom or the molecule is taken to a higher energy state because of excitation and its fall to ground state results in the emission of light, which is called luminescence. There are different sources of excitation, namely, ultra-violet (UV) light, x-rays, γ-rays, etc. For instance, some minerals show some kind of luminescence under ultra-violet light exposure and some need x-ray bombardment. The presence of atomic centers whose energy levels are protected from the thermal vibrations of the atoms of the bulk medium, for example, the transitions of inner 4f electrons in lanthanide rare-earth ions [30], is the specific characteristic which provides an inorganic solid the luminescent property. Luminescence phenomena can also be observed in organic solids. While the luminescence of inorganic solids is mostly

due to impurity atoms or other lattice defects, the luminescence in organic solids is attributed to molecular complexes [31].

After the absorption of radiation, the emission of light takes place in a characteristic time t and this parameter allows us to sub-classify the process of luminescence. Conventionally emissions with decay time shorter than 10^{-8} s are referred as fluorescence and those with decay time greater than that are known as phosphorescence [29] and this phenomenon is shown in Fig. 2.1. While fluorescence takes place simultaneously with the absorption of radiation and stops immediately when the radiation ceases, phosphorescence continues to be observed after the excitation has been removed. In other words, phosphorescence takes place under the involvement of some

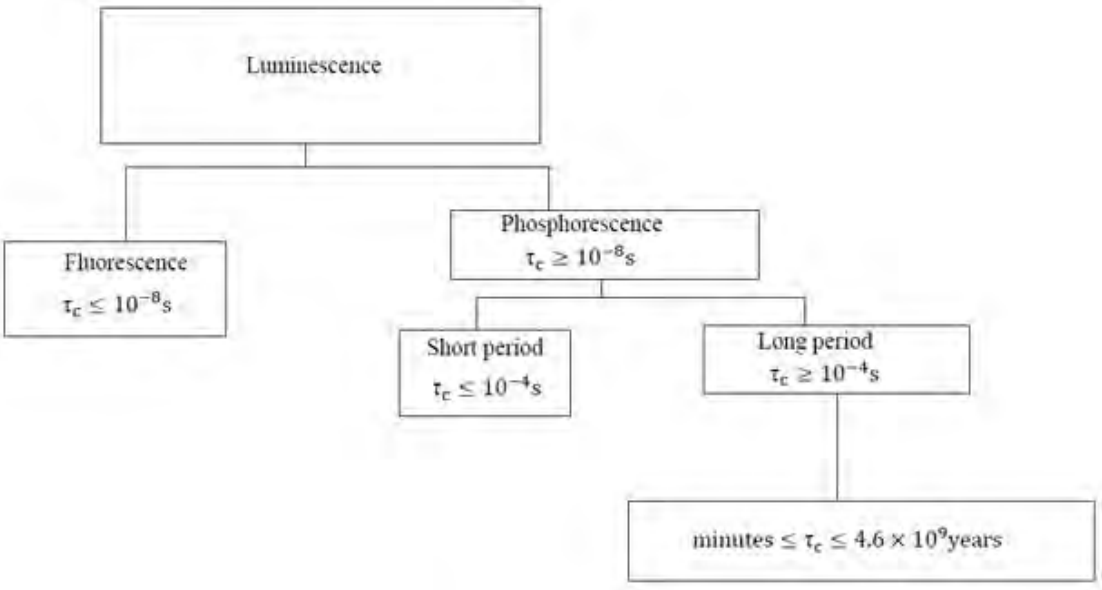

Figure 2.1: The types of luminescence based on the characteristic time t for the emission of light to take place [1].

metastable state M, which is an energy level from which transitions to any lower energy levels are forbidden [1]. Thus, the luminescence that occurs after an electron

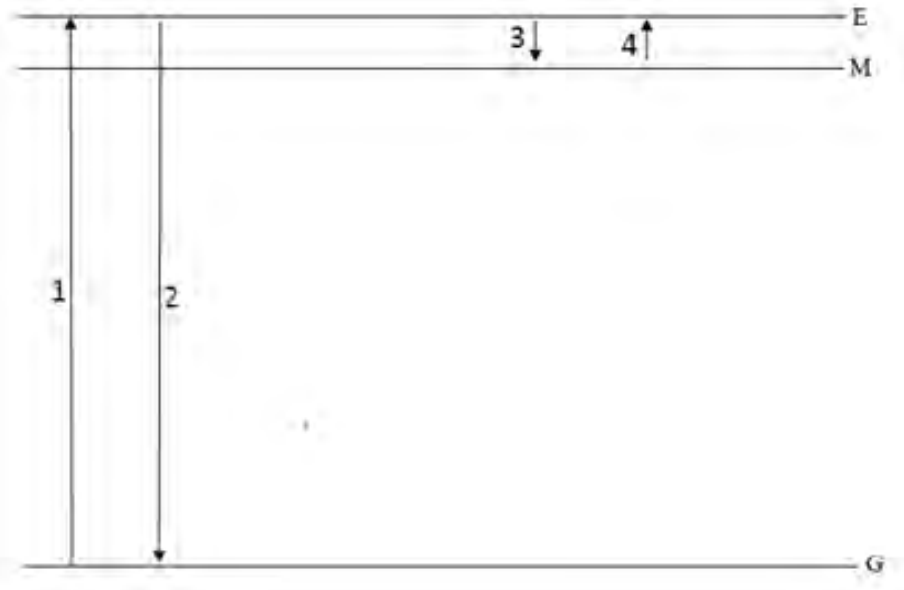

Figure 2.2: Energy level diagram illustrating (1) excitation, (2) emission, (3) falling to metastable state, and (4) depopulation of the metastable state.

is brought to a metastable state as a result of the excitation of the system is called phosphorescence. If a system brought to its metastable state is completely unperturbed, then it would remain in such a state for a relatively long period. Absorption transition from the ground state (G) to M is also forbidden, though it can be reached indirectly as shown in Fig. 2.2.

For example, after an electron has attained the state E as a result of excitation shown by transition 1, it can fall to M (transition 2). Consider the conditions that M is separated from E by a small energy gap and the system is in thermal equilibrium with its surrounding medium. Under such cases, the electron can return to state E following depopulation of the state M upon the application of some thermal energy. From there, transitions can take place as described in the case of fluorescence (transition 2). Therefore, phosphorescence spectrum contains emissions which are also

present in fluorescence. Since the emission intensity changes with even small change in temperature, phosphorescence is sensitive to changes in temperature in contrast to fluorescence.

To describe light emitting or luminescent material the Greek word 'phosphor' is usually used and it means 'light bearer' [1]. A phosphor emits energy from an excited electron as light and the excitation of the electron is triggered by absorption of energy from one of the external excitation sources discussed above. An excited electron occupies a quantum state whose energy is above the minimum energy ground state. In semiconductors and insulators, the electronic ground state is commonly referred to electrons in the valence band, which is completely filled with these electrons. The excited quantum state often lies in the conduction band, which is empty and separated from the valence band by gap, E_g. Therefore unlike metallic materials, small continuous change in electron energy within the band is not possible. Instead a minimum energy equal to the band gap energy is necessary to excite an electron in semiconductors and insulators, and the energy released by de-excitation is often nearly equal to the band gap. The band gap of semiconductor material is such that at room temperature, very few electrons are promoted from the valance band to the conduction band leaving holes in the valence band. In general, luminescence emission is explained by the transfer of energy from radiation to the electrons of the solid, thus exciting the electrons from a ground state to an excited state. The emission of a luminescent photon takes place when an excited electron returns to a lower energy state.

An electron excited to an upper energy level can return to the ground state by re-emitting a photon of the same energy as was absorbed. This phenomenon is called

resonance fluorescence. Depending on the presence of other metastable states relative to the excited state energy level, emission of photon of lower energy (Stoke's shift) or higher energy (anti-Stoke's shift) as compared to the absorbed energy can be observed when an excited electron relaxes to the ground state [32]. The wavelength of the emitted light is characteristic of the luminescent substance and not of the incident radiation. Usually, most studies of luminescence phenomena are concerned with the emission of visible light, but other wavelengths can be emitted, such as ultra-violet or infra-red.

2.2 Types of Luminescence

According to the type of radiation used to excite the emission, luminescence can be classified in to different types. These are photoluminescence, electroluminescence, thermoluminescence, cathodoluminescence, chemiluminescence, bioluminescence, triboluminescence, radioluminescence (scintillation), ionoluminescence, etc.

2.2.1 Photoluminescence

Photoluminescence occurs after excitation with light (i.e., radiation within the optical range). This excitation with electromagnetic radiation imparts external energy on an electron in a semiconductor or insulator and makes it excited to a higher energy quantum state. If the electron returns (relaxes) to a lower energy quantum state by radiating a photon, the process is called photoluminescence (PL) [33, 34]. This can be described as an excitation to a higher energy state and then a return to a lower energy state accompanied by the emission of photon. In PL phenomena, the

period between absorption and emission is of the order of 10 nanoseconds, which is extremely short. The PL intensity depends on the measurement temperature and the energy of the exciting light. The PL emission can be divided in to fluorescence and phosphorescence as discussed above.

2.2.2 Electroluminescence

When a material emits electromagnetic radiation as a result of the application of an electric field, the process is called electroluminescence (EL) [35, 36]. The photon emitted results from radiative recombination of electrons and holes created in the phosphor by the voltage between the two electrodes. One of the electrodes is transparent to the wavelength of the light emitted by the device. In other words, electroluminescence is the efficient generation of light in a non-metallic solid or gas by an applied electric field or plasma. Another type of electroluminescence is that produced by some crystals when an electric current passes through them. In this case the current or electrons excites electrons that occupy energy levels involved with chemical bonds inside the crystal. When the excited electrons decay back to their ground state, they emit visible light. Both organic and inorganic light emitting diodes (LEDs), operating on a different principle, has now become a widely used application of electroluminescence [36, 37].

2.2.3 Thermoluminescence

Thermoluminescence (TL), which is also called radiation induced thermally stimulated luminescence or simply thermally stimulated luminescence (TSL), is the thermally stimulated emission of light following the previous absorption of energy from

radiation[1, 28, 38]. The primary causes for the induction of TL in a given material are the ionization radiations such as x-rays, γ- rays, UV light, etc, to which the sample is pre-exposed. However, the application of heat stimulates the release of the stored energy in the sample due to pre-exposure to the ionizing radiations which in turn produces luminescence. Therefore, heat has only a secondary role in the process of TL.

The three essential conditions necessary for the production of TL are:

- The material must be an insulator or semiconductor.
- The material must have at some time absorbed energy during exposure to radiation.
- Heat should be applied to the material to trigger luminescence.

Moreover, the particular characteristic of a TL material is that, once heated to excite the light emission, the material can not be made to emit TL again by simply cooling the specimen and re-heating. For the luminescence emission to occur again, the material should be re-exposed to one of the ionizing radiations, where upon heating the sample once again produces light emission [1].

2.2.4 Cathodoluminescence

Cathodoluminescence (CL) is the characteristic visible radiation (color) occurring due to bombardment by electrons (cathode rays) [39, 40, 41]. Luminescence in CL is typically more intense than that produced by ultraviolet light and is also observed in minerals that do not luminesce under ultraviolet light. It is a very useful form of luminescence since beams of electrons are used for many purposes. For example, the

electron microscope employs beams of electrons to produce high resolution images of small specimens and in some cases, the beam produces CL from the specimen. This is important for the study of minerals in rocks where the presence of transition metal trace elements can cause the mineral to give off a distinctive color light. The CL of a sample reveals geochemical, rather than optical, variations in a sample, which provides important compositional, textural, and structural information not readily obtained by other methods. However, CL is most useful when used in conjunction with other studies such as optical microscopy, x-ray diffraction, electron microprobe, scanning electron microscopy, and geochemistry.

2.2.5 Chemiluminescence

Chemiluminescence is produced as a result of a chemical reaction usually involving an oxidation reduction process [42, 43]. The most common mechanism for such an emission is the conservation of chemical energy, released in a highly exothermic reaction, into light energy in the visible region. In some chemical reactions energy can be transferred to electrons in the chemical bonds. As these electrons decay down to lower excited states, they emit light. Some of these reactions proceed slowly, so the light can be emitted for a considerable time. This is known as chemiluminescence. This is distinct from more vigorous chemical reactions where so much heat is released that the chemicals actually catch fire or otherwise glow red hot (incandescence). However the process of chemiluminescence remains to be not fully understood. Lyoluminescence, which is the phenomenon of light emission during the dissolution of previously irradiated solids in suitable solvents is a type of chemiluminescence [44].

2.2.6 Bioluminescence

Electronic excited states of the biomolecules can be produced due to biochemical reactions inside the cells of the living organisms such as fire flies, glow-worms, some bacteria, fungi and many sea creatures (such as planktons) both near surface and at great depths and interesting luminescence phenomena can be observed from these living beings [45, 46]. The chemical reactions are the enzymic oxidations. For example, the oxidation of luciferin in the presence of enzyme luciferase is responsible for occurrence of bioluminescence [46].

2.2.7 Triboluminescence

Triboluminescence is the emission of light on applying an external mechanical energy inducing stress. It could be excited by cutting, cleaving, grinding, rubbing, and compressing or by impulsive deformation of solids. Because of this it can also be called mechanoluminescence. B. V. Bukvetskii et al, described the phenomenon of triboluminescence as the glow resulting from crystal destruction or friction [47, 48] and stated its importance in the process of converting mechanical energy into light energy. It has been observed that all piezoelectric crystals exhibit triboluminescence and it is sometimes called piezoluminescence.

2.2.8 Radioluminescence (Scintillation)

Radioluminescence is produced by ionizing radiation [49, 50]. Some polymers contain organic molecules which emit visible light when exposed to such radiations as x-rays, γ-rays, or cosmic rays. It is also called scintillation because it is used as a technique to detect individual light pulses generated by the incidence of each x- or (γ-ray) photon

or a nuclear particle [49]. Such light pulses are called scintillations, since like a spark they are very short-lived. The intensity of the scintillation (light pulse) is directly proportional to the incident gamma ray photon energy when it is totally absorbed. The measurement of the pulse intensity, therefore, provides the means for knowing the gamma ray energy. The mechanism of light emission in radioluminescence and cathodoluminscence is same because in both the cases it is the electrons, incident primarily from cathode rays or the secondary electrons produced after the first interaction of the incident x-ray photon or nuclear particle, which cause the excitation of the luminescent species in the bulk sample.

2.2.9 Ionoluminescence

Another interesting method of producing luminescence is the visible light produced when fast ions collide with organic and inorganic compounds. This is called ionoluminescence and it can also be defined as a phenomenon of non-thermal light emission induced by high energy accelerated particles or ion beams [51, 52]. An early application of ionoluminescence was to luminous clock dials. These relied upon a rather hazardous method of making light that involved radioactivity. A radioactive material, such as radium, was mixed with a material that displays luminescence, such as zinc sulphide. As the radium decays, it emits alpha particles and other radiation. This excites electrons in the luminescent material to give off light. This is very handy, since the light persists indefinitely, limited only by the half-life of the radium isotope used, ^{226}Ra, which is 1600 years.

2.3 Characteristic Luminescence

Characteristic luminescence occurs by doping the host lattice with either transition (3d) or rare-earth (4f) metal ions (impurities) that substitute for host lattice cations. An electron gets excited to a higher energy level in the atom itself. Rare earth ions from Ce^{3+} (atomic number of 58) to Yb^{3+} (70) have partially filled 4f orbitals with energy levels characteristic to each ion and show a variety of luminescent properties around the visible region. Many of these ions can be used as luminescent ions in phosphors. There are 15 rare earth materials and the lanthanides are those rare earths with the atomic numbers between 57 (La) and 71 (Lu). The 4f electronic energy levels of lanthanide ions are characteristic of each ion. The levels are not affected much by the environment because 4f electrons are shielded from external electric fields by the outer $5s^2$ and $5p^6$ electrons. This is in strong contrast with transition metal ions, whose 3d electrons, located in an outer orbit, are heavily affected by the environmental or crystal electric field [53]. Typical phosphors used in cathode ray tube (CRTs) and Field emission displays (FEDs) consist of a host matrix doped with activators such as the rare earths (4f) and the transition metals (3d) [54].

Among the various types of luminescence discussed above, attention is given to TL phenomenon in this study. This is owing to its wide applications in various disciplines of science. However, before discussing some of its wide applications, it is useful to discuss mechanism of TL and the role of defect centers in a given specimen.

2.4 Defect Centers and Mechanism of Thermoluminescence

As discussed above, TL is a two step process involving excitation by exposure to ionizing radiations and thermal stimulation. Irradiation of a sample causes transitions of electrons between the valence band and the conduction and creating free electrons in the conduction band and free holes in the valence band. Though some electrons and holes undergo recombination almost instantaneously during irradiation, some still diffuse in the lattice and remain trapped in the defect centers. These imperfections in the crystal, associated with impurities and/or lattice defects may create new localized energy levels in the forbidden band gap whose positions depend on the nature of the imperfections/defects and the host lattice [1]. Some of these defects are capable to trap an electron or a hole. Therefore the centers are referred to as electron or hole traps and after trapping an electron or hole the new defects are called trapped electron or trapped hole centers, respectively.

In other words, the presence of certain types of defects in the regular structure of a TL material which should be capable of capturing electrons or holes during exposure to ionizing radiations is very important for the induction of TL in the concerned material. This means that TL is very sensitive to the presence of defects or impurities in a given sample. Furthermore, the captured electrons/holes should be retained in the defect centers (also called TL centers) until the sample is heated to an appropriate temperature to read the TL. The term 'center' is used to designate these structures since they are present as an isolated entities and are not part of the regular lattice, which is a continuous repetition of the unit cell of a crystalline material.

There is also another type of defect which is associated with impurities, for example, ions of transition elements. This is usually the main cause of a characteristic color from certain minerals (as discussed in section 2.3) and the color is due to absorption bands caused by electronic transitions between energy levels in the band gap. The wave functions of the transition ions (in particular 4f ions) are highly localized. As mentioned above, the energy levels in the band gap depend on the nature of the imperfection, lattice defect or impurity and can in principle be located at any energy position varying from just below the bottom of the conduction band to just above the top of the valence band.

A variety of defects which are associated with energy levels in the forbidden band gap are also produced during exposure to ionizing radiation. As long as the concentration of radiation-induced defects is small, the number of defects usually increases with increasing radiation dose. Ultimately, for very high doses, one might expect that the concentration of the radiation-induced defects saturates. i.e., with increasing dose the concentration of radiation-induced defects reaches a maximum value. Due to their long-term exposure to ionizing radiation extremely old minerals are often metamict, which means that the long-range order is absent and the structural properties of these minerals are similar to those of amorphous materials like glasses. These heavily damaged minerals are not suited for TL dating purposes. As a result of the structural changes during the long-term exposure, the physical properties, in particular the TL controlling properties have changed drastically.

Due to their high mobility, free electrons and holes produced by ionizing radiation can migrate in the crystal until they are trapped by different trap centers such as impurities, luminescent centers and other imperfections in the crystal. A trap is

characterized by the energy E that a trapped electron (or hole) must acquire from lattice vibrations to escape to the conduction band (or valence band). A necessary condition for a mineral to be a suitable luminescent material for TL dating is that the relevant traps are deep, i.e., not easily emptied [1]. This implies that the energy of the trapped electron should be located sufficiently far from the bottom of the conduction band. Similarly, the energy of the trapped hole should be located sufficiently far from the top of the valence band. In TL, during the heating stage, different kinds of transitions of electrons and holes can take place during the detrapping process from their respective trap centers so that luminescence can occur. These transition options, which may or may not involve the delocalized bands, are discussed below.

2.4.1 Transitions involving delocalized bands

The alteration in occupancy of the various localized energy states, which can be implemented by electronic transitions from one energy state to another, is an essential feature of all luminescence processes [1, 28]. For both electrons and holes, several kinds of transitions are possible and some are shown in the Fig. 2.3. Because of irradiation, a valence electron from a host atom is excited into the conduction band in which state it has enough energy to move freely through the lattice (transition (a)). Thus, this transition corresponds to the process of ionization and is a result of the absorption of energy from an external source. Since for every free electron in the conduction band a free hole is left behind in the valence band, the process of ionization results in the creation of free electron-hole pairs which may wonder through the crystal until they become localized at defect (trap) centers. This is shown as the trapping of electrons (transitions (b)) and holes (transition (e)). However, through

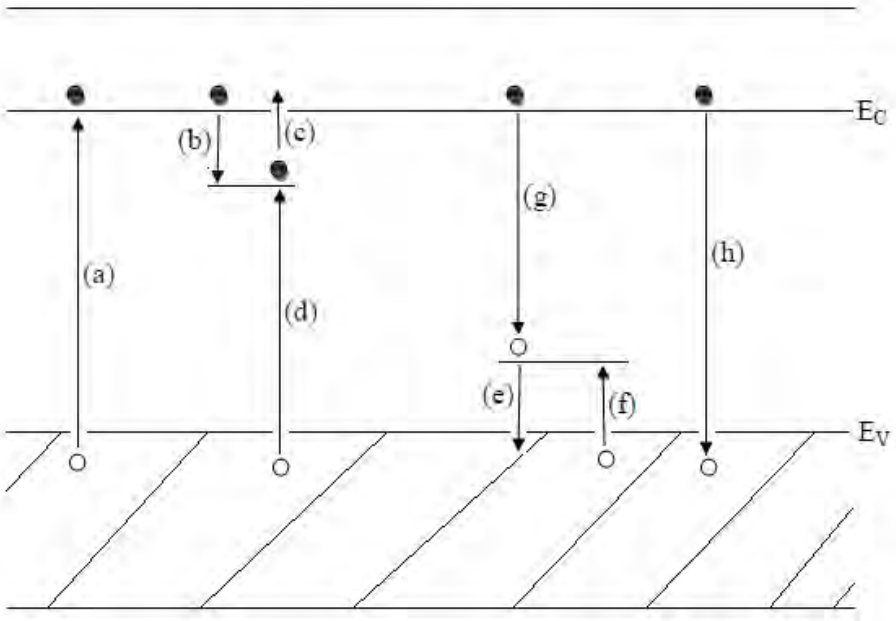

Figure 2.3: Common electronic transitions in crystalline semiconductors and insulators: (a) ionization; (b) and (e) electron and hole trapping respectively; (c) and (f) electron and hole release; (d) and (g) indirect recombination; (h) direct recombination. Electrons are represented by solid circles and electron transitions by solid arrows. Holes are represented by open circles and hole transitions by open arrows [1].

thermal excitation, the localized electrons and holes may be released from their traps (transitions (c) and (f)) to become free and move through the crystal. The free electrons and holes have also an option to undergo recombination with a charge carrier of opposite sign at recombination centers. This can take place either directly (transition (h)), or indirectly by recombining with a previously trapped carrier (transitions (d) and (g)). If either of these recombination mechanisms is accompanied by the emission of light (i.e., it is radiative) then luminescence results.

2.4.2 Transitions not involving delocalized bands

Unlike the above discussion, which is strictly valid for transitions involving the delocalized bands, electron and hole transitions can occur directly between centres in many materials without the carriers being raised into the conduction and valence bands [1]. Transitions of this type are important in luminescence processes (includ-

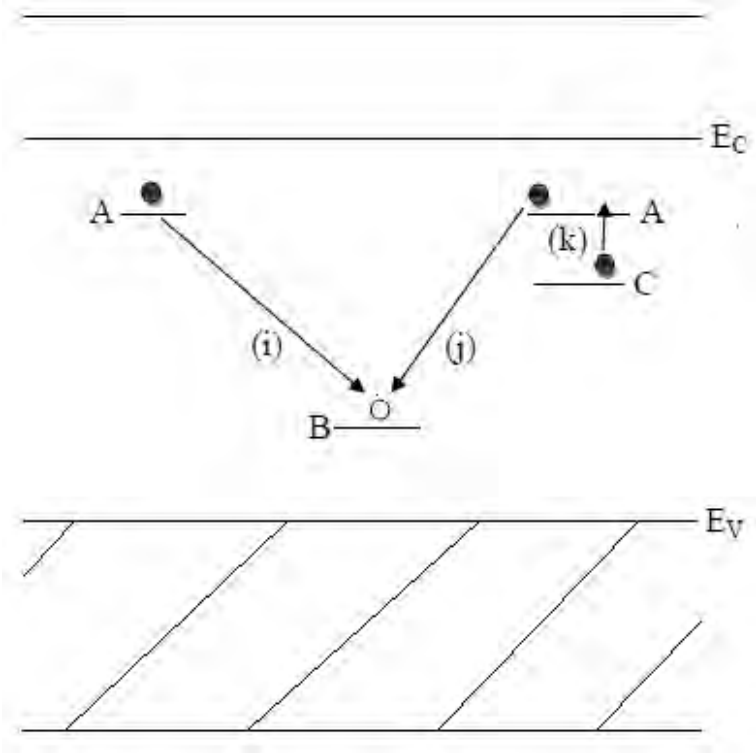

Figure 2.4: Electron transitions in a semiconductors or insulators not involving the delocalized bands [1].

ing TL) of many luminescent materials (phosphors).

Fig. 2.4 depicts a typical center-to-center transition of electrons that can take place. In this Figure, though only electron transitions are represented for simplicity, similar transitions also occur for holes. Transition (i) shows recombination of an electron trapped at level A with the hole trapped at level B.

This type of recombination commonly happens if energy levels A and B are within the same atom. Good examples of substances which exhibit this kind of recombination are rare earth elements. For example, due to this type of transition, luminescence from thallium in potassium chloride occurs when an electron from the $3P_1$ state in thallium decays to its ground state $1S_o$ with the emission of light of wavelength 305 nm [1]. This is one of the earliest classical examples of this kind of recombination. Moreover, luminescence can also be induced when dopants are incorporated into the lattice of different host materials and this luminescence is primarily a characteristic of the particular rare earth used, and not of the host material [55].

Rare-earth-doped materials are becoming popular as luminescent phosphors because of the fact that the transitions within the dopants are normally radiative. If levels A and B in Fig. 2.4 are not within the same atom, a transition of type (i) can still take place by tunneling. This is commonly true if the defects responsible for the levels are situated close to each other few lattice constants apart in the host lattice. This type of recombination is reported in a variety of organic and inorganic materials [56, 57, 58]. An alternative possibility is that an electron has to be elevated to a higher energy level before recombination with a trapped hole can take place. Thus, in Fig. 2.4, an electron at level C has to be raised to A (transition (2)) before recombination (transition (3)) can take place. The fact that electron transitions of this sort do not involve excitation into the conduction band has a consequence that there will not be any accompanying conductivity phenomena, while transitions involving delocalized bands (Fig. 2.3) will be associated with changes in conductivity.

2.5 Applications of Thermoluminescence

The modernization and development in the instrumentation and better understanding of TL have helped the professionals to solve their problems in many fields. The present research on TL has explored its very high application potential in various fields such as archaeology, analysis of defects in solids, radiation dosimetry, geology, forensic sciences, quality control in industry for controlling the quality of many glass, ceramics, and semiconductor products; biology and biochemistry for studying the properties (involving different chemical reactions) or contents of proteins and leaves. Moreover, TL has also interesting applications in space science, thermostimulated luminescence (TSL) photography, radiation physics, petroleum exploration, etc. In this section, the applications of TL for defect analysis in solids and dosimetry are discussed briefly.

2.5.1 Defect analysis in solids

TL is very sensitive to traces of impurities or defects within the host material of a given sample and experiments on TL yields useful information on the properties of the various types of defect present within an insulator or semiconductor [1, 62, 63]. This includes the position of the defect within the energy gap and sometimes the type of defect itself. There are early reports on the effect of impurities on the TL properties of various materials [64, 65, 66]. In general the impurities give rise to the localized energy levels within the forbidden energy gap and that these are crucial to the TL process. For the purpose of detecting the presence properties of these defect levels, the analysis of TL glow curves is important. In addition to defect levels produced by external means such as irradiation or doping, there are also those due to defects, such

as lattice vacancies and interstitials inherently present in the material. The presence of this type of imperfection is also crucial to the TL process in many materials.

Recent research on defect analysis in various materials focusses on the determination of the position of the defect (trap) level just beneath the edge of the conduction band [4, 7, 38]. This can be achieved through analysis of TL glow curves by employing various methods such as heuristic method, initial rise method, the whole TL glow curve method, heating rate method, peak shape method and isothermal decay method. These techniques for analysis of TL glow curves to locate the trap depth within the band gap are discussed in detail in chapter 3.

2.5.2 Radiation dosimetry

TL has an interesting application in the field of radiation dosimetry [65, 66, 67]. It is clear that the absorption of radiation increases the level of TL observed from a given sample by filling the localized energy levels with trapped electrons while the absorption of heat from the environment tends to reduce the numbers of trapped electrons by detrapping them. Therefore, the intensity of TL from the sample is the result of a competition between trap filling by radiation and trap emptying by thermal excitation. Since many materials display an intensity of TL which is proportional to the amount of radiation absorbed [62], TL may be used as a means of radiation dosimetry. The first proper application of TL to dosimetry was in 1953 when LiF was used to measure radiation following an atomic weapon test [1]. The eligibility of LiF for radiation dosimetry is mainly because of its high sensitivity and it was used as small pellets to measure internal radiation doses received by cancer patients treated with radioactive isotopes [68]. The procedure was that the patients were

made to swallow small LiF pellets which were recovered after passage through the digestive system. Then, the accumulated dose received by the patients was obtained by measuring the TL from the pellets and comparing it with that produced in similar crystals which had been irradiated with a known dose of radiation. Other well known TL dosimetry (TLD) phosphors in use today include Al_2O_3, $Li_2Ba_4O_7$, and Mg_2SiO_4 [69].

In order to check whether a given material is appropriate for dosimetric application, investigation of its TL properties with increase in external radiation dose (ultra-violet, x-rays, γ-rays, etc) is quite important. In some TLD phosphors, the TL intensity grows linearly with dose [69]. However, in most other materials used in radiation dosimetry, different degrees of deviation from linearity are observed [70, 71]. Therefore, the phenomena of superlinearity (where the intensity growth is more than linear) and sublinearity (where the intensity growth is less than linear) can be observed from the TL response of a given TLD phosphor with dose.

2.6 Models of Thermoluminescence

There are different models of thermoluminescence. A simple energy level scheme consisting of two localized levels (one act as trap (TR) and the other act as recombination center (R)) is shown in Fig. 2.5. It is also called one trap and one recombination center (OTOR) model. The traps are assumed to be electron traps and the recombination centers are hole traps. The traps and the recombination centers get filled up by the respective type of charge carriers following irradiation of the specimen. The electrons are ejected out of the traps (detrapped) and become free to move in the conduction band during the heating stage after absorption of enough energy E

corresponding to the trap depth.

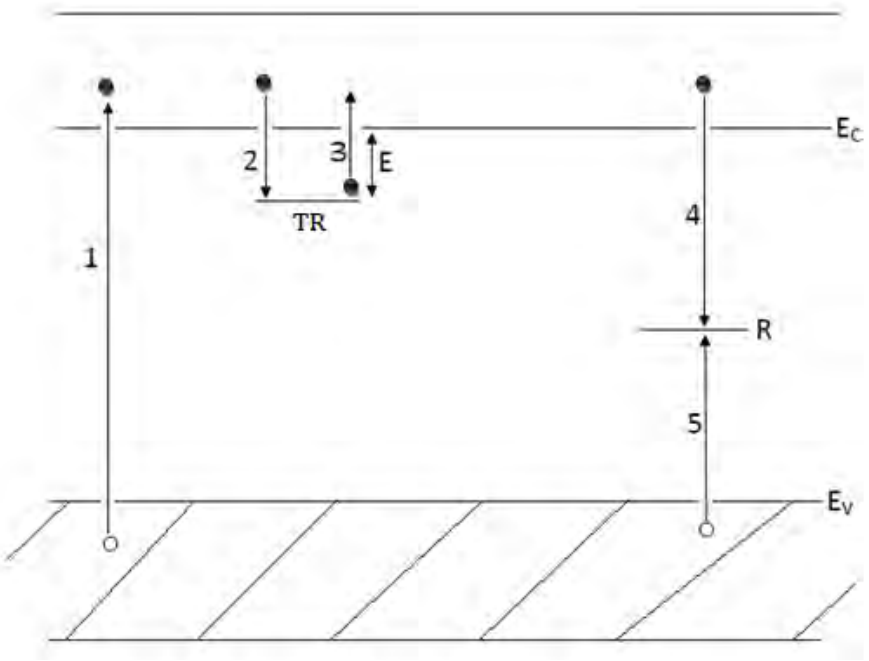

Figure 2.5: Two level model for thermoluminescence. Allowed transitions: (1) ionization; (2), (5), trapping; (3) thermal release (detrapping); (4) radiative recombination and emission of light.

During the random motion of the electrons in the conduction band following ionization (irradiation) and thermal release, the electrons may recombine with holes trapped at recombination center (R) emitting light. Alternatively the electrons may also fall back into an empty trap. This is called retrapping. Thus the transport of electrons from the traps to the recombination centers to emit luminescence may be described in terms of rate of excitation, retrapping and recombination. These three rates for the OTOR model are given by [28, 29]

$$R_{ex} = n\ s\ \exp\left(-\frac{E}{kT}\right), \tag{2.6.1}$$

$$R_{ret} = n_c \; A \; (N - n), \tag{2.6.2}$$

$$R_{rec} = n_c \; A_r \; n_h, \tag{2.6.3}$$

where R_{ex}, R_{ret}, R_{rec}, respectively are the excitation, retrapping and recombination rates, N and n, respectively are the total and the filled concentration of the thermally active traps, n_c is the concentration of the charge carriers in the conduction band, n_h is the concentration of holes in the recombination center, E is the activation energy of the trap, which is also called the trap depth, T is the sample temperature, k is the Boltzmann constant, A and A_r, respectively, are the retrapping and the radiative recombination probability coefficients. The values of these coefficients depend on the capture cross sections σ and σ_r of the traps and the recombination centers, respectively: ($A = \sigma v$ and $A_r = \sigma_r v$ where v is the velocity electron in the conduction band). The physical scheme used in formulating any particular model of TL determines the value of n_h. Since the overall charge neutrality condition should be ensured, the value of n_h is the sum of all the filled traps in the sample, which means the filled active traps n and any deeper level traps which are thermally not affected, at the given temperature T. It is assumed that all the excited charge carriers relax from conduction band instantly either into the recombination center or alternatively into the empty traps, with no significant number of these being left behind in the conduction band. This is called the quasi-equilibrium condition. The fraction η of the excited carriers which produces luminescence during heating stage is given by the following equation [1],

$$\eta = \frac{R_{rec}}{R_{ret} + R_{rec}}. \tag{2.6.4}$$

Here, η is also called the luminescence efficiency and its value strongly depends on the values of the parameters in Eq. 2.6.1 to Eq. 2.6.3. However, the expression of η would change according to the applicable physical model since the denominator in Eq. 2.6.4 may increase depending on the existence of other possible routes of relaxation such as non-radiative recapture in deeper level traps.

There are two early models of TL proposed by Randall and Wilkins, and Garlick and Gibson. These models are discussed below.

2.6.1 Randall and Wilkins model

This is the first theoretical model of TL suggested by Randall and Wilkins (RW) [60]. Their suggestion was under the assumption that the retrapping may be negligible ($R_{ret} = 0$) and hence according to Eq. 2.6.4, $\eta = 1$. Therefore, the TL intensity I is directly proportional to R_{ex}.

$$I = c\ R_{ex} = c\ n\ s\ \exp\left(-\frac{E}{kT}\right). \tag{2.6.5}$$

The temperature T can be expressed in terms of the linear heating rate β as $T = T_0 + \beta t$ and c is a constant representing the optical efficiency factor relating the luminescence output to the electron release rate and the measuring instrument's efficiency to collect the light. The value of the constant c can be taken to be unity since it influences only the intensity of the glow curve and it has no effect on the characteristics like the shape of the glow curve and its decay pattern. Rearranging Eq. 2.6.5, yields [28],

$$\frac{dn}{n} = -s\ \exp\left(-\frac{E}{kT}\right)\ dt. \tag{2.6.6}$$

Using the assumption of linear heating rate i.e., $dT/dt = \beta$, Eq. 2.6.6 may be written as,

$$\frac{dn}{n} = -\left(\frac{s}{\beta}\right)\ \exp\left(-\frac{E}{kT}\right)\ dT. \tag{2.6.7}$$

The expression of n at any temperature T during the heating process can be obtained by integrating Eq. 2.6.7 and is expressed as,

$$n = n_0\ \exp\left[-\int\left(\frac{s}{\beta}\right)\exp\left(-\frac{E}{kT'}\right)\ dT'\right], \tag{2.6.8}$$

where T' in the integral runs from initial temperature T_0 to final temperature T, n_0 is the initial concentration of trapped electrons. Plugging this expression for n in Eq. 2.6.5, one obtains the expression for TL intensity $I(T)$ as a function of temperature T as,

$$I(T) = n_0\ s\ \exp\left(-\frac{E}{kT}\right)\ \exp\left[-\int\left(\frac{s}{\beta}\right)\ \exp\left(-\frac{E}{kT'}\right)\ dT'\right]. \tag{2.6.9}$$

Eq. 2.6.9 gives the TL intensity the glow curve. The integral in this equation is expressed in terms of special function as,

$$\int \exp\left(-\frac{E}{kT}\right)\ dT = \exp\left(-\frac{E}{kT}\right)\ T + \frac{E \times ExpIntegralEi\left(-\frac{E}{kT}\right)}{k}, \tag{2.6.10}$$

where $ExpIntegralEi\left(-\frac{E}{kT}\right)$gives the exponential integral function $Ei\left(-\frac{E}{kT}\right)$.

The profiles of change in the filled trap population n, the thermal excitation probability p and the TL intensity I as a function of temperature T during the heating stage are shown in Figs. 2.6, 2.7, and 2.8 respectively. As shown in Fig. 2.7, the initial part of the glow curve rises exponentially. Moreover, the probability of thermal excitation p given by $s\ \exp\left(-\frac{E}{kT}\right)$ also rises exponentially as shown in Fig. 2.8. In the initial rise part of the glow curve, the value of n may be considered constant at n_0 which is the initial concentration of electrons in traps. This property

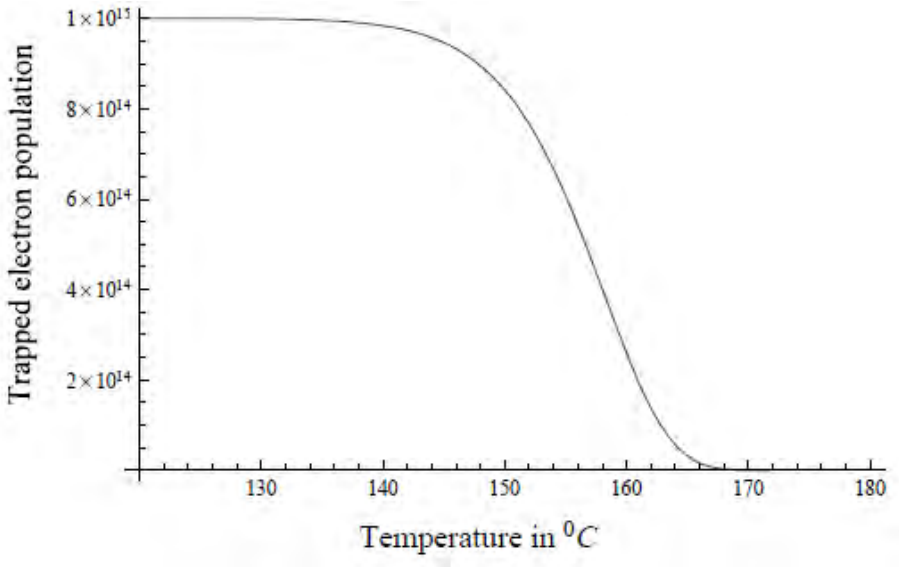

Figure 2.6: Profile of trapped electron population n. Calculations are carried out using the Randall- Wilkins model. Input parameters used are $E = 0.4\ eV$, $s = 10^{12}\ s^{-1}$, $\beta = 1\ ^0C\ s^{-1}$. The initial value of n is $10^{15}\ cm^{-3}$.

is useful to determine the values of the thermoluminescence kinetic parameters such as the trap depth E and the frequency factor s by a method called initial rise method. The methods of analysis of TL glow curves will be discussed in detail in chapter 3. When the number of trapped charges n, is appreciably diminished, the TL intensity curve ceases to rise in the exponential fashion. It attains a maximum value before falling and ultimately falls to zero when all the traps are emptied.

The following are the characteristics of the glow curves of this model:

- The glow curve has an asymmetric nature. This means that it rises comparatively slowly and falls relatively sharply (see Fig. 2.7).

- As E increases, the glow peak shifts to higher temperature. Higher value of E means stronger binding of the trapped charge and higher thermal energy is needed to release it. The glow peaks for different values of E are shown in Fig.

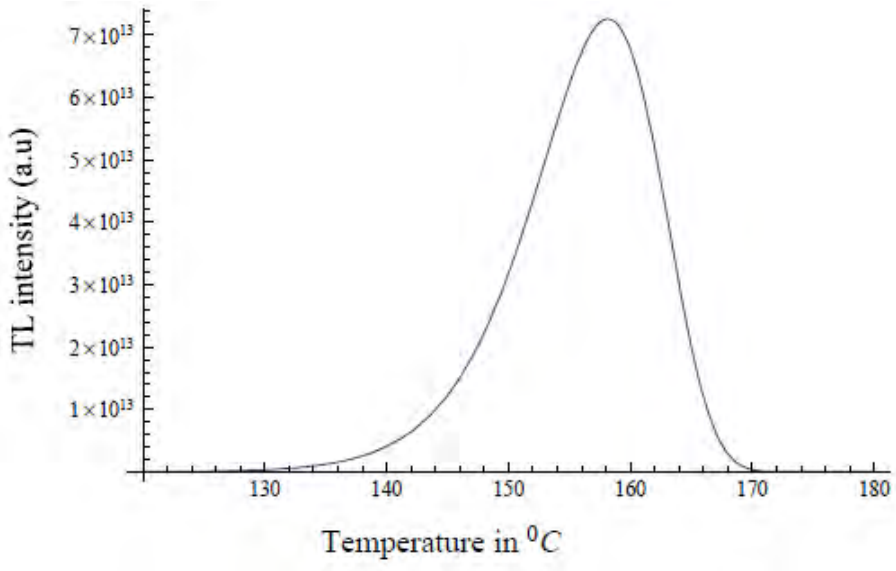

Figure 2.7: TL intensity versus temperature in Randall- Wilkins model with the same input paramaters as in Fig. 2.6.

2.9 for constant values of s and b. It can be observed that with increase in the value of E the peak height is reduced.

- For given values of E and b, the glow peak shifts to lower temperature as s is increased. Thus, it is clear that E and s have opposite effects on T_M. This is simple to understand since higher s means faster escape of the trapped change from the excited state of the trap. Higher s leads also to increase in peak height.

- For given values of E and s, the peak temperature T_M increases as heating rate β is increased.

- The glow peak characteristics, namely the peak temperature T_M and the peak shape remain unchanged when the initial filled concentration n_0 of the traps is changed. This means that the peak characteristics are independent of radiation dose given to the sample. However, the intensity (the area as well as the height

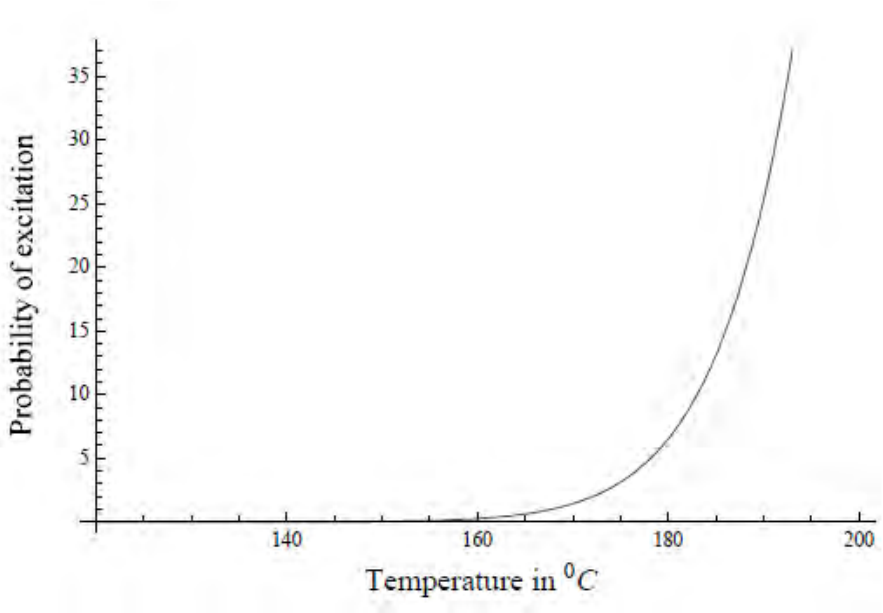

Figure 2.8: Profile of probability p of excitation as a function of T during heating Randall- Wilkins model. The same input parameters as in Fig. 2.6 are used. This increment in p for all T is, however, ideal.

of the peak) increases in direct proportion to n_0 for given E, s and β. In other words, the intensity is directly proportional to dose given to a sample, assuming that the trap filling is directly proportional to the dose. These characteristics are unique to RW model and are of prime importance in the application of TL in radiation dosimetry as well as in kinetics analysis of the glow curves.

2.6.2 Garlick and Gibson model

Using the same OTOR model, Garlick and Gibson (GG) modified the model of TL intensity proposed by RW [61]. According to GG model, an electron which is de-trapped into the conduction band from the trap centers after absorption of thermal

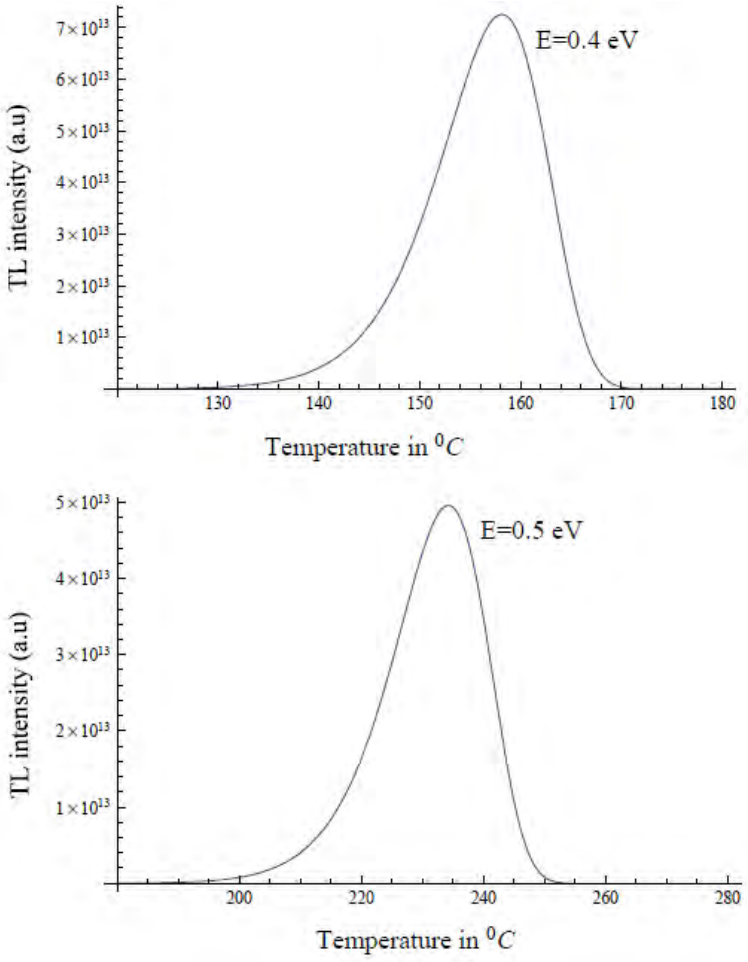

Figure 2.9: Change in temperature T_M of glow peak maximum with change in E. The values of other parameters are the same as in Fig. 2.6.

energy has two options, i.e., it may either recombine with a hole trapped at recombination center to produce luminescence or may be retrapped by any of the vacant traps. However, in RW model, retrapping is assumed to be negligible and the detrapped electrons are assumed to recombine directly with the trapped holes giving luminescence. Let A and A_r, respectively, be the probability coefficients for retrapping and recombination. The recombination and retrapping terms, respectively, are proportional to $A_r\ n$ and $A\ (N-n)$, where N is the total number of the traps and n

is the instantaneous number of available recombination centers. In the OTOR model n is also equal to the number of filled traps, so that the charge neutrality condition is maintained. The recombining fraction η of this combined probability of transitions for any excited carrier, then is,

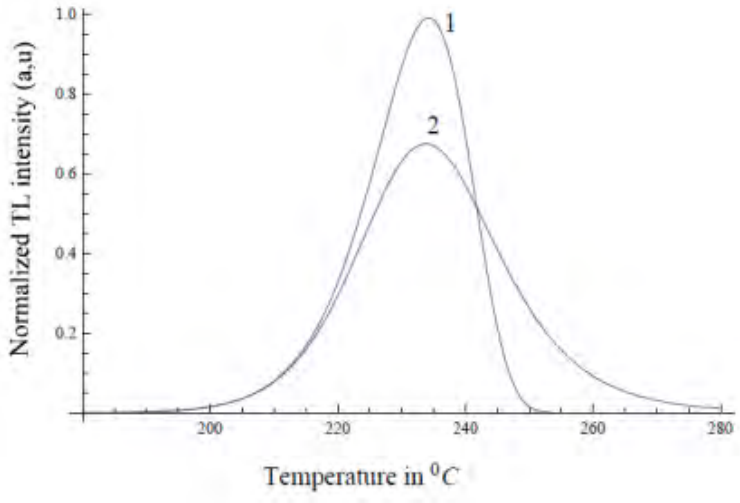

Figure 2.10: First order (1) and second order (2) peaks with $E = 0.5\ eV$, $s = 10^{12}\ s^{-1}$, $n_0 = N = 10^{15}\ cm^{-3}$.

$$\eta = \frac{A_r\ n}{A_r\ n + A\ (N - n)}. \tag{2.6.11}$$

According to Garlick and Gibson (GG), the probability of rerapping is equal to the probability of recombination, i.e., $A_r = A$. Therefore, the value of η in GG model becomes $\eta = n/N$ and the TL intensity $I(T)$ previously given by Eq. 2.6.5 would be modified by a factor equal to n/N. Thus, in GG model,

$$I(T) = -\frac{dn}{dt} = \left(\frac{n}{N}\right)\ n\ s\ \exp\left(-\frac{E}{kT}\right) = \left(\frac{n^2}{N}\right)\ s\ \exp\left(-\frac{E}{kT}\right). \tag{2.6.12}$$

It can be seen that the TL intensity $I(T)$ is proportional to n^2 in GG model, and is called second order kinetics which is discussed in detail in the next section. Again

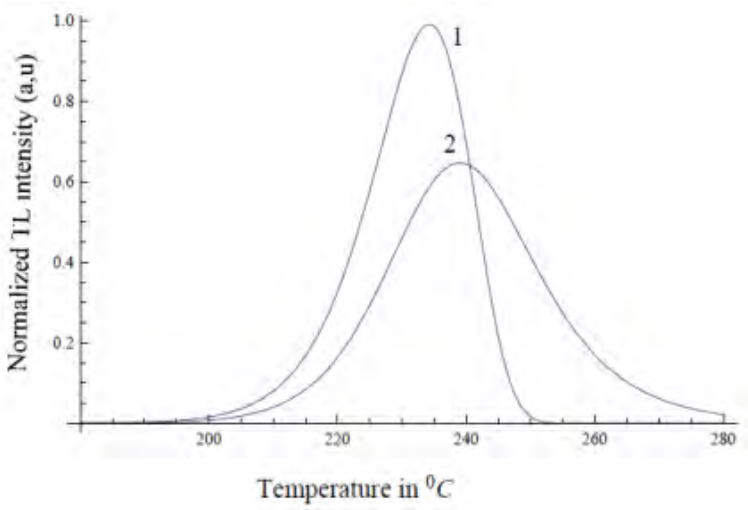

Figure 2.11: First order (1) and second order (2) peaks with $E = 0.5\ eV$, $s = 10^{12}\ s^{-1}$, $n_0 = 10^{15}\ cm^{-3}$, $N = 2 \times 10^{15}\ cm^{-3}$, $\beta = 1\ ^0C\ s^{-1}$.

assuming linear heating rate $dt = dT/\beta$ and integrating Eq. 2.6.12 one obtains the value of n at any temperature T as,

$$n(T) = \frac{n_0}{1 + \frac{1}{N}\ \left(\frac{s}{\beta}\right)\ n_0\ \int \exp\left(-\frac{E}{kT'}\right)\ dT'}, \tag{2.6.13}$$

Substituting Eq. 2.6.13 in to Eq. 2.6.12, the following equation for the glow curve can be obtained [28],

$$I(T) = n_0^2\ \left(\frac{s}{N}\right)\ \exp\left(-\frac{E}{kT}\right)\ \left[1 + \frac{n_0\ s}{\beta\ N}\int \exp\left(-\frac{E}{kT'}\right)\ dT'\right]^{-2}. \tag{2.6.14}$$

It is worth noting that, if $n \ll N$ (low dose sample) so that $A\ N$ becomes much greater than $A_r\ n$, second order kinetics can be obtained in OTOR model even if $A_r \neq A$. In this case, $\eta = A_r\ n/A\ N$ and in Eq. 2.6.12, n/N gets replaced by $A_r\ n/A\ N$ and in Eq. 2.6.14, s/N gets replaced by $sA_r/A\ N$. Therefore,

$$I(T) = n_0^2\ \left(\frac{s\ A_r}{N\ A}\right)\ \exp\left(-\frac{E}{kT}\right)\ \left[1 + \frac{n_0\ s\ A_r}{\beta\ N\ A}\int \exp\left(-\frac{E}{kT'}\right)\ dT'\right]^{-2}. \tag{2.6.15}$$

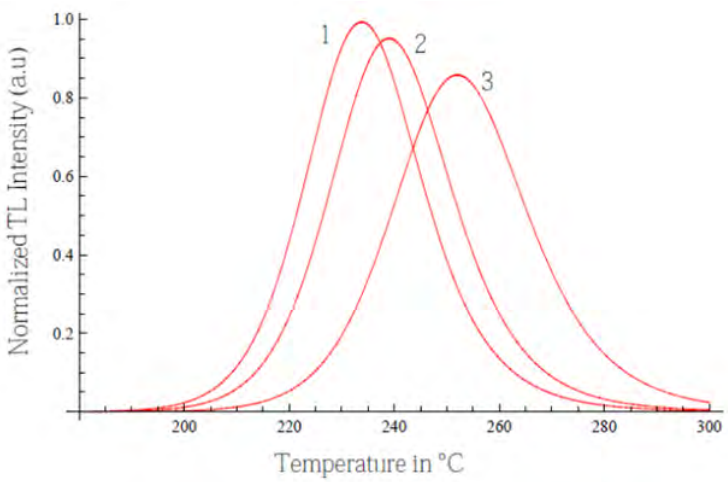

Figure 2.12: Second order peaks with (1) $n_0/N = 1$, (2) $n_0/N = 0.5$, and (3) $n_0/N = 0.1$. In addition, $E = 0.5\ eV$, $s = 10^{12}\ s^{-1}$ and $\beta = 1\ ^0C\ s^{-1}$ for all the peaks.

Thus, it should be noted that in the case of $A_r \neq A$, the second order kinetics is obeyed only in low dose samples ($n \ll N$), whereas it is valid at all doses for the case when $A_r = A$. The characteristics of the glow curves computed from GG model (Eq. 2.6.12) may be described as follows.

- The fall of the glow curve is slightly slower than its rise (see Figs. 2.10 and 2.11). This is in contrast to the first order kinetics case in which the fall is faster than the rise.

- For a given set of parameters E, s, β and n_0/N the temperature of maximum intensity (T_M) is on the higher side as compared to that of the first order, except when $n_0 = N$ (traps filled to saturation) (see Figs. 2.10 and 2.11) in which case the T_M for the first order and the second order kinetics is nearly same.

- The glow peaks shift to higher temperature and become progressively wider in shape as the value of n_0/N is reduced, i.e. smaller is the dose, higher the T_M

and wider are the peaks (see Fig. 2.12). This is in contrast to the first order kinetics case in which T_M is independent of n_0/N.

The other properties, namely the dependence of T_M on E, s and β as expected are similar to that of the first order kinetics case.

2.7 Order of Kinetics

2.7.1 First and second order kinetics

In TL theory, the term order of kinetics has been taken from chemistry. It is related to the rate of chemical reaction and the change in the concentration of reactants. When the rate of a chemical reaction is directly proportional to the change in the concentration of only one of the reactant, it is called mono molecular kinetics or first order kinetics. However, if the rate of chemical reaction is directly proportional to the change in the concentration of both the reactants, it is called bi-molecular kinetics or second order kinetics. The reaction following second order kinetics may be written as [72],

$$-\frac{dn}{dt} = C\ n(t)\ m(t). \tag{2.7.1}$$

In other words, in first order kinetics, the electron retrapping probability is assumed to be zero and the TL intensity I at any temperature T during heating stage depends only on the concentration n of electrons in the active traps at that temperature [72]. Randall and Wilkins demonstrated that a TL glow curve corresponding to a single electron trapping state and a single kind of recombination center results in first-order kinetics if there no retrapping of the detrapped electrons. The equation governing this process was shown in Eq. 2.6.6. RW model is called a 'classical' first order case

among researchers dealing with TL due to the assumption of no retrapping. However, in some cases the physical situation of 'negligible retrapping' has been termed first order kinetics.

A case of non-first order kinetics is obtained if the values of the TL intensity are dependent also on the concentration h of the recombination centers in addition to the concentration of electrons n in traps. According to some early investigators of TL phenomena, second-order kinetics is obtained if the probability of retrapping is non-zero. For OTOR case in GG model, when $A_r = A$ and the concentration h of recombination center is equal to the concentration n of electrons in traps, it becomes a case of second order kinetics. If $A_r = A$, the 'reaction' rate between the released charges from the traps and the recombination center becomes equal to n^2 (as shown in Eq. 2.6.12 which means we have kinetic order equal to 2. For the condition when $A_r \neq A$, a value of kinetic order between 1 and 2 is obtained instead of being exactly equal to 2. Thus, though a chemical reaction can be described in terms of first order or second order kinetics in chemical kinetics, all values of the kinetic order between 1 and 2 are also possible in TL phenomena. Such cases do not fit in to first order or second order kinetics and are called general order kinetics. This is discussed in detail in the following section.

2.7.2 General order kinetics

May and Partridge (MP) suggested a more general expression for TL emission which would satisfy not only the first order and second order kinetics expressions when $b = 1$ and $b = 2$ respectively, but would also include all other possible values of b including its non-integral values between 1 and 2 or even outside this range. Accordingly, they

proposed the following expression for TL intensity [28, 73]

$$I(T) = -\frac{dn}{dt} = n^b s' \exp\left(-\frac{E}{kT}\right), \tag{2.7.2}$$

where s' and b are the empirical constants called frequency factor and the order of kinetics, respectively. Therefore, this expression for TL intensity is called general order kinetics. There is a general practice of applying Eq. 2.7.2 to any experimental glow peak to do kinetic analysis though it is based on OTOR model. This is under the assumption that it includes all plausible physical schemes that may be applicable to the glow peaks. The solution of this equation gives the following temperature dependent expression for the TL glow peak,

$$I(T) = n_0^b\ s'\ \exp\left(-\frac{E}{kT}\right)\ \left[1 + \frac{(b-1)\ n_0^{b-1}\ s'}{\beta}\int \exp\left(-\frac{E}{kT'}\right)\ dT'\right]^{-\frac{b}{b-1}}, \tag{2.7.3}$$

where $b \geq 2$. Eq. 2.7.3 was simplified by Chen [74] under the assumption that $n_0^{b-1}\ s' = s$. The role of $n_0^{b-1}\ s'$ was assumed to be similar to that of the frequency factor in the first order kinetics mainly because of the fact that it has the dimension s^{-1} like the frequency factor. However, to avoid confusion, later workers have designated it as s'' instead of s. Therefore, equation Eq. 2.7.3 becomes,

$$I(T) = n_0\ s''\ \exp\left(-\frac{E}{kT}\right)\ \left[1 + \frac{(b-1)\ s''}{\beta}\int \exp\left(-\frac{E}{kT'}\right)\ dT'\right]^{-\frac{b}{b-1}}. \tag{2.7.4}$$

It is important to note that greater degree of retrapping (indicated by greater value of b) is found to raise the value of the temperature T_M corresponding to the maximum intensity.

2.7.3 Mixed order kinetics

Since the expression of the general order kinetics discussed above is only empirical a better alternative (expression) which fit neither in first order nor second order is

required in dealing with TL glow peaks. To fill this gap, the mixed order kinetics was originally proposed by Visocekas [75]. Chen et al. [76] have further elaborated on the model proposed by Visocekas and suggested that mixed order kinetics has merit over general order kinetics since it is derived from a physically meaningful model whereas the general order kinetics is only empirical. The equation for the mixed order glow curve when the linear heating rate of $dT/dt = \beta$ is used is given by [77, 78],

$$I(T) = \frac{s'\ C^2\ \alpha\ \exp\left[\frac{s'\ C}{\beta}\int \exp\left(-\frac{E}{kT'}\right)\ dT'\right]\ \exp\left(-\frac{E}{kT}\right)}{\left\{\exp\left[\frac{s'\ C}{\beta}\int \exp\left(-\frac{E}{kT'}\right)\ dT'\right] - \alpha\right\}^2}, \tag{2.7.5}$$

where α is the kinetic order parameter in mixed order kinetics and is defined as $\alpha = n_0/(n_0 + C)$ and C is the population of the thermally disconnected deep traps (TDDTs) [77]. The TDDTs may be assumed to be totally filled, so that they do not capture the carriers liberated from the active traps during heating.

Chapter 3

Analysis of Thermoluminescence Glow Curves and Characterization Techniques

3.1 Introduction

The models and factors affecting TL have been discussed in detail in chapter 2. However, it is important to analyze the TL emission characteristics to get the mechanisms involved in the process. Also the knowledge of TL kinetic parameters, which can be analyzed using different methods, is crucial to determine TL applications of studied samples. In general, research activities in the area of TL over the past years led scientists in three different directions. The first approach is concentrated on the determination of TL kinetic parameters such as activation energy (E), frequency factor (s) and order of kinetics (b) relevant to the TL glow curves. The second approach is related to studies on defect centers. The third approach makes use of the capability of deep traps in insulating materials to store charge carriers above room temperature for a long time for applications in the field of dosimetry and dating.

In fact, the main objective of studying TL is to extract data from the TL glow

curves and use these data to determine the various TL kinetic parameters associated with the sample under investigation. Though arriving at the correct values of these parameters is not an easy task, their calculation is an important step in arriving at an acceptable level of understanding of the underlying processes in TL emission. Moreover, a great deal of efforts has been directed towards the development of a reliable method of analysis. The methods used for the analysis of the TL glow curves are, heuristic method (first approximation of E), initial rise method, the whole glow curve method, the variable heating rate method, peak shape method, isothermal decay method, and computer glow curve deconvolution method. These methods begin by selecting the TL kinetic equations appropriate to a particular model and continue by introducing a simplifying assumption into these equations in order to arrive at an analytical expression which describes the variation in TL intensity with temperature, in terms of the desired parameters [59]. From these equations, even reaching at simpler expressions which relate the parameters directly to the data is possible. Therefore in this chapter, the simplified methods of analysis used to evaluate the TL kinetic parameters will be briefly discussed. Moreover, some useful characterization techniques employed during the study are also briefly discussed. The synthesized nanophosphor is characterized using x-ray diffraction (XRD), photoluminescence (PL) spectroscopy, ultra-violet Visible (UV-VIS) spectroscopy, and thermoluminescence (TL) spectroscopy. The basic working principle of each technique (device) is explained.

3.2 Methods of Analysis

3.2.1 Heuristic method (First approximation of E)

These are the first approximations for the evaluation of activation energies. However, the accuracy expected in these methods is, in general, poor. From TL experiments, D. Curie [79] deduced the following empirical relation between the activation energy (E) and the maximum temperature of the glow peak T_M for a given value of β/s.

$$E = \frac{T_M - T_0}{K}. \tag{3.2.1}$$

Here, E is in eV, T_M is in Kelvin, and T_0 and K are constants varying with the value of β/s as given in Table 3.1.

β/s (^oK)	K ($^oK/eV$)	T_0 (^oK)
10^{-4}	833	35
10^{-5}	725	28
10^{-6}	642	22
10^{-7}	577	17
10^{-8}	524	13
10^{-9}	480	10
10^{-10}	441	7
10^{-11}	408	6
10^{-12}	379	6
10^{-13}	353	5
10^{-14}	331	5
10^{-15}	312	4

Table 3.1: The values of the parameters T_0 and K for different input values of β/s [79].

Therefore, for a given value of T_M, E can easily be evaluated.

3.2.2 Initial rise method

This method of analysis was first suggested by Garlcik and Gibson [80]. It is commonly used to determine the activation energy when only one glow peak is presented and analyzed. However, when the glow peak is more complex, a wide peak and some holders appear in the structure, the application of the initial rise method is not valid since multiple trapping levels are considered and then the thermoluminescence analysis becomes difficult to perform [81]. The underlying principle in this method is that the dependence of the amount of trapped electrons $n(T)$ is negligible in the low temperature tail of TL glow peak and it can be assumed to be approximately constant. In other words, very little detrapping will take place at this low temperature region indicating that this method is independent of the order of kinetics. With rise in temperature, the first exponential in Eq. 2.6.9 increases, whereas the value of the second term remains close to unity and this remains valid when the TL intensity I has risen by no more than 15 percent of the maximum intensity of the glow peak I_M. The second term in equation Eq. 2.6.9 decrease with further increase in temperature $T > T_C$ and the competition between the two terms in this equation results in the peak shape of the TL glow curve.

Applying the assumption of constant $n(T)$, the intensity in the initial part of the glow curve may be expressed as,

$$I(T) \propto \exp\left(-\frac{E}{kT}\right). \tag{3.2.2}$$

Fig. 3.1 depicts the initial rise part of a single TL glow peak. In using this method, a graph of $\ln(I)$ versus $1/kT$ is made and a straight line of slope $-E$ is obtained. The activation energy E is evaluated from the slope of this line without any knowledge of the frequency factor s. Ilich [82] proposed a graphical approach as alternative

method and is shown in Fig. 3.2. By using a point I_C on the isolated TL glow peak and drawing the tangent at the point $N = (T_C, I_C)$, the slope can be calculated assuming that $I(T)$ is given by:

$$I(T) = C \ \exp\left(-\frac{E}{kT}\right). \tag{3.2.3}$$

Taking the derivative of Eq. 3.2.3, one obtains

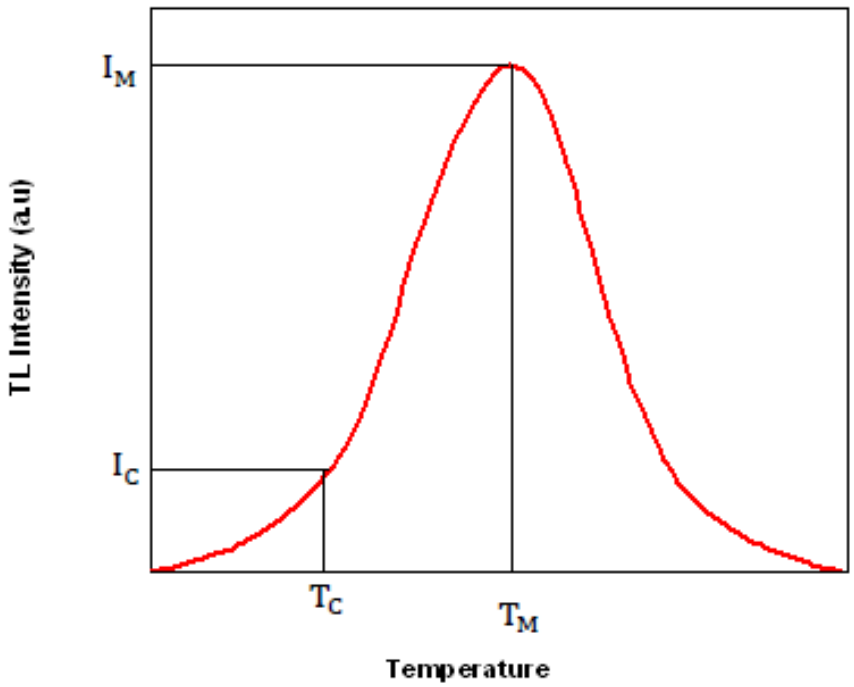

Figure 3.1: The initial rise part of TL glow curve.

$$\frac{dI}{dT} = C \ \frac{E}{kT^2} \ \exp\left(-\frac{E}{kT}\right) = I \ \frac{E}{k \ T^2}. \tag{3.2.4}$$

The slope of the tangent at point N is obtained by setting $T = T_C$. Eq. 3.2.4 then becomes,

$$\frac{dI}{dT} = I_C \ \frac{E}{k \ T_C^2}. \tag{3.2.5}$$

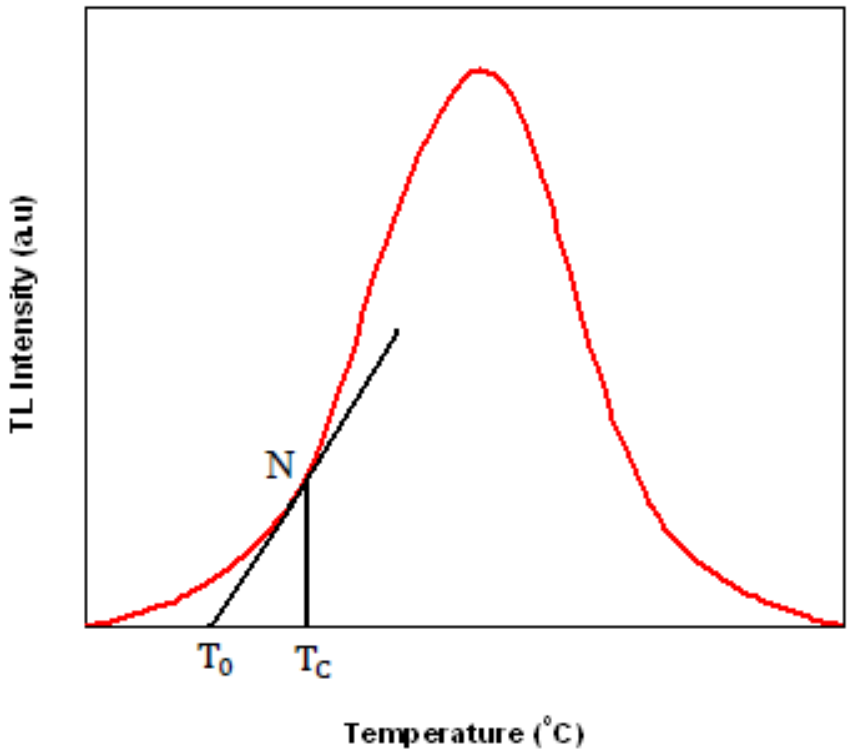

Figure 3.2: The graphical method proposed by Ilich.

In order to determine the point $M = (T_0, 0)$ where the graph intersects the X-axis, the following equation of the tangent line is used,

$$I - I_C = \frac{I_C\ E}{k\ T_C^2}(T - T_C). \tag{3.2.6}$$

Using $I = 0$, Eq. 3.2.6 becomes

$$E = k\ \frac{T_C^2}{T_C - T_0}. \tag{3.2.7}$$

Therefore, Eq. 3.2.7 gives the estimated value of the activation energy. In recent years, the initial rise method was extended to multiple trapping levels in thermoluminescent materials [83]. The quantity E_{eff} corresponding to an average value over the E_i values of each single sub-level is taken into consideration as a consequence, the trapping

parameter s, which is of course considered as an effective value, is calculated once E_{eff} is obtained. The following precautions should be made while using this method.

- The initial rise part of the glow peak under study should be free from any contribution from any nearby glow peaks, and
- There should be no lag in temperature between the heater plate and the sample and no temperature gradient across the sample thickness. This means that the sample layer should be very thin and it should be firmly deposited on the heater pan. Use of slow heating rate is desirable to avoid temperature lag between the heater pan and the sample.

Therefore, though this method can be applicable to any order of kinetics, it is not applicable if the resolution of the TL glow peak is poor due to the presence of nearby overlapping peaks.

3.2.3 The whole TL glow curve method

The methods described in the initial rise method utilize only the initial rising portion of a glow peak, thus the number of data points which may be used to calculate E is severely limited. This may be overcome by using not just one small section of the curve but the whole peak (the whole or 'total' glow peak method) and this enables E, s and the kinetic order b, to be calculated. Thus, this method is also known as 'area method' or 'whole glow peak' method of analysis, and is based on the measurement of the integral under a glow peak. It can be applied when a well isolated and clean peak is available. It is possible to estimate the value of the integral $n(T)$ of the TL intensity over a certain temperature region using the area under the glow curve

between a given temperature T_0 in the initial rise region, up to the final temperature T_F at the end of the glow peak, as shown in Fig. 3.3.

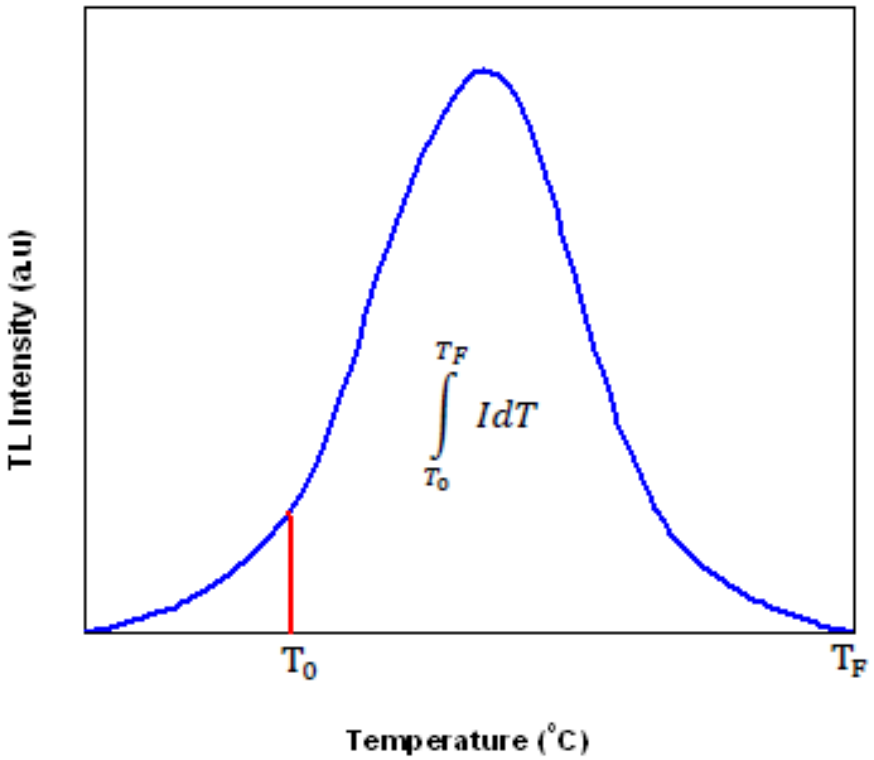

Figure 3.3: Calculation of the area $n(T)$ in the whole glow peak measurement method.

$$n = \int I \, dt = \frac{1}{\beta} \int I \, dT. \tag{3.2.8}$$

Assuming first order kinetics and substituting the Randall-Wilkins relation given in Eq. 2.6.7, the following relation can be obtained.

$$\ln\left(\frac{I}{\int I dT}\right) = \ln\left(\frac{s}{\beta}\right) - \frac{E}{kT}. \tag{3.2.9}$$

From Eq. 3.2.9, one can see that in the case of first order kinetics, the term $\ln[I/n(T)]$ is a linear function of E/kT with a slope $-E$ and an intercept equal to $\ln(s/\beta)$.

Different authors proposed the same method in the case of general order kinetics [84, 85]. However, in this case the equation is,

$$\ln\left(\frac{I}{n^b}\right) = \ln\left(\frac{s'}{\beta}\right) - \frac{E}{kT}, \tag{3.2.10}$$

which is graphically processed by plotting $\ln\left(I/n^b\right)$ versus $1/kT$. For the case when the order of kinetics b is known, one can obtain a broad range of temperatures in which the curve is a straight line. However, when the order of kinetics is unknown, several lines are drawn with various values of b and the best straight line is chosen.

3.2.4 Methods of analysis based on the various heating rates

Variable heating rate (VHR) is one of the most widely used technique for the analysis of TL glow curves. It considers the evolution of the TL maxima at different heating rates while all other parameters are held constant. When the heating rate increases, the position of the TL maximum T_M shifts toward higher temperatures (see Fig. 3.4) and the heating rate β can be related to the T_M of its corresponding peak using an equation of the following form [86, 87]:

$$\frac{\beta\ E}{kT_M^2} = s\ \exp\left(-\frac{E}{kT_M}\right), \tag{3.2.11}$$

where k is the Boltzmann constant (in units of eV/K) and E is the activation energy (in units of eV). This method requires several measurements of the glow peak with different β and first suggested by Hoogenstraaten [88]. Higher values of β or faster heating rates produce a shift in temperature relatively towards higher values of T_M as shown in Fig. 3.4. By means of the VHR method, E and s can be derived from the variation of $\ln\left(T_M^2/\beta\right)$ as a function of $1/kT_M$. When $\ln\left(T_M^2/\beta\right)$ is versus $1/kT_M$ is plotted, the resulting graph consists of a straight line of slope E and intercept

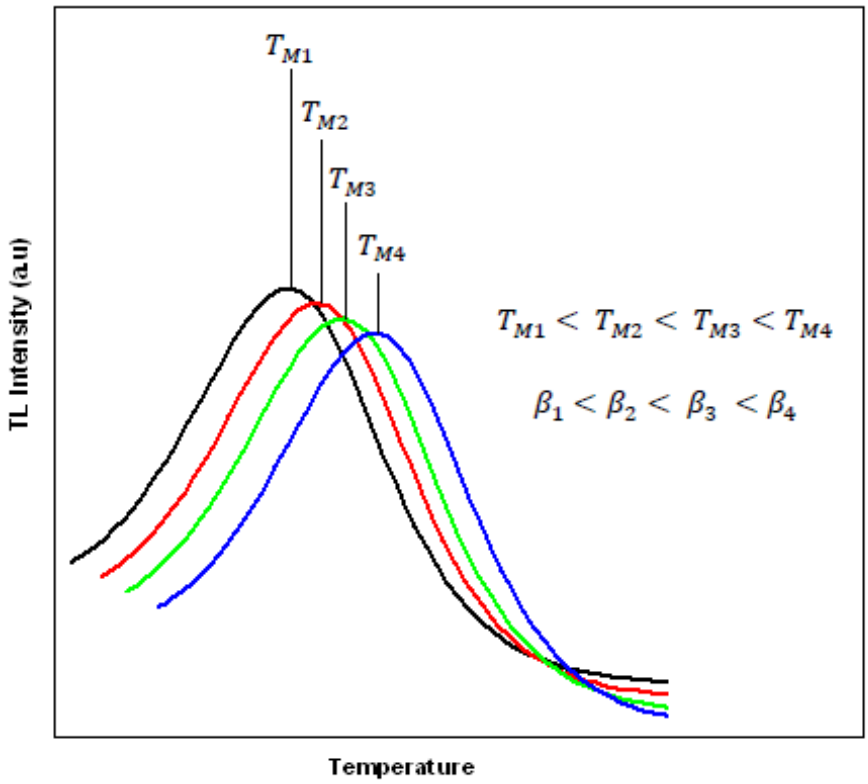

Figure 3.4: The change in temperature T_M of maximum intensity with heating rate.

$\ln(E/sk)$. Therefore, the values of the kinetic parameters E and s can be determined from the slope and intercept.

3.2.5 Method of analysis based on the shape of the glow curve

A popular method of analyzing glow curve in order to evaluate the TL kinetic parameters E, s and b is by considering the shape of the peak. This method essentially uses only three temperature points, namely T_M, T_1 and T_2; where T_M is the peak maximum temperature, T_1 and T_2, respectively, are the temperatures on the rising

and falling side of T_M corresponding to half intensity as shown in Fig. 3.5. This

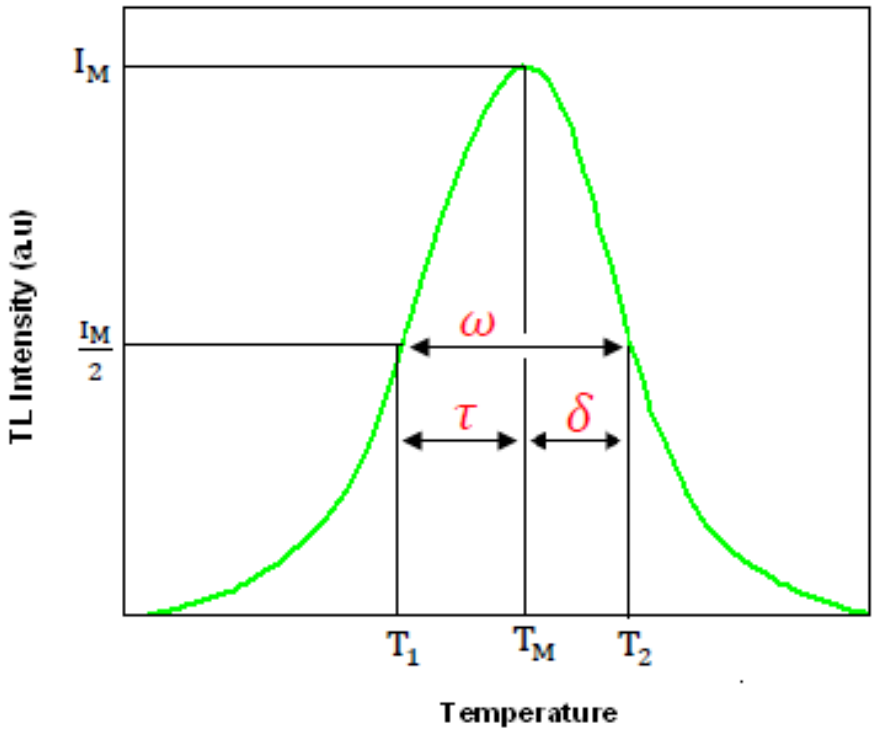

Figure 3.5: The geometrical shape parameters ω, τ and δ.

method was developed on the approximation that the glow peak may be described as consisting of two right angled triangles of same height. Order of kinetics depends on the shape factor of the glow peak μ which is in turn related to the temperatures T_M, T_1 and T_2 as follows [89]:

$$\mu = \frac{\delta}{\omega} = \frac{T_2 - T_M}{T_2 - T_1}, \tag{3.2.12}$$

where $\omega = T_2 - T_1$ is the half width of the full glow peak and $\delta = T_2 - T_M$ is the half width towards the fall off side of the glow peak and $\tau = T_M - T_1$ (see Fig. 3.5).

First order peak is characterized by $\mu = 0.42$ and a second-order peak by $\mu = 0.52$. For the general case in which kinetic order is not necessarily equal to 1 or 2, Chen [90]

investigated the correlation between μ and the three parameters, namely the activation energy, the pre-exponential factor and the kinetics order. Chen used the glow curve of general order kinetics for this study and found that μ is strongly dependent on the order of kinetics and practically independent of the activation energy and the frequency factor. The computations covered values of the kinetic order between 0.7 and 2.5, the activation energy between 0.1 and 1.6 eV, and the frequency factor between 10^5 and 10^{19} s^{-1}. The result is shown in Fig. 3.6 and it is used to find the value of the order of kinetics from the measured value of μ in an experimentally measured glow peak.

In Fig. 3.5, $\tau = T_M - T_1$ is the half width at the low temperature side of the peak. In other words, δ and τ are the widths of the two right angled triangles. Another geometrical factor γ is defined as δ/τ. The activation energy is evaluated from Chen's equations for general order kinetics [90, 91]. That is,

$$E_\alpha = c_\alpha \left(\frac{kT_M^2}{\alpha}\right) - b_\alpha \, (2kT_M), \tag{3.2.13}$$

where α represents ω, τ or δ.

$$c_\tau = 1.510 + 3.0 \, (\mu - 0.42), \tag{3.2.14}$$

$$c_\delta = 0.976 + 7.3 \, (\mu - 0.42), \tag{3.2.15}$$

$$c_\omega = 2.52 + 10.2 \, (\mu - 0.42), \tag{3.2.16}$$

$$b_\tau = 1.58 + 4.2 \, (\mu - 0.42), \tag{3.2.17}$$

$$b_\delta = 0, \quad b_\omega = 1. \tag{3.2.18}$$

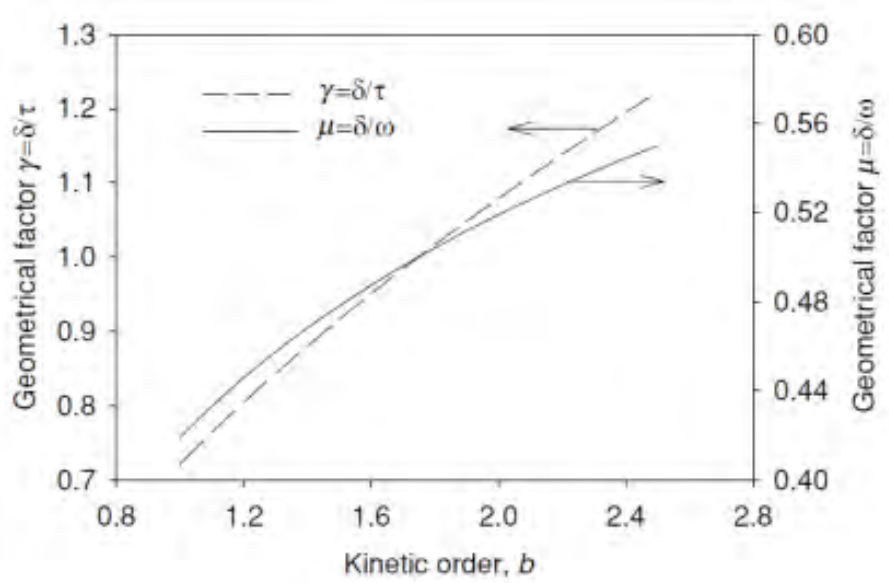

Figure 3.6: The relation between kinetic order b and geometrical shape factors μ and γ [28].

The possible source of error in this method is that it is an approximate method in the sense that the value of the peak shape factor μ is not totally independent of the E and s values. The purity of the glow peak is an essential requirement for the accuracy of the results. In addition, correct measurement of T_M, T_1 and T_2 is essential to get the values ω, τ and δ. Moreover, it is important to note that before applying the peak shape method, one should test the glow peak for shift in T_M with change in dose. In case there is no consistent shift, as stated earlier, one should assume the glow peaks to belong to the first order kinetics.

3.2.6 Isothermal decay method

The methods of TL analysis discussed above deals with determination of the TL kinetic parameters from the form, or shape, or position of the glow peak which itself is produced during a non-isothermal rise in sample temperature. However, in isothermal decay analysis, the sample temperature is kept constant and the luminescence intensity is followed as a function of time. In other words, this is a method of analysis that does not employ any particular heating cycle. This method of analysis, therefore, deals with phosphorescence rather than TL, but by raising the temperature, at which the phosphorescence decay is being monitored, the deep traps which take part in TL can be sampled and their trap depths determined. The common experimental procedure in an isothermal decay experiment consists of quickly heating the sample after irradiation to a specific temperature, and keeping the sample at this temperature for a given time interval. The light output known as phosphorescence decay is measured as a function of time. Therefore, it is possible to evaluate the decay rate of trapped electrons. Graphs of the TL intensity versus time t at constant temperature are called isothermal decay curves.

Garlick and Gibson [92] illustrated the method of isothermal decay analysis for first order kinetics. The isothermal decay curves at a temperature T_i for TL peaks following first-order kinetics are exponential graphs as a function of time, and is given by

$$I = I_0 \ \exp\left[-s \ \exp\left(-\frac{E}{kT_i}\right) t\right]. \tag{3.2.19}$$

Eq. 3.2.19 shows that a graph of $\ln(I)$ versus time is linear for first order kinetics

peaks, and that the slope of the line is expressed as,

$$m_i = -s \ \exp\left(-\frac{E}{kT_i}\right). \tag{3.2.20}$$

Taking the natural logarithm of Eq. 3.2.20, the following relation is obtain,

$$\ln\left(|slope|\right) = \ln(s) - \frac{E}{kT_i}. \tag{3.2.21}$$

The plot of the $\ln\left(|slope|\right)$ versus $1/kT$ should be a straight line with $slope = -E$ and a Y-intercept equal to $\ln(s)$. If two different constant temperatures, T_1 and T_2, are used during the experiment, two different slopes m_1 and m_2 are obtained and Eq. 3.2.21 gives

$$\ln\left(\frac{m_1}{m_2}\right) = \frac{E}{k}\left(\frac{1}{T_2} - \frac{1}{T_1}\right). \tag{3.2.22}$$

The activation energy E can be calculated using Eq. 3.2.22. Moreover, the application of isothermal decay analysis for general order kinetics has been suggested in [93, 94] and the order of kinetics b can possibly be evaluated. Using the assumption of constant temperature and integrating the general-order expression given in Eq. 2.6.14 with respect to time t, one obtains,

$$I(t) = I_0 \ \left[1 + s' \ n_0^{b-1} \ (b-1) \ t \ \exp\left(-\frac{E}{kT}\right)\right]^{\frac{b}{1-b}}, \tag{3.2.23}$$

where $I_0 = s' \ n_0^b \ \exp\left(-\frac{E}{kT}\right)$. I_0 and n_0, respectively, the initial TL intensity and the initial concentration of trapped charges, $I(t)$ is the TL intensity at time t, T is the temperature of the isothermal decay and $s' = s/N$ is the effective frequency factor. Eq. 3.2.23 can also be expressed as,

$$\left(\frac{I(t)}{I_0}\right)^{\frac{1-b}{b}} = \left[1 + s' \ n_0^{b-1} \ (b-1) \ t \ \exp\left(-\frac{E}{kT}\right)\right]. \tag{3.2.24}$$

From Eq. 3.2.24, it can be seen that a plot of the quantity $\left(I(t)/I_0\right)^{\frac{1-b}{b}}$ versus time should be a straight line when a suitable value of b is found. Further use of different

isothermal decay temperatures results in the determination of a set of straight lines with slopes given by,

$$m = s' \; n_0^{b-1} \; (b-1) \; t \; \exp\left(-\frac{E}{kT}\right). \tag{3.2.25}$$

Determination of the activation energy E and the effective frequency factor $s'' = s' n_0^{b-1}$ then follows from the slope and intercept of the plot of $\ln(m)$ versus $1/kT$. The limitation of using isothermal decay data is that it may be difficult to obtain an exact estimate of the best linear fit, since small differences may occur between the graphs for various values of b.

3.2.7 Curve fitting method

The curve fitting technique is also capable of analyzing the glow peaks of a real sample. The popularity of the curve fitting technique has stemmed from the advancements in computational techniques, in which large number of numerical data points may be handled. The basic approach for glow curve fitting involves choosing the appropriate equation to fit the data. For example, one may choose the Randall-Wilkins (RW) equation of the glow peaks (Eq. 2.6.9). This would implicitly mean that all the glow peaks in the multi-peak glow curve belong to first order kinetics ($b = 1$). One may then carry out a three parameter fit namely using E, s, and n_0 as fitting parameters. However, in most cases, the glow curve fitting is carried out using the general order kinetics equation of the glow peak (see Eq. 2.6.15).

3.3 General Precautions in Glow Curve Analysis

One of the most important procedures in glow curve recording is accurate measurement of temperature. If the sample is in the form of fine powder it should be firmly deposited on the heater plate for uniform heating. The sample may be in the form of thin polished plate of approximately 0.5 mm or less thickness. If the sample is in the form of fine powder one may use small amount of the powder which may be uniformly spread on the heater plate over about 1 cm^2 area uniformly. In addition, the glow peaks to be analyzed should be free from any satellites associated with the glow peak under study. For this purpose, satellites on the lower temperature side may be removed by preheating the sample to a selected temperature. This phenomenon is called thermal cleaning.

3.4 Characterization Techniques

3.4.1 X-ray diffraction (XRD)

X-ray diffraction (XRD) is an efficient analytical nondestructive technique which is used for many purposes such as investigation of structural properties of crystalline materials, phase identification, determination of crystallite size, evaluation of lattice constants, and determination of degree of crystallinity in a mixture of amorphous and crystalline substances [95]. The basic components of x-ray diffractometer are x-ray tube, a sample holder and an x-ray detector [96]. X-rays are produced in the x-ray tube and it consists of an evacuated chamber with a tungsten filament at one end of the tube, called the cathode, and a metal target at the other end, called an anode. The electrons are driven to the anode (target) due to the large voltage difference

maintained across these electrons (usually tens of thousands of volts). Thus, x-rays are produced at the point of impact and radiate in all directions. Fluorescent screens are widely used today in x-ray diffraction work for detection of x-rays. A fluorescing crystal may also be used in conjunction with a phototube; the combination, called a scintillation counter, is a very sensitive detector of x-rays [96]. A schematic diagram of x-ray diffraction is shown in Fig. 3.7. The x-ray tube acts as the source of x-rays and the detector counts the number of x-rays scattered by the sample. Moreover, the incident angle θ is always 1/2 of the detector angle 2θ.

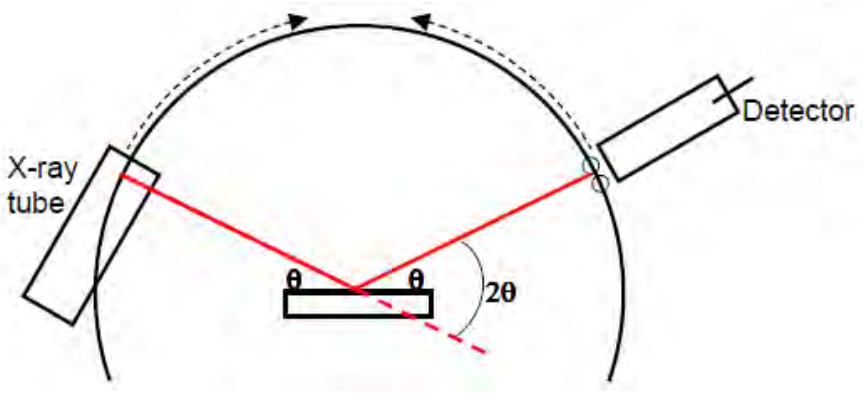

Figure 3.7: Schematic diagram of x-ray diffraction. The incident angle, θ, is defined between the x-ray source and the sample. The diffracted angle, 2θ, is defined between the incident beam and the detector angle.

Bragg's law

Bragg's law is the basis of XRD analysis. Consider a beam of monochromatic x-rays entering a crystal with one of its planes oriented at an angle θ to the incoming beam as shown in Fig. 3.8. When ray 1 reflects off the upper atomic plane at an angle θ, ray 2 is still in the crystal. At the time of exit of ray 2 from the crystal, it travels a distance of 2 d $sin\theta$ further than ray 1. If this distance is equal to an integral

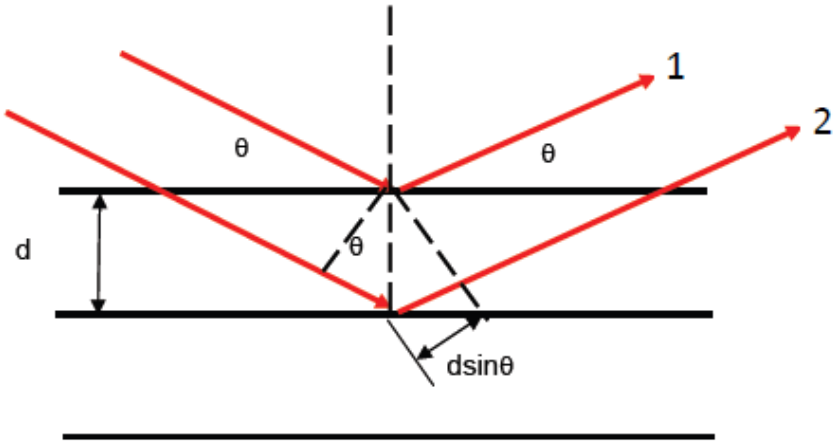

Figure 3.8: Two incident x-rays entering a crystal with interplanar spacing d.

number of wavelengths ($n\lambda$), then rays 1 and 2 will be in phase on their exit from the crystal and constructive interference will occur. However, if the distance 2 d $sin\theta$ is not an integral multiple of wavelengths, then destructive interference will occur and the waves will not be as strong as when they entered the crystal. Thus, the condition for the constructive interference to occur is

$$n\ \lambda = 2\ d\ \sin\theta. \tag{3.4.1}$$

This is known as Bragg's law for x-ray diffraction [97]. Thus, if we know the wavelength λ of the x-rays going in to the crystal and we can measure the angle θ of the diffracted x-rays coming out of the crystal, the d-spacing between the atomic planes is given by;

$$d = \frac{n\ \lambda}{2\ \sin\theta}. \tag{3.4.2}$$

In this study, Bruker D8 x-ray advance diffractometer operating at 40 kV and 40 mA using $Cu\ K_\alpha = 0.15406$ nm is used for structural analysis of the samples.

3.4.2 Photoluminescence spectroscopy (PL)

As discussed in detail in chapter 2, photoluminescence is luminescence by which electromagnetic radiation i.e., photons are used to excite a material. When light is directed onto the sample and gets absorbed, it imparts excess energy into the material causing excitation or creation of electron-hole pairs. This excess energy can be released by the sample through the emissions of light as the system relaxes to its ground state [98], a process called photoluminescence. Photoluminescence spectroscopy is a contactless, nondestructive method of probing the electronic structure of materials. In PL, the emission properties of materials are measured by using photons to induce

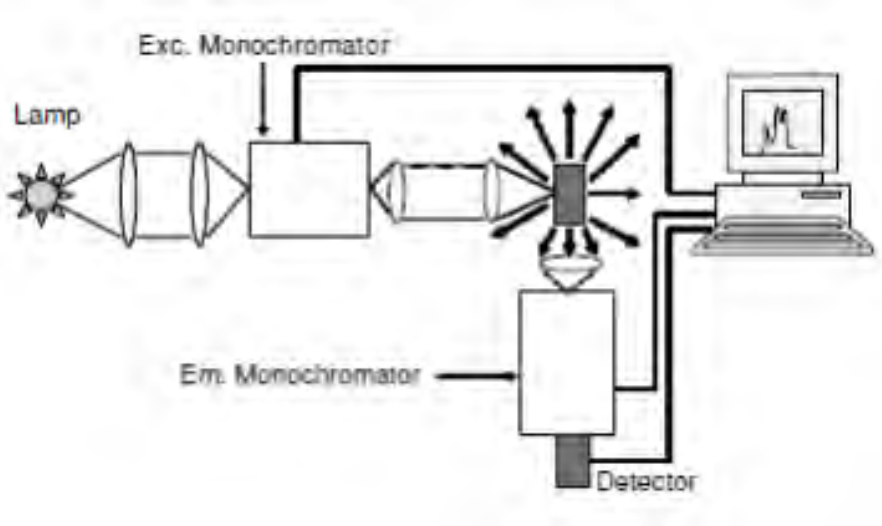

Figure 3.9: A schematic diagram showing the main elements for measuring PL spectra [99].

excited electronic states in the material system and analyzing the optical emission as these states relax. A typical experimental arrangement to measure PL spectra is shown in Fig. 3.9. The sample is excited by light, which is followed by a monochromator (the excitation monochromator) or a laser beam. A focusing lens is used to

collect the emitted light while a second monochromator (the emission monochromator) analyzes it. A suitable detector is also connected to a computer for displaying the PL excitation or emission spectra. Therefore, two kinds of spectra (the excitation and emission spectra) can be registered. In excitation spectra, the emission wavelength is fixed at any emission wavelength while the excitation wavelength is scanned in a certain spectral range. In emission spectra, the excitation wavelength is fixed and the emitted light intensity is measured at different wavelengths by scanning the emission wavelength [99]. Sensitivity is one of the strengths of PL technique, allowing very small quantities or low concentrations of material to be analyzed [99].

In this study, the excitation and emission spectra were measured at room temperature using a Cary Eclipse fluorescence spectrophotometer model: LS-55 with a built-in 150 W Xenon flash lamp.

3.4.3 Ultra-violet visible (UV-VIS) spectroscopy

Ultraviolet-visible (UV-VIS) spectroscopy or ultraviolet-visible spectrophotometry refers to absorption spectroscopy (A) or reflectance spectroscopy (R) in the ultraviolet-visible spectral region. It can also measure the amount of light transmitted (T) through the sample. In the UV-VIS spectrum, an absorbance versus wavelength graph measures transitions from the ground state to excited state, while photoluminescence deals with transitions from the excited state to the ground state. An excitation spectrum is a graph of emission intensity versus excitation wavelength. An excitation spectrum looks very much like an absorption spectrum. The greater the absorbance is at the excitation wavelength, the more molecules are promoted to the excited state and the more emission will be observed. By running a UV-VIS

absorption spectrum, the wavelength at which the molecule absorbs energy most and is excited to a large extent can be obtained.

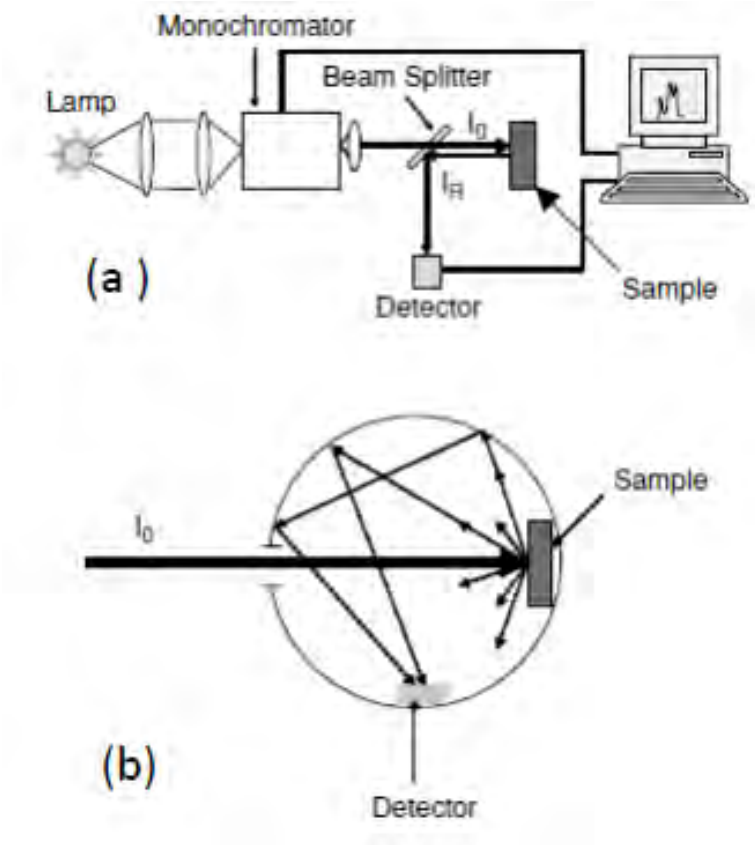

Figure 3.10: (a) An experimental arrangement used to measure direct reflectance spectra, (b) A schematic drawing of an integrating sphere for measuring diffuse reflectance spectra. As indicated in (a), I_0 is the incident intensity minus the reflection losses I_R at the surface [99].

Absorption and reflectance measurements both give complimentary information. Reflectance can be registered in two different modes: (i) direct or (ii) indirect. Direct reflectance measurements are made with well polished samples at normal incidence while diffuse reflectance is generally used for unpolished or powdered samples. For direct refelectance measurements (Fig. 3.10a), monochromatic light is passed through

a semitransparent lamina (the beam splitter in the Figure). This lamina deviates the light reflected in the sample toward a detector. For diffuse refelectance measurements (Fig. 3.10b), an integrating sphere (a sphere with a fully reflective inner surface) is used. Such a sphere has a pinhole through which the light enters and transmitted toward the sample.

The diffuse reflected light reaches the detector after suffering multiple reflections in the inner surface of the sphere. The integrating spheres can be incoprporated as additional instrumentation into conventional spectrophotometers. In this work, a Perkin Elmer Scan-Lambda 950 UV-VIS spectrophotometer ($LAMBDA^{TM}$ 950) was used to record the reflectance characteristics of samples.

3.4.4 Thermoluminescence (TL) spectroscopy

When a phosphor is excited with some external source of radiation and then heated, an increase after glow called thermally stimulated luminescence (TSL) is recorded because of the recombination of electrons detrapped from deep traps within the phosphor. This emission is also called TL and the temperature dependence of the TL intensity is called glow curve. The measurement of glow curve of a sample proceeds as follows.

- The sample is cooled to a low temperature (or at least room temperature). Liquid nitrogen is often used as coolant.
- The sample is excited by UV light (or other sources of excitation) until the traps are populated with electrons or holes.
- The excitation is terminated and the temperature of the sample is raised at a

constant rate while the intensity is recorded.

The TSL glow curves in this study were obtained by TL reader type TL1009I offered by Nucleonix systems Pvt. Ltd., India interfaced to a PC where the TL signals were analyzed. It is a versatile controller based unit facilitating the user to subject the TL sample under study to the desired heating profile, to record the digitized glow curve. A complete electronics hardware circuits (comprising of power electronics, low/high voltage supplies, temperature controller, micro controller based data acquisition circuits, sample heating system, drawer assembly, etc.) are enclosed in a single enclosure [98]. The system also contains some of the software features like glow curve acquisition, analysis, filing, printing, plotting, overlapping, maker data reporting, etc. This integral TL reader unit gets connected to the personal computer system through USB port.

Fig. 3.11 illustrates a schematic diagram of a typical TL experiment. The sample is mounted on a coldfinger that is made of copper because of its good conductivity. It is equipped with a high power heater to rapidly rise the sample temperature during the heating stage. It is also placed in a cryostat and is under vacuum. The Xenon lamp is used as radiation source, filtered by the monochromator. During the heating of sample at a constant heating rate, the thermoluminescence is recorded by a light sensitive detector. The photomultiplier tube is used to detect the light. The photomultiplier is connected to a photo-counting system that records the thermoluminescence signal as a function of sample temperature [100].

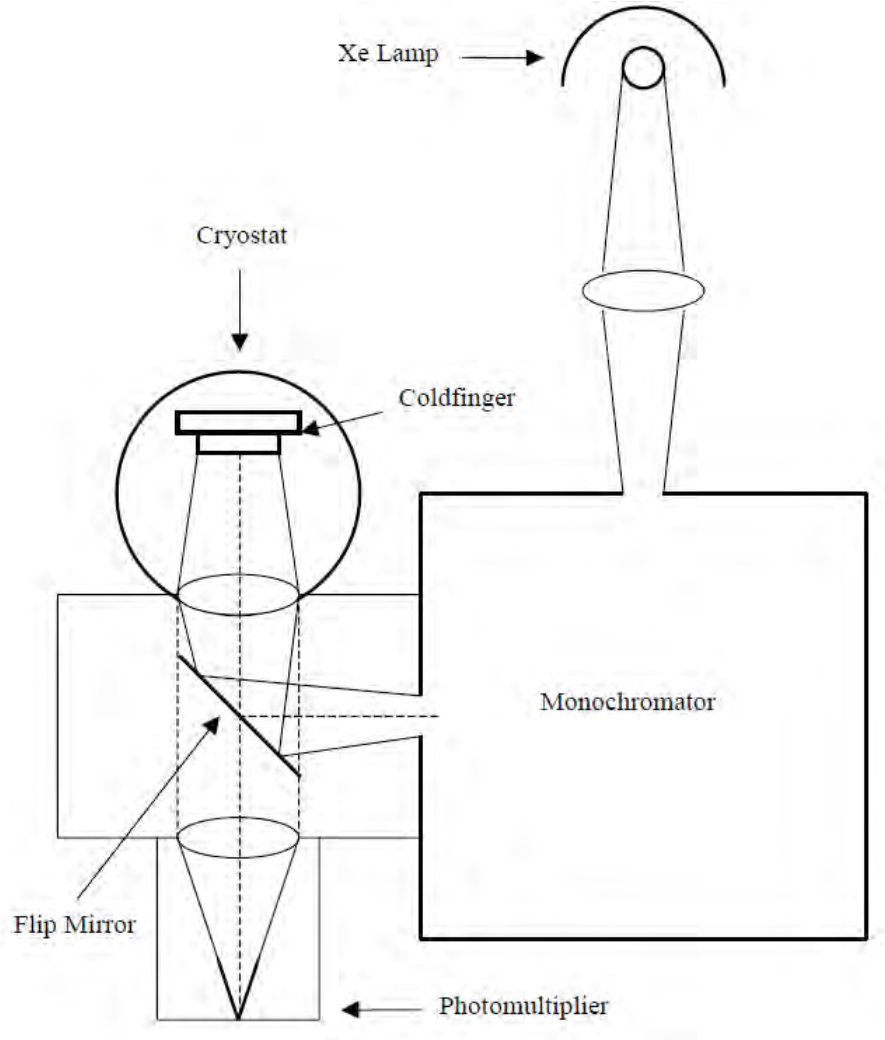

Figure 3.11: A schematic diagram of typical TL experiment [100].

Chapter 4

Thermoluminescence from Silicon Quantum Dots in Two Traps-One Recombination Center Model

4.1 Introduction

The light emission from silicon quantum dots is an active research area because of its potential applications in the silicon-based optoelectronic devices [1, 28, 101, 102]. The efficiency of the silicon light emitting devices can be increased with the help of different mechanisms. In particular, the possible increase in the intensity of TL from quantum dots caused by the confinement has been studied in [103]. It was shown that the confinement increases the probability of radiative recombination and enhances the intensity of the TL. A quantum confined structure is one in which the motion of the carriers (electron and hole) are confined in one or more directions by

potential barriers. In quantum dots (QDs), the charge carriers are confined in all three dimensions and the spatial extent of the electronic wave function is comparable with the particle size. It was shown that the confinement increases the probability of radiative recombination and enhances the intensity of the TL. The efficiency of TL from silicon quantum dots is enhanced because of two main reasons [103]. Firstly, the quantum confinement effect causes an increase of surface states (because of the high surface to volume ratio); so that the particles may provide more accessible carriers (holes and electrons) for the TL recombination. Secondly, in nano-particles the wave functions of electron and hole are overlapped effectively, which results in the increase of their radiative recombination probability (A_r). Electrons and holes created during the irradiation of a semiconductor will be trapped in some metastable states if they do not recombine rapidly and they need an energy which is equal to the trap depth to be released back to the conduction band to give luminescence. This energy is also called activation energy. If the detrapping process is caused by heating or thermostimulation, the luminescence is called thermoluminescence (TL) [104, 105, 106, 107, 108].

Traps and trapped carriers in nanoparticles are abundant and luminescence might be improved if the trapped carriers are effectively released from the traps by stimulation with energy equal to the trap depth. TL is a good way to detect the recombination emission caused by detrapping of carriers thermally [108]. TL continues to be an active area of research because of its immense contribution in the fields of personal and environmental dosimetry, dating of archeological artifacts, sediments and study of defects in solids [104]. In particular, light emission from silicon quantum dots has

got recent attention because of its potential applications in the silicon-based optoelectronic devices [109, 110]. There are different mechanisms of increasing the efficiency of the light emitting device. In experiments, the possible increase in the intensity of TL from nanoparticles due to the confinement effect and increase in the surface states have been studied [107]. It was shown that both increase the probability of radiative recombination and enhances the intensity of the TL.

The TL from different materials has been studied by many research groups using different models. The OTOR model was discussed in detail by Randall and Wilkins as seen in section 2.8.1. In this model, the peak of the TL intensity corresponding to each peak depends on the level of the trap beneath the edge of the conduction band; the shallower the trap, the higher the intensity peak. In other words, retrapping has no effect on the intensity peaks. The rate equation governing the TL process and the intensity of the TL in OTOR model are given by Eqs.2.6.6 and 2.6.9, respectively.

The interactive-multi-trap-system (IMTS) model has also been reported in literature [28]. This model assumes; one active electron trap (TR), one thermally disconnected deep trap (TDDT) that cannot be thermally activated, and one recombination center as shown in Fig. 4.1. In IMTS model, though there is an effect of retrapping to the thermally disconnected deep trap, its effect on TL peaks is not clearly observed as there is only one active electron trap taking part in the TL process. Basically, in reality we often have more than one active electron traps taking part in TL process and the intensity peaks completely depends on the retrapping condition in this case. The kinetic equations for this model are

$$\frac{dn}{dt} = -s\ n\ \exp\left(-\frac{E}{kT}\right) + n_c\ A\ (N-n), \tag{4.1.1}$$

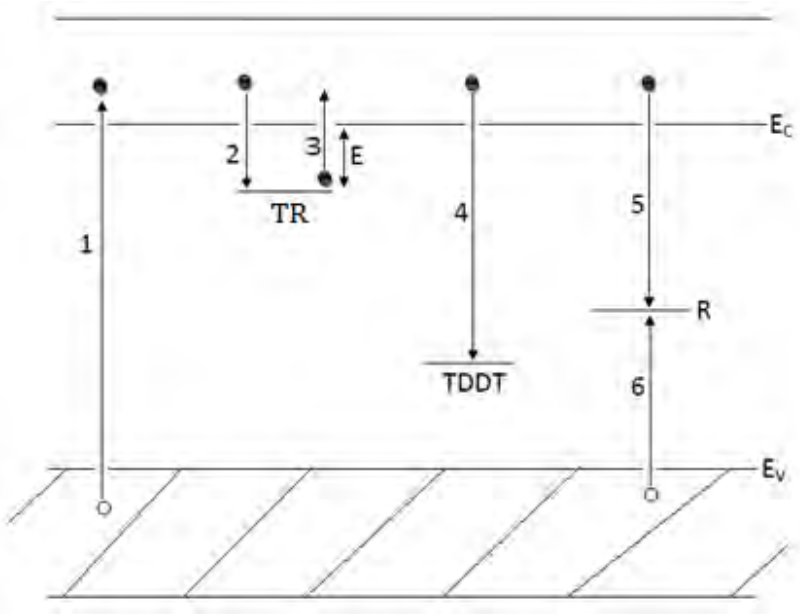

Figure 4.1: IMTS model for TL. Allowed transitions: (1) ionization; (2), 4, (6), trapping; (3) thermal release (detrapping); (5) radiative recombination and emission of light.

$$\frac{dm}{dt} = n_c \; A_m \; (M - m), \tag{4.1.2}$$

$$\frac{dn_c}{dt} = s \; n \; \exp\left(-\frac{E}{kT}\right) - n_c \; A \; (N - n) - n_c \; A_m \; (M - m), \tag{4.1.3}$$

where n is the instantaneous concentration of electrons in the active trap (cm^{-3}), s is the frequency factor (s^{-1}), E is the activation energy of the active trap (eV), k is the Boltzmann constant (JK^{-1}), n_c is the instantaneous concentration of electrons in the conduction band (cm^{-3}), A is the probability coefficient of electron retrapping to the active trap ($cm^3 \; s^{-1}$), N is the total concentration of traps in the active trap (cm^{-3}), m is the instantaneous concentration of electrons in the TDDT (cm^{-3}), A_m is the probability coefficient of electron retrapping to the TDDT ($cm^3 \; s^{-1}$)), and M

is the total concentration of traps in the TDDT (cm^{-3}). Moreover, because of the conservation of charge in the crystal, the concentration of holes in the recombination center at any moment must be equal to the total instantaneous concentration of electrons $n + m + n_c$.

Though OTOR and TDDT models are extensively studied, there is still gap in considering more number of traps which is a condition existing in real experimental situation. Therefore, considering a model dealing with more number of traps is important. Let us consider small Si quantum dots of different size with size dependent radiative recombination rate and study the effect of retrapping on TL intensity peaks corresponding to each trap for second order and a case beyond second order kinetics assuming two active electron traps and one recombination center model. In addition, we study the variation of concentration of electrons in each trap and the intensity of the TL.

4.2 Statement of the Problem

Let us consider an energy band scheme having three localized levels as shown in Fig. 4.2. The two levels act as traps (TR_1 and TR_2) and the other acts as recombination center (R). The absorption of radiation of energy greater than the band gap energy results in the ionization of valence electrons, producing free electrons in the conduction band and free holes in the valence band respectively (transition 1).

The electrons and holes may either recombine with each other or become trapped at the trap centers. In order for recombination to occur holes first become trapped at centers (R) (transition 7). Recombination takes place via the annihilation of the

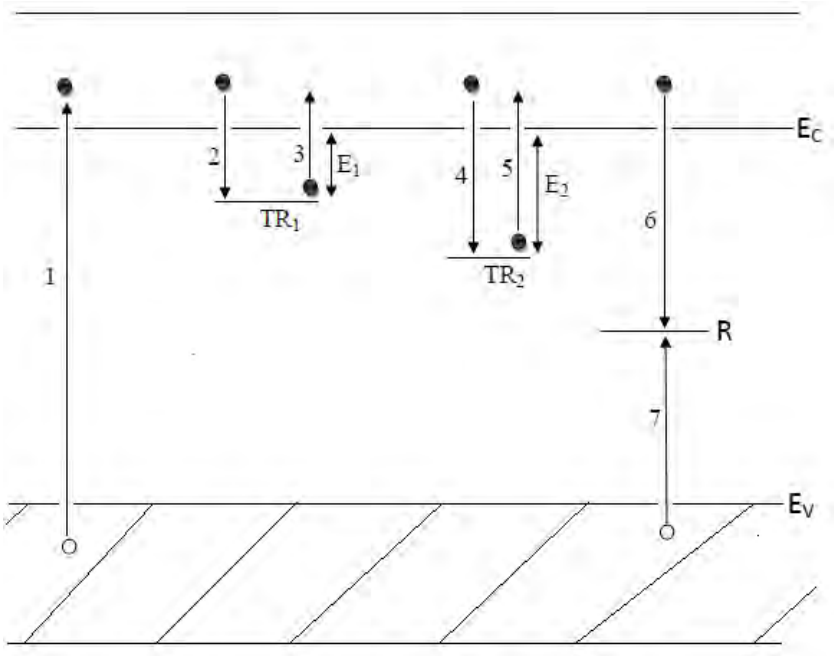

Figure 4.2: Three level model for thermoluminescence. Allowed transitions: (1) ionization; (2), (4) and (7) trapping; (3) and (5) thermal release; (6) radiative recombination and emission of light.

trapped holes by free electrons (transition 6). If the recombination transition is assumed to be radiative, then luminescence will result. The free electrons may also become trapped at levels TR_1 and TR_2 (transitions 2 and 4) in which case recombination can only take place if the trapped electrons absorb enough energy E_1 and E_2, respectively, to be released back to conduction band (transitions 3 and 5), from where recombination is possible. In other words, the TL occurs when the trapped electrons absorb enough energy in the form of heat to be released back to the conduction band from where there is possible recombination of electrons and holes. The energy required for the trapped electrons to be released back to the conduction band is called the trap depth (activation energy). Now let us write down the rate equations governing the TL process.

4.3 Electron Rate Equations

Let us consider two active electron traps with energy levels E_1 and E_2 below the bottom of the conduction band. The electron rate equations can be written as:

$$\frac{dn_1}{dt} = -s_1\ n_1\ \exp\left\{-\frac{E_1}{kT}\right\} + n_c\ A_1\ (N_1 - n_1), \tag{4.3.1}$$

$$\frac{dn_2}{dt} = -s_2\ n_2\ \exp\left\{-\frac{E_2}{kT}\right\} + n_c\ A_2\ (N_2 - n_2), \tag{4.3.2}$$

$$\frac{dn_c}{dt} = s_1\ n_1\ \exp\left\{-\frac{E_1}{kT}\right\} + s_2\ n_2\ \exp\left\{-\frac{E_2}{kT}\right\} -$$

$$n_c\ \left[A_1\ (N_1 - n_1) + A_2\ (N_2 - n_2) + A_r\ n_h\right]. \tag{4.3.3}$$

Here, n_i $(i = 1, 2)$ is the concentration of trapped electrons on the levels E_i, N_i $(i = 1, 2)$ is the total concentration of traps on the levels E_i, k is the Boltzmann constant; s_i and A_i are the probability of electron to escape from the i^{th} trap and the re-trapping probability on the i^{th} energy level; n_c and n_h, respectively, are the concentration of the electrons in the conduction band and holes in the hole trap, and A_r is the electron-hole radiative recombination probability. It is assumed that, initially, all holes are trapped to the hole trap. Eqs. 4.3.1 to 4.3.3 are closed by the quasi-neutrality condition

$$n_1(t) + n_2(t) + n_c(t) = n_h(t). \tag{4.3.4}$$

Basically the temperature of the system depends on time $T = T(t)$. This dependence is controlled by the conditions of experiment. The generally acceptable is the linear heating rate

$$T(t) = T_0 + \beta\ t, \tag{4.3.5}$$

where β is the heating rate. The system of Eqs. 4.3.1 to 4.3.3 presents the rate equations governing the process of TL. The intensity of the TL is given by

$$I(T) = A_r \; n_h(T) \; n_c(T). \tag{4.3.6}$$

The above presented system of equations is nonlinear with varying coefficients. It cannot be solved analytically in general case. Let us consider two generally accepted approaches of studying the kinetics of the TL.

4.4 First Order Kinetics

The simplest approach, which allows one to solve our system of equations analytically, is called the first order kinetics. It assumes that the retrapping of electrons is negligible. In this case the solutions of Eqs. 4.3.1 and 4.3.2 with account of Eqs. 4.3.5 can be written as

$$n_i(T) = n_{i0} \; \exp\left[-\frac{s}{\beta}\int \exp\left(-\frac{E_i}{kT}\right) dT\right], \tag{4.4.1}$$

where n_{i0} $(i = 1, 2)$ are the initial concentration of electrons in the traps. It is generally accepted that the density number of electrons in the conduction band $n_c(t)$ is slowly varying function of time and practically is a constant on the typical times of the TL

$$\frac{dn_c}{dt} \approx 0. \tag{4.4.2}$$

Using Eqs. 4.3.3, 4.3.5, 4.4.1, and 4.4.2, we obtain the intensity of the TL from each trap in the first order kinetics.

$$I(T) = n_{i0} \; s_i \; \exp\left(-\frac{E_i}{kT}\right) \exp\left[-\frac{s}{\beta}\int \exp\left(-\frac{E_i}{kT}\right) dT\right], \tag{4.4.3}$$

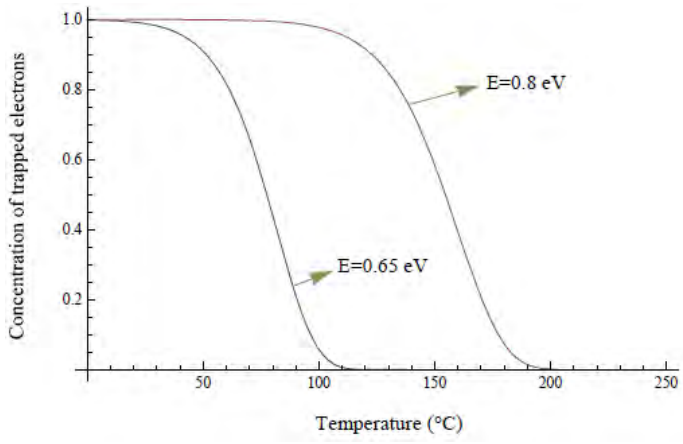

Figure 4.3: The normalized concentration of electrons $n_1(T)$ and $n_2(T)$ in the first trap ($E_1 = 0.65\ eV$) and second one ($E_2 = 0.8\ eV$) versus the temperature T (in ^0C) for first order kinetics with the following values of parameters: $n_1(0) = n_2(0) = 10^{15}\ cm^{-3},\ \beta = 1\ ^0C/s,\ s_1 = s_2 = 10^8\ s^{-1}$.

where $(i = 1, 2)$. The graphs depicting the concentration of electrons on the traps $n_1,\ n_2$ and the intensity of TL versus the temperature T for the typical parameters of the TL systems are presented in Figs. 4.3 and 4.4, respectively. Fig. 4.3 depicts that the first trap ($E_1 = 0.65\ eV$) is activated at $T_1 \approx 40\ ^0C$ and the second one ($E_2 = 0.8\ eV$) at $T_2 \approx 100\ ^0C$. Fig. 4.4 shows the two maxima of the intensity of TL in arbitrary units at the temperatures corresponding to the thermal activation of the traps. The maximum of intensity of TL from the first trap is higher than that from the second trap because $E_1 < E_2$. To take into account the effects of electron retrapping one has to use more general approach that is called general order kinetics.

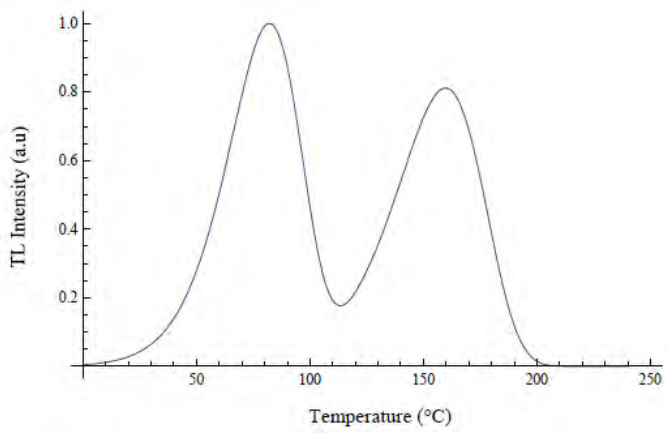

Figure 4.4: The intensity of TL in arbitrary units versus temperature T for first order kinetics with the same parameters as in Fig. 4.3.

4.5 Second Order and a Case Beyond Second Order Kinetics

In this model, the retrapping terms with the coefficients A_1 and A_2 are taken into account. It considerably complicates the system of Eqs. 4.3.1 to 4.3.3 that becomes nonlinear and cannot be solved analytically in general case. We solved this system of equations numerically with the help of Mathematica 8 with the same parameters as have been used in the previous section. But now it is necessary to specify the additional parameters: the retrapping probabilities A_1, A_2, and the electron-hole radiative recombination probability, A_r. The latter one depends on the size of quantum dot. It is clear that the confinement must increase the radiative recombination probability [107].

For the typical quantum dots the retrapping probability is of the order of $10^7\ cm^3\ s^{-1}$. We chose $A_1 = A_2 = 5 \times 10^7\ cm^3\ s^{-1}$ and ignore the possible corrections associated with the confinement. The coefficient A_r depends on the size of quantum dot. The

D in nm	A_r in $cm^3\ s^{-1}$
2	2×10^7
4	3×10^6
6	4×10^5
8	5×10^4

Table 4.1: Approximate size dependence of radiative recombination rate A_r of the quantum dots [103]. D is the diameter of the dots.

graph of experimental data on the size dependence of A_r for silicon quantum dots of diameter (D) 2-8 nm is given in [103] and we summarized them in Table 4.1. It illustrates the rate of the radiative recombination as a function of quantum dot size for our model. Figs. 4.5 and 4.6 show the variation of the concentration of electrons in the traps with activation energies $E_1 = 0.65\ eV$ and $E_2 = 0.8\ eV$, respectively, for quantum dots of different diameters D from 2 to 8 nm for general order kinetics. The

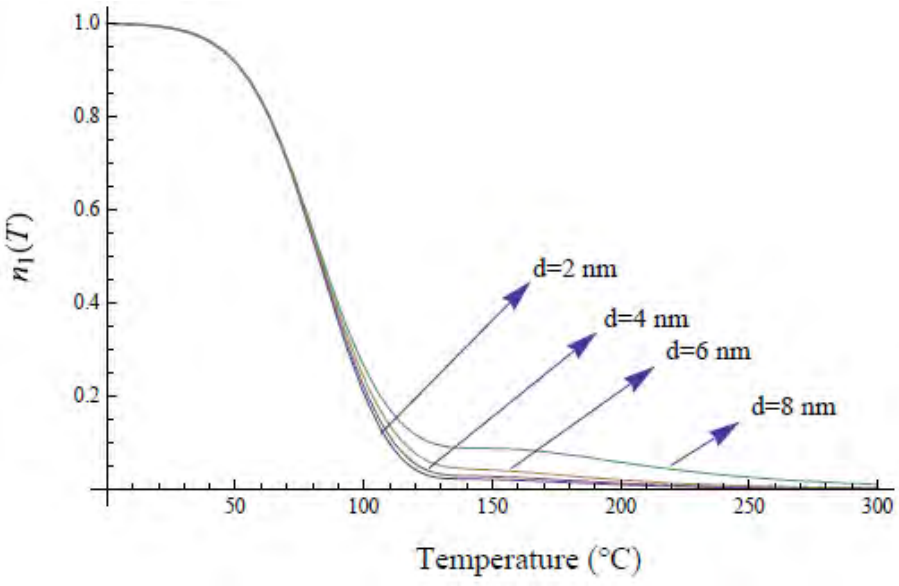

Figure 4.5: Variation of concentration of electrons $n_1(T)$ in the shallower trap ($E_1 = 0.65\ eV$) for general order kinetics.

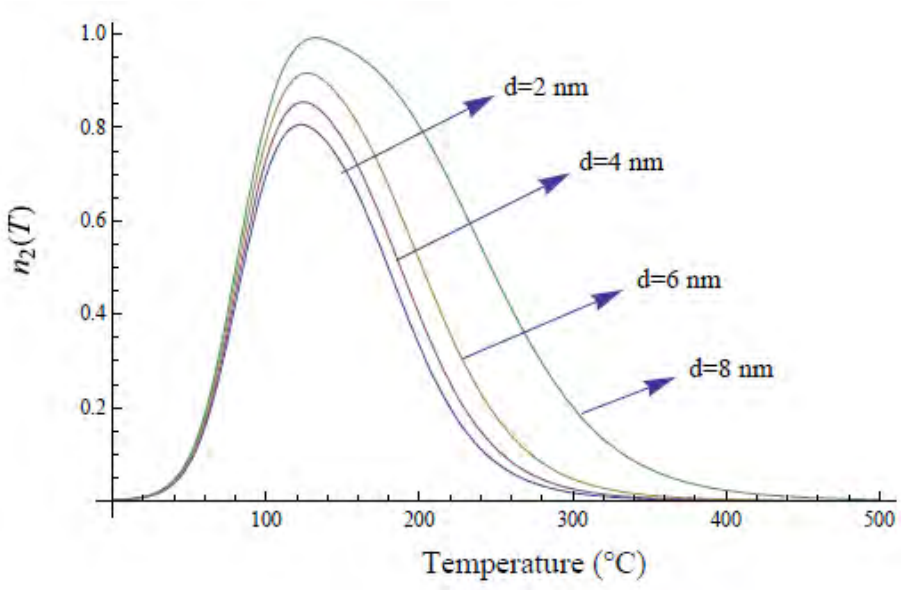

Figure 4.6: Variation of concentration of electrons $n_2(T)$ in the deeper trap ($E_2 = 0.8\ eV$) for general order kinetics.

electrons that are released from the first trap level ($E_1 = 0.65\ eV$) can be retrapped by the deeper trap ($E_2 = 0.8\ eV$). This is the reason why the concentration of electrons in the deeper trap initially increases with temperature as indicated in Fig. 4.6. However, the concentration of electrons in the shallower trap decreases with rise in temperature as shown in Fig. 4.5.

Table 4.1 shows that the number of the carriers, which are recombined radiatively per unit time, increases with a decrease in the quantum dot size. Using the data of in Table 4.1 and Eq. 4.3.6, we generated the temperature dependent TL intensity for the dot whose diameter varies from 2 nm to 8 nm as presented in Fig. 4.7. The intensity increases with decreasing in the dot size indicating that the quantum confinement effect enhances radiative recombination rate. There are two peaks of the TL intensity and they correspond to the two different active electron trap levels. We also found that positions of the TL intensity peaks corresponding to the first trap practically do

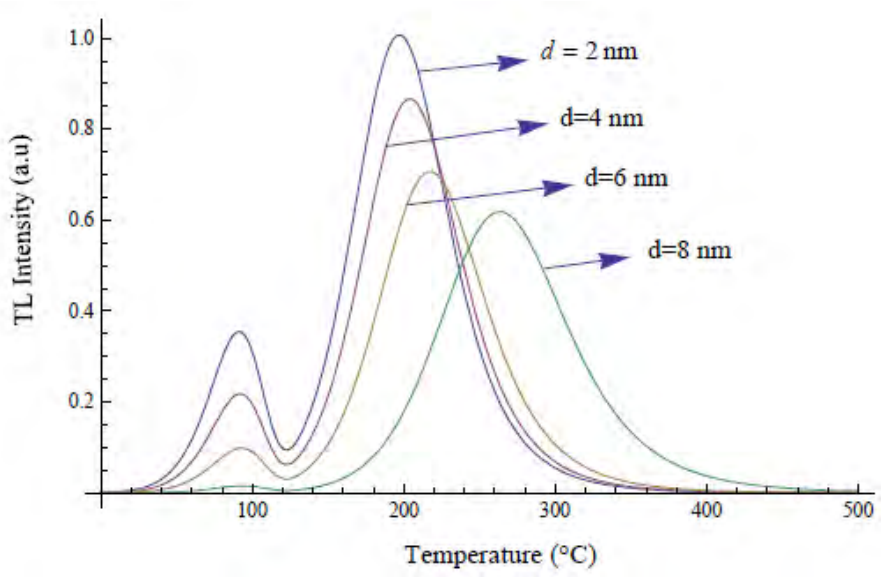

Figure 4.7: Variation of TL intensity I versus temperature for general order kinetics.

not shift with the temperature. At the same time, the intensity peaks of the second trap shift to the high temperatures with increasing in the dot size. The TL peaks of the first trap are lower comparing with the peaks of the second trap as shown in Fig. 4.7. It can be explained by the fact that during the excitation of the first trap only some of its electrons recombine with the holes emitting light while some of them are trapped by the second trap. This is indicated in the initial rise in the concentration of the trapped electrons in the second trap (Fig. 4.6).

4.6 Conclusion

The TL glow curves of silicon quantum dots of diameter 2-8 nm in the model of two active electron traps and one recombination center have been numerically simulated within the frame of the first and general order kinetics. There are two peaks of the TL intensity corresponding to the two active electron trap levels. The first order kinetics

does not take into account the retrapping effects and the calculated TL intensity does not depend on the quantum dot size. As a result, this approach gives the higher TL intensity compared with the general order kinetics. We focused on the results obtained within the frame of the general order kinetics approach as the more realistic one. The results show that the TL intensity increases with a decrease in the quantum dot size. This can be explained in terms of the quantum confinement effect. In our investigation, we account it with the help of extrapolation of the experimental data on the probability of radiative transitions on the quantum dot size. We obtained that the trap with deeper electron level $E_2 = 0.8\ eV$ (we call it the second trap) provides the higher TL intensity as compared with the trap of shallower level $E_1 = 0.65\ eV$ (the first trap) but at higher temperatures. Both traps show an increase in the TL intensities with a decrease in the quantum dots size. We claim that this conclusion will be true for any traps provided that $E_1 < E_2$.

The proposed model of TL in the case of quantum dots with the active electron energies $E_1 < E_2$ and different sizes $D_1 > D_2$ can give a considerable increment in the second peak of TL. To our mind the ensemble of quantum dots of two kinds with different energy of the trapped electrons and different size of may have interesting TL properties and deserves further study.

Chapter 5

Thermoluminescence Properties of UV-irradiated $Ca_3Y_2(Si_3O_9)_2$ Nanophosphor

5.1 Introduction

Calcium yttrium silicate $Ca_3Y_2(Si_3O_9)_2$ is one of the most important phosphors in the silicate family. It belongs to a space group C2/c with Ca and Y atoms randomly sharing 6, 7 and 8- fold coordination symmetry sites in the composition [111, 112, 113]. Though the structural properties of this phosphor material are first studied in 1997 [112], it has attracted much attention in the years following this first report. The structure of this material can be seen as an arrangement of two types of layers; namely, the metal ions (Ca^{2+}/Y^{3+}) and SiO_4 tetrahedrons. Two oxygen atoms of every SiO_4 tetrahedron are shared with another SiO_4 tetrahedron resulting in the

formation of ternary Si_30_9 rings with Ca/Y atoms coupled with them [111, 112]. This arrangement of the metal ions is found to reduce their interaction capability and opens an opportunity to introduce a relatively high content of luminescent impurities without thermal quenching [111, 114]. The photoluminescence (PL) properties of different rare earth doped $Ca_3Y_2(Si_30_9)_2$ have been studied in recent years [111, 112, 113, 114]. However, the thermoluminescence (TL) properties of this material have not been investigated to the best of our knowledge. Therefore, study of its TL properties is important for possible applications in the field of dosimetry. TL is one of the radiation induced defect related process in which the energy stored in the material is released in the form of emitted light by heating the irradiated material [1, 28, 38, 115]. The intensity of the emitted light as a function of temperature forms TL glow curve. TL finds favor in diverse scientific disciplines because of its several applications. Energy stored in the crystal is released with the emission of light while heating the irradiated material and the intensity of the emitted light as a function of temperature forms TL glow curve. The nature of the glow peaks which are generated from the intensity of the emitted light as a function of temperature depends on the properties of the trapping states responsible for TL [38]. In other words, the position, shape, and intensities of the glow peaks are related to the properties of the trapping states responsible for the TL [38]. TL kinetic parameters such as activation energy (E), the frequency factor (s) and the order of kinetics (b) determine the dosimetric properties of a material as they give us valuable information about the mechanism responsible for the TL emission in the material. Therefore, reliable dosimetric studies of any TL material include a good knowledge of its kinetic parameters. Therefore, in this chapter, the TL kinetic parameters such as E, s, and b of $Ca_3Y_2(Si_30_9)_2$ host material are reported.

Moreover, its isothermal decay curve and optical properties are also investigated.

5.2 Experimental Details

5.2.1 Solution combustion method of synthesizing nanophosphor

The solution combustion method is an important chemical route for the synthesis and processing of advanced ceramics (structural and functional), catalysts, composites, alloys, inter-metallics and nanomaterials [116]. The method has generated more interest in the field of nanomaterials such as luminescence materials (phosphors) and other ceramic materials, because of fine particle sizes, multi-component, crystalline and homogeneous materials can be achieved at relatively low temperature and less time [117]. In this technique, a saturated aqueous solution of the desired metal salts and a suitable organic fuel is made to boil, until the mixture ignites and a self sustaining and rather fast combustion reaction occurs, resulting in a dry, usually crystalline, fine oxide powder [118, 119, 120, 121, 122, 123]. To form a mixed oxide, a mixture containing the desired metal ions, in the form of, for instance, water soluble nitrate salts, a fuel such as urea, glycine or ethylene glycol can be used. Usually redox reactions such as this are exothermic in nature and often lead to explosion if not controlled, but in this technique the combustion metal nitrates-urea mixtures usually occurs as a self propagating and non-explosive exothermic reaction. The large amounts of gases formed can result in the appearance of a flame, which can reach temperatures in excess of 1000 ^oC. The energy released from the exothermic reaction between the nitrates and fuel, which is usually ignited at a temperature much lower

than the actual phase transformation temperature, can rapidly heat the system to a high temperature and sustain it long enough, even in the absence of an external heat source for the synthesis to occur [124]. The luminescent materials (phosphors) prepared by this method have low density, fluffy texture and ultra fine particles. As more gases are released, either agglomerates are not formed or disintegrated into fine particles [125]. In recent years, with the development of the synthesis technologies on materials, several chemical methods have been applied to prepare luminescence powders [126], of which combustion synthesis is the most important one. There are many merits of the combustion synthesis. First, the process is conducted in the liquid state, so that each component can be accurately controlled and uniformly mixed. Second, the process, which has been extensively applied to preparation of various nanoscale materials, takes only a few minutes [127]. Third, it involves inexpensive processing equipments. Fourth, the final product is obtained in only one step using the chemical energy of the reactants, and finally the final products are of high purity due to libration of volatile impurities [128].

$Ca_3Y_2(Si_30_9)_2$ white powder was synthesized with the solution combustion route using $CaNO_3, YNO_3$, TEOS and Urea as a starting materials. First, the starting materials were dissolved in 10 ml de-ionized water and kept under magnetic stirring for one hour. The mixture was then contained in China crucible and quickly put in to a muffle furnace pre-heated to 600 ^oC. After few minutes, the solution precursors boiled, swelled, evolved a large amount of gases and were ignited yielding product. After keeping the product for 10 minutes in the furnace, dry foam-like powder of $Ca_3Y_2(Si_30_9)_2$ was then pulled out quickly. It was then grinded into powder using mortar and pestle which were pre-cleaned with water and ethanol.

5.2.2 Characterization techniques

The crystal structure of this material was studied by x-ray diffraction (XRD) using a Bruker D8 advance x-ray diffractometer operating at 40 kV and 40 mA using Cu $K_\alpha = 0.15406\ nm$. For TL measurements, the sample was prepared into disc of 5 mm in diameter and 1 mm thick. A UV source was used for TL excitation prior to heating. The TL is detected using TL reader type TL1009I offered by Nucleonix systems Pvt. Ltd., India interfaced to a PC where the TL signals were analyzed. The sample was heated from 0 to 400 ^oC after a UV dose of 5 minutes.

5.3 Results and Discussion

5.3.1 XRD analysis

Fig. 5.1 shows the XRD pattern of the synthesized $Ca_3Y_2(Si_30_9)_2$. It shows monoclinic phase of the powder and the diffraction peaks match well with the standard JCPDS card number 87-0459. The average crystallite size of the prepared powder was determined from Scherrer equation [129] which is given by,

$$D = \frac{0.9\lambda}{\beta \cos\theta}, \tag{5.3.1}$$

where D is the crystallite size, λ is the x-ray wavelength (0.15406 nm), β is the full width at half maxima (FWHM) and θ is the diffraction angle. The values of 2θ with the corresponding values of FWHM and crystallite size for some prominent peaks are given in Table 5.1. The average crystallite size of the prepared phosphor is 28 nm. The strain (ε) developed in the synthesized powder was evaluated from the following

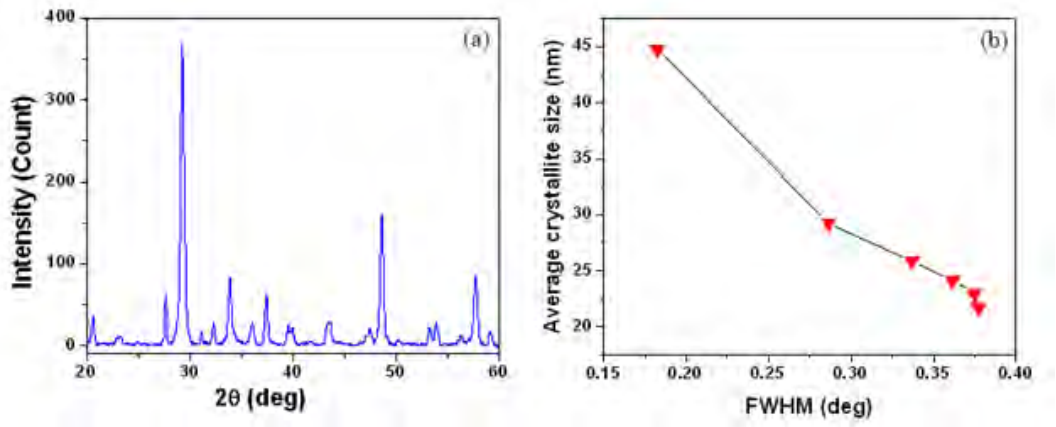

Figure 5.1: (a) XRD pattern of the synthesized $Ca_3Y_2(Si_30_9)_2$ sample, and (b) FWHM with the corresponding crystallite size.

relation [130] and is also given in Table 5.1.

$$\varepsilon = \frac{\beta \cot\theta}{4}, \tag{5.3.2}$$

where β and θ are as defined above.

2θ (degree)	$FWHM$ (degree)	Crystallite size (nm)	Strain
27.667	0.18260	44.80	0.18538
29.300	0.37715	21.77	0.36068
33.905	0.36133	24.21	0.29634
37.443	0.28635	29.29	0.21123
48.640	0.33667	25.89	0.18623
57.629	0.37470	22.98	0.16994

Table 5.1: FWHM, crystallite size and strain of the synthesized $Ca_3Y_2(Si_3O_9)_2$ host material.

5.3.2 Thermoluminescence analysis

The TL glow curve of $Ca_3Y_2(Si_30_9)_2$ host material obtained at heating rate of 1 $^0C/s$ after UV dose of 5 minutes is shown in Fig. 5.2 (a). From the analysis of glow

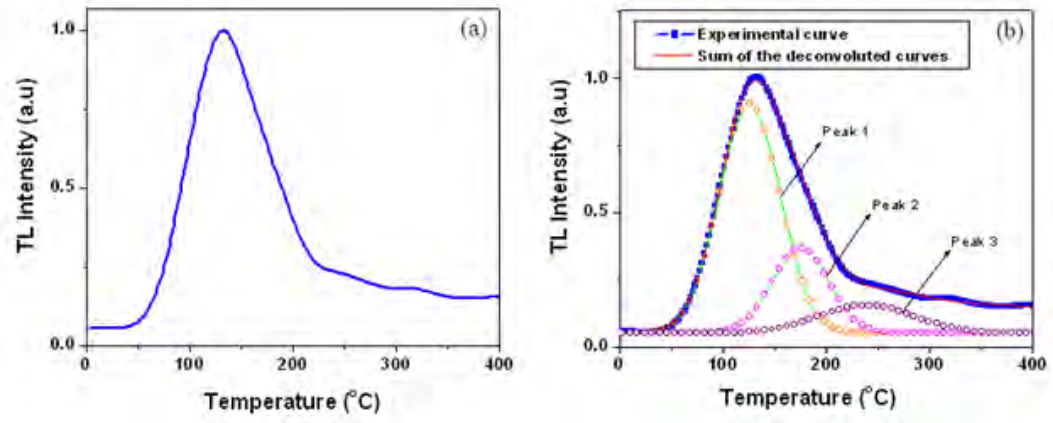

Figure 5.2: (a) TL glow peak for heating rate of 1 ${}^0C/s$ and UV dose of 5 minutes, and (b) deconvoluted glow curve of $Ca_3Y_2(Si_30_9)_2$ host material.

curve deconvolution, it can be observed that the glow peak can be well fitted by three constituent peaks as shown in Fig. 5.2(b). The determination of the TL kinetic parameters of $Ca_3Y_2(Si_30_9)_2$ host material is made using peak shape method. This method, which considers the shape of the glow peaks [1, 28], is reported to be a popular method of analyzing glow curves in order to evaluate the kinetic parameters E, s and the order of kinetics b and it is discussed in detail in Chapter 3. In other words, this technique for evaluating the TL kinetic parameters is based on the values of the peak temperature T_M, and the temperatures T_1 and T_2 located on the left and right sides of T_M, respectively, corresponding to half of the peak intensity. The order of kinetics depends on the shape factor of the glow peak, μ which is also related to the temperatures T_M, T_1, and T_2 according to Eq. 3.2.12. The activation energy is evaluated from Chen's equations for general order kinetics (Eqs. 3.2.13 to 3.2.18) [1, 28]. Moreover, the frequency factor s can be calculated using the following equation

for general order kinetics [1, 28]. That is,

$$\frac{\beta E}{kT_M^2} = s\ \exp\left(-\frac{E}{kT_M}\right)\left[1+(b-1)\left(\frac{2kT_M}{E}\right)\right], \tag{5.3.3}$$

where β is the heating rate and k is the Boltzmann's constant. The values of the shape factor μ, E, and s of the glow peaks are summarized in Table 5.2. The glow peaks obey general order kinetics. The relationship between the order of kinetics b and the geometrical factor μ is given in [1, 28].

	$T_1\ (^oC)$	$T_M\ (^oC)$	$T_2\ (^oC)$	τ	δ	ω	μ	b	$E\ (eV)$	$s\ (s^{-1})$
1	89	125	162	36	37	73	0.51	1.96	0.56	4.6×10^6
2	140	176	212	36	36	72	0.50	1.90	0.70	2.7×10^7
3	162	242	314	80	72	152	0.47	1.81	0.85	6.8×10^7

Table 5.2: μ, E, and s of the glow peaks 1, 2, and 3 of $Ca_3Y_2(Si_30_9)_2$ host material.

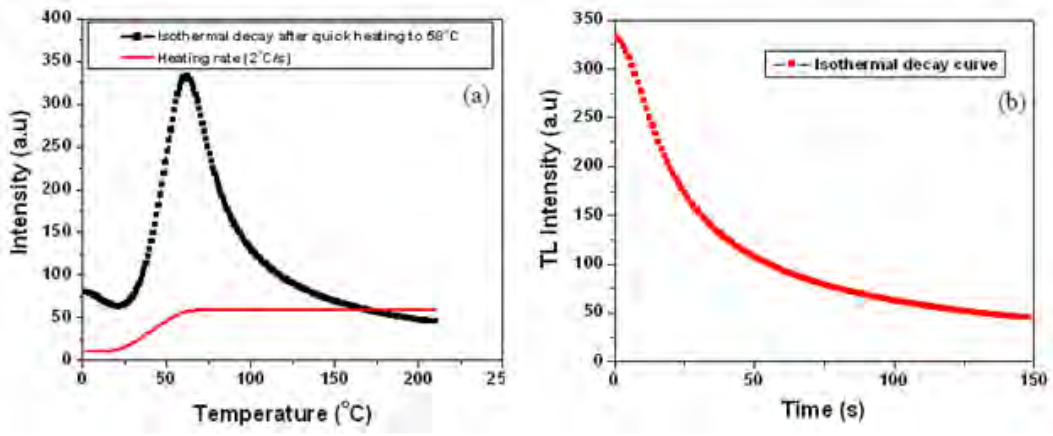

Figure 5.3: Graphs of (a) the sample quickly heated at 2 $^oC/s$ to 58 ^oC, and (b) its phosphorescence decay curve.

The values of the activation energy E for peaks 1, 2, and 3 estimated using initial rise method are 0.52, 0.66, and 0.81, respectively. The isothermal decay curve of the prepared sample was also investigated. After 5 minutes of UV exposure, the sample

was quickly heated to a temperature of 58 ^oC at heating rate of 2 $^0C/s$ (Fig. 5.3(a)). Keeping the sample at this temperature, the phosphorescence decay is measured as a function of time (Fig. 5.3(b)) and it is considerably fast. Glow curve fitting using Kitis

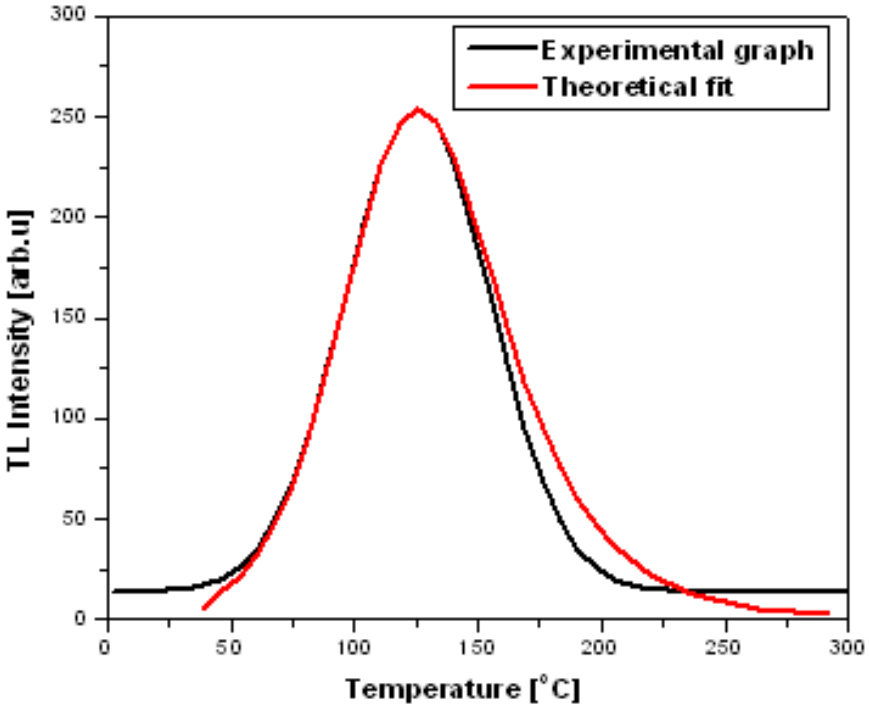

Figure 5.4: Experimental data and the theoretically fitted graph using Kitis et al equation.

et al equation was also performed. The following analytical equation of temperature dependent TL intensity was developed by Kitis et al for peaks following general order kinetics [28].

$$I(T) = I_M \; b^{b-1} \; \exp\left(\frac{E}{kT} \times \frac{T - T_M}{T_M}\right) \times$$

$$\left\{1 + (b-1)\,\frac{2kT_M}{E} + (b-1)\,\frac{T^2}{T_M^2}\,\left[1 - \frac{2kT}{E}\right] \exp\left(\frac{E}{kT} \times \frac{T - T_M}{T_M}\right)\right\}^{-\frac{b}{b-1}}. \quad (5.3.4)$$

The expression depends on the maximum TL intensity I_M and the temperature corresponding to the maximum TL intensity T_M. Here, glow curve fitting of peak 1 is presented. Using $I_M = 254,\ T_M = 398\ K,\ E = 0.56\ eV$, and $b = 1.96$, it is theoretically fitted applying the above equation and a good fit was obtained as shown in Fig. 5.4. It is important to note that the theoretical curve nicely agree with the experimental glow curve in low temperature region. However, they tend to move apart at high temperature region and this could be because of thermal quenching effect. The calculated values are compared with the experimental data in Table 5.3 for the first 15 data points.

Let us now further discuss about the glow curve of $Ca_3Y_2(Si_30_9)_2$ host material shown in Fig. 5.2 using theoretical approaches. Analysis of glow curve deconvolution shows that the broad glow curve of this material can be best fitted with three peaks of trap parameters shown in Table 5.2. Showing the existence of one single glow peak with the three different traps and trap parameters shown in Table 5.2 is quite important. This can be done using numerical solutions of the rate equations governing the TL process applying three traps one recombination center model. The consideration of only one recombination center is just to simplify the theoretical problem and the theoretical comparison is done using quantum dot of diameter 8 nm with radiative recombination probability indicated in Table 4.1

	T (^oC)	TL Intensity (Experimental)	TL Intensity (Theoretical)
1	45.66017	20.27676	13.4837
2	52.91186	25.69919	20.9934
3	60.16356	34.67155	31.8534
4	67.41525	48.49479	47.0334
5	74.66695	68.26884	67.4192
6	81.91864	94.42865	93.4927
7	89.17034	126.24341	124.866
8	103.67373	196.3975	194.811
9	110.92542	226.35149	225.249
10	118.17712	246.70638	246.172
11	125.42881	254.03313	254.076
12	132.68051	247.04618	248.133
13	139.9322	226.97204	230.351
14	147.1839	197.19749	204.607
15	154.43559	162.33579	175.208

Table 5.3: The first 15 data points for comparison of the experimental data and theoretical result.

Consider an energy band scheme having four localized levels (Fig. 5.5). The three levels act as traps (TR_1, TR_2 and TR_3) and the other acts as recombination center (R). As discussed before, the ionization of valence electrons shown in transition 1 due to absorption of external energy produces free electrons in the conduction band and free holes in the valence band. The electrons and holes then become trapped at the trap centers though there is probability of recombination with each other. Usually in theoretical models, it is assumed that holes first become trapped at centers (R) (transition 9) in order for recombination to occur so that recombination takes place via the annihilation of the trapped holes by free electrons (transition 8) resulting in luminescence. For the case where electrons are trapped at levels (TR_1, TR_2 and TR_3) (transitions 2, 4 and 6), recombination can only take place if the trapped

electrons absorb enough energy E_1, E_2 and E_3, respectively, in the form of heat to be released back to conduction band (transitions 3, 5 and 7), from where there is possible recombination of electrons and holes. For these three active electron traps

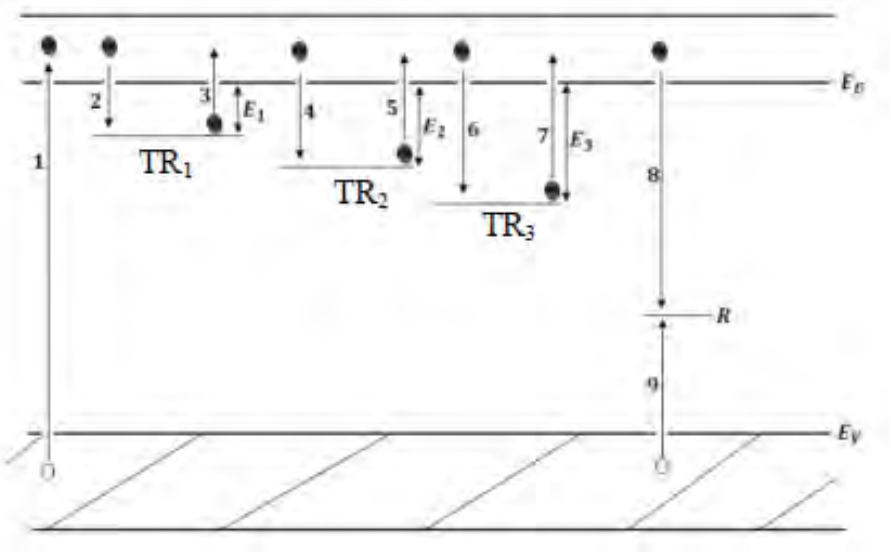

Figure 5.5: Four level model for thermoluminescence. Allowed transitions: (1) ionization; (2), (4), (6) and (9) trapping; (3), (5) and (7) thermal release; (8) radiative recombination and emission of light.

with energy levels E_1, E_2 and E_3 below the bottom of the conduction band, the rate equations can be written as:

$$\frac{dn_1}{dt} = -s_1\ n_1\ \exp\left\{-\frac{E_1}{kT}\right\} + n_c\ A_1\ (N_1 - n_1), \tag{5.3.5}$$

$$\frac{dn_2}{dt} = -s_2\ n_2\ \exp\left\{-\frac{E_2}{kT}\right\} + n_c\ A_2\ (N_2 - n_2), \tag{5.3.6}$$

$$\frac{dn_3}{dt} = -s_3\ n_3\ \exp\left\{-\frac{E_3}{kT}\right\} + n_c\ A_3\ (N_3 - n_3), \tag{5.3.7}$$

$$\frac{dn_c}{dt} = s_1\ n_1\ \exp\left\{-\frac{E_1}{kT}\right\} + s_2\ n_2\ \exp\left\{-\frac{E_2}{kT}\right\} + s_3\ n_3\ \exp\left\{-\frac{E_3}{kT}\right\} -$$

$$n_c\ \left[A_1\ (N_1 - n_1) + A_2\ (N_2 - n_2) + A_3\ (N_3 - n_3) + A_r\ n_h\right]. \tag{5.3.8}$$

Here n_i $(i = 1, 2, 3)$ is the concentration of trapped electrons on the levels E_i (cm^{-3}), N_i $(i = 1, 2, 3)$ is the total concentration of traps on the levels E_i (cm^{-3}), k is the Boltzmann constant, s_i is the probability per unit time of an electron to escape from the i^{th} trap, A_i is the re-trapping probability on the i^{th} energy level $(cm^3\ s^{-1})$. The other parameters $A_r,\ n_c$ and n_h are as defined before.

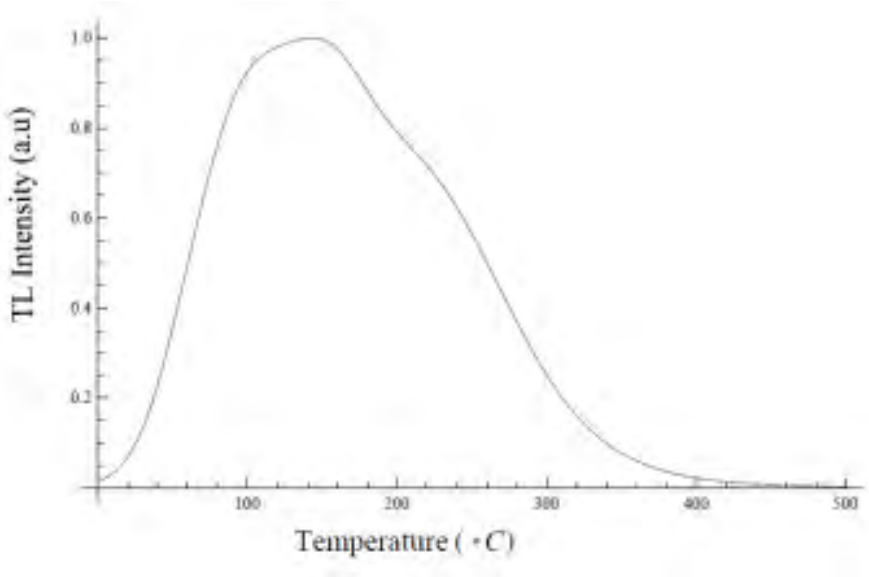

Figure 5.6: Numerically simulated glow curve using the experimentally determined TL kinetic parameters.

It is assumed that $N_1 = N_2 = N_3 = N$. The term s is commonly called the 'frequency factor', although when applied to TL it is often called 'attempt-to-escape frequency'. As explained before, the usual interpretation of s is that it represents

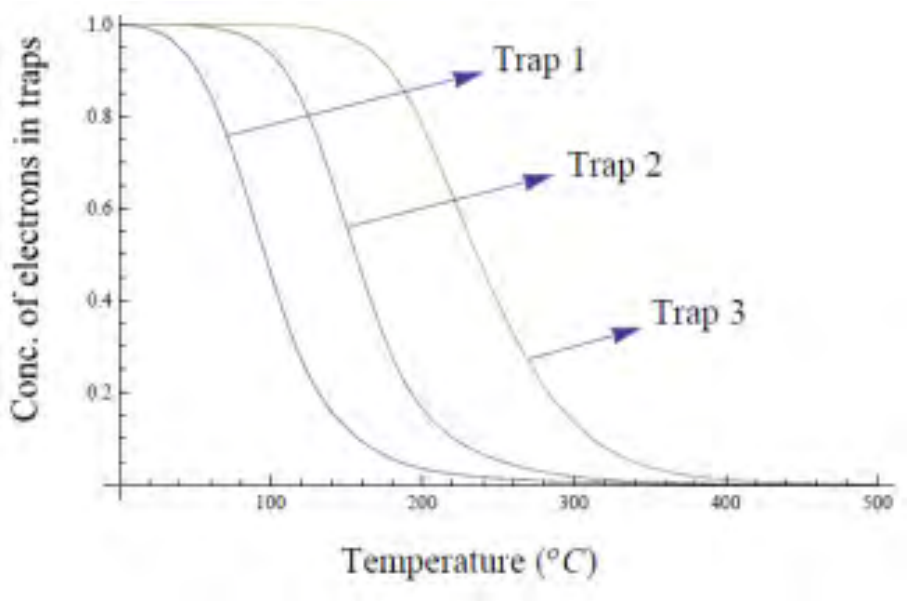

Figure 5.7: Numerically simulated curves for variation of concentration of electrons in the three identified traps of $Ca_3Y_2(Si_30_9)_2$ host material using the experimentally determined TL kinetic parameters.

the number of times per second that a bound electron interacts with lattice phonons times transition probability [1]. The maximum value expected for s is therefore the lattice vibration frequency, namely $10^{12} - 10^{14}\ s^{-1}$. The system [1, 28, 38, 114] is closed by the quasi-neutrality condition,

$$n_1(t) + n_2(t) + n_3(t) + n_c(t) = n_h(t). \tag{5.3.9}$$

Here $n_h(T)$ is the instantaneous concentration of holes in hole trap. Linear heating rate β defined in equation Eq. 4.3.5 was used during the experiment. The value of the heating rate for the glow curve shown in Fig. 5.2 is 1 $^oC/s$. As defined before, the recombination term in equation Eq. 5.3.8 is $A_r\ n_h(T)\ n_c(T)$. Numerical solution of equations (Eqs. 5.3.5 to 5.3.8) using Mathematica 8 gives a glow curve shown in Fig. 5.6 for the same experimentally determined trap parameters except that

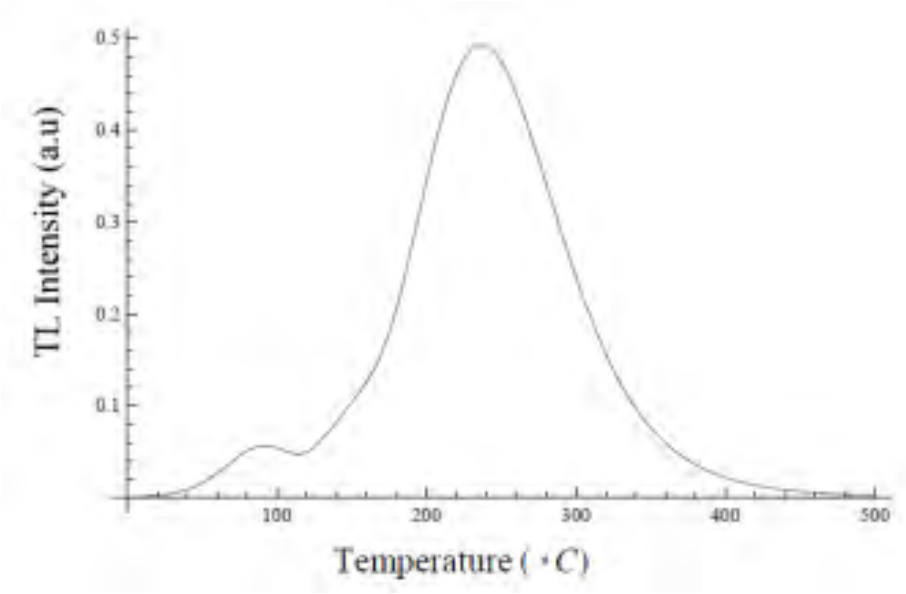

Figure 5.8: Numerically simulated glow curve for general values of $n_{10},\ n_{20},\ n_{30}$, and N.

$n_{10} = n_{20} = n_{30} = N$, i.e., all the traps on each trap level are initially fully filled. The peak maximum and the glow curve profile of the numerical result are much similar to the experimental glow curve. Therefore, it can be concluded that following irradiation with UV dose, all traps on each trap level of $Ca_3Y_2(Si_30_9)_2$ host material are initially fully filled.

The numerical result of the corresponding variation of electrons in traps 1, 2 and 3 of $Ca_3Y_2(Si_30_9)_2$ host material during the heating stage is depicted in Fig. 5.7. The concentration of electrons in each trap has the same initial value because of the assumption $n_{10} = n_{20} = n_{30} = N$ and it decreases with increasing temperature. However, for general values of $n_{10},\ n_{20},\ n_{30}$, and N, a completely different result is obtained. The generated glow peak and variation of concentration of electrons in each trap for this case are shown in Figs. 5.8 and 5.9, respectively. The rise in the concentration of electrons in traps 2 and 3 is due to the retrapping of electrons to the

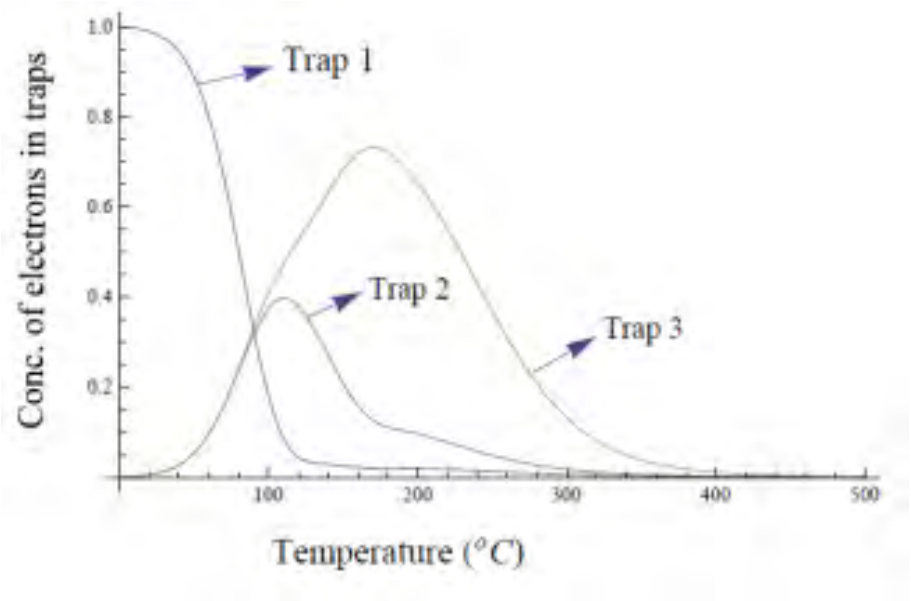

Figure 5.9: Numerically simulated curves for variation of concentration of electrons in the three identified traps of $Ca_3Y_2(Si_30_9)_2$ host material for general values of $n_{10},\ n_{20},\ n_{30}$, and N.

vacant traps which are not initially occupied by electrons.

5.4 Optical Properties

Among the optical methods, UV-VIS diffuse reflectance spectroscopy is one of the most employed techniques to describe the optical properties present in the solids. The band gap energy of $Ca_3Y_2(Si_30_9)_2$ is estimated from the reflectance spectrum shown in Fig. 5.10(a) by applying the Kubelka-Munk (K-M) method. The K-M method is based on the following equation [11-12]:

$$F(R) = \frac{(1-R)^2}{2R}, \tag{5.4.1}$$

where R is the reflectance and $F(R)$ is a parameter that is proportional to the absorption coefficient α. A modified K-M function is obtained by multiplying the function

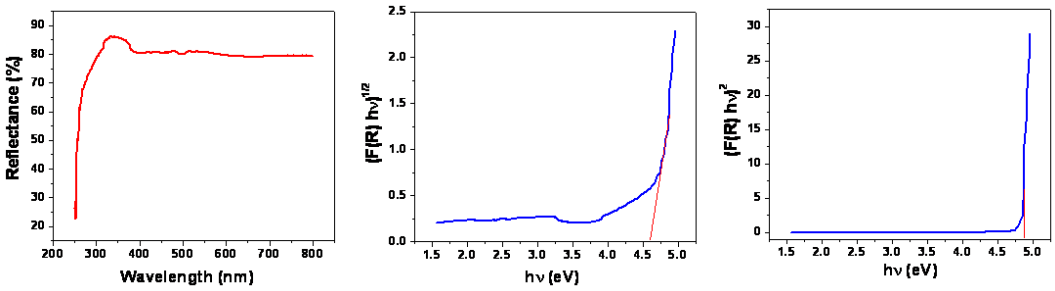

Figure 5.10: Graphs of (a) Reflectance as a function of wavelength, (b) $[F(R)\ h\nu]^{\frac{1}{n}}$ versus energy $h\nu$ for indirect allowed transition (n=2), and (c) $[F(R)\ h\nu]^{\frac{1}{n}}$ versus energy $h\nu$ for direct allowed transition ($n = 1/2$) of the prepared sample.

$F(R)$ by $h\nu$, where h is Planck's constant and ν is the frequency of vibration. As it is proposed in [131, 132], the modified function is related to the band gap (E_g) of the material by,

$$F(R) \times h\nu = C\ (h\nu - E_g)^n, \tag{5.4.2}$$

where C is a proportionality constant.

The value of n is 1/2 for direct allowed transition, 3/2 for direct forbidden transition, 2 for indirect allowed transition and 3 for indirect forbidden transition. Figs. 5.10(b) and 5.10(c), respectively show the evaluation of $[F(R)\ h\nu]^{\frac{1}{n}}$ versus $h\nu$ for $n = 2$ and $n = 1/2$. The band gap energy of the sample is estimated by extrapolating the slope of $[F(R)\ h\nu]^{\frac{1}{n}}$ versus $h\nu$ curves to the energy axis. To the best of our knowledge, the type of the band gap of $Ca_3Y_2(Si_30_9)_2$ (direct or indirect) has not been reported in literature. Therefore, in this work, the estimation of the band gap is made for both direct and indirect allowed transitions and the two values are compared. The band gap of the synthesized phosphor calculated using the modified K-M method is of the order of 4.6 eV for indirect allowed transition and 4.9 eV for direct allowed transition. The band gap estimated for indirect allowed transition is in

a good agreement with estimated value reported by Yi-Chen Chu et al [133]. Yi-Chen Chu et al reported that the band gap of $Ca_3Y_2(Si_30_9)_2$ host material synthesized by solid state reaction can be roughly estimated using a wavelength of 288 nm which is of the order of 4.3 eV.

5.5 Conclusion

The structural, TL, and optical properties of $Ca_3Y_2(Si_30_9)_2$ host material synthesized by solution combustion method is studied. Important TL kinetic parameters such as activation energy (E), the frequency factor (s) and the order of kinetics (b) are determined by employing peak shape method. Glow curve deconvolution analysis shows that the glow peak can be well fitted by three constituent peaks obeying general order kinetics. From glow curve fitting using Kitis et al equation, a good fit is obtained showing that the evaluated trap parameters are correct. The prepared sample shows considerably fast phosphorescence decay. Moreover, the values of the optical band gap determined using both direct and indirect allowed transitions are comparable.

Chapter 6

Synthesis and Luminescence Properties of $Ca_3Y_2(Si_30_9)_2 : x\ Ce^{3+}$ Nanophosphor

6.1 Introduction

Most phosphors are composed of a transparent microcrystalline host (or a matrix) and an activator, i.e., a small amount of intentionally added impurity atoms distributed in the host crystal. Therefore, the luminescence processes of a phosphor can be divided into two parts: the processes mainly related to the host, and those that occur around and within the activator. These dopants introduced into the host may reside in different positions inside the host structure. Recently, inorganic compounds doped with rare earth elements form an important class of phosphors [134, 135], and have attracted much attention because of their versatile applications, for example,

in cathode ray tubes, photodiodes, lamps and x-ray detectors, bio-detectors, in lamp industries, color display, radiation dosimetry etc [136, 137, 138, 139]. Silicate family is an attractive class of materials for wide range of applications due to their special properties such as visible light transparency, chemical resistance, high temperature strength, low thermal expansion, high conductivity, good chemical and thermal stability [7].

As discussed in Chapter 6, the Ca and Y atoms in $Ca_3Y_2(Si_30_9)_2$ are sharing 6, 7 and 8-fold coordination symmetry sites in the composition as shown in Fig. 6.1 [111, 140, 141]. $Ca_3Y_2(Si_30_9)_2$ is reported to be a suitable host material for white emission when activated by different rare earth elements [111, 140]. This is particularly important for white light emitting diodes (w-LEDs) requiring a single host for solid state lightening. It exhibits three different crystallographic Y sites namely, Y_1 (coordination number (CN) 8), Y_2 (CN 7) and Y_3 (CN 6) and they can be randomly occupied by Cerium ion (Ce^{3+}). The occupation of Y_1 and Y_2 sites by Ce^{3+} has been reported for $Ca_3Y_2(Si_30_9)_2 : x$ (Ce^{3+}, Mn^{2+}) prepared by the conventional solid state method [140]. In general, different dopant concentration and synthesis routes results in different luminescence properties of a material. In this aspect, further investigation of the PL and study of the TL properties of $Ca_3Y_2(Si_30_9)_2 : x\ Ce^{3+}$ prepared by solution combustion technique is quite interesting. TL is one of the radiation induced defect related process in which the energy stored in the material is released in the form of emitted light by heating the irradiated material [1, 28, 38]. Therefore, in this Chapter, in addition to the structural study, the PL and TL properties of $Ca_3Y_2(Si_30_9)_2 : x\ Ce^{3+}$ are investigated for possible applications in w-LEDs and radiation dosimetry.

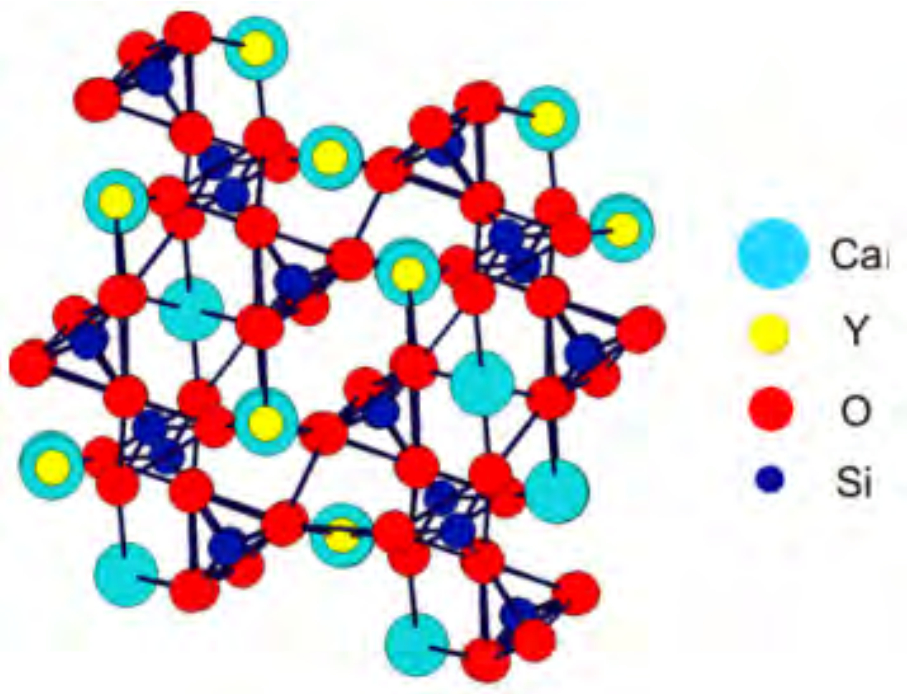

Figure 6.1: Unit cell of $Ca_3Y_2(Si_30_9)_2$ [111]. Ca and Y randomly occupy the same three sites of 6-, 7 and 8- fold coordination symmetries.

6.2 Optical Transitions in Ce^{3+}

Cerium (Ce) is one of the rare earth elements in the lanthanide group with electronic configuration $[Xe]4f^15d^16s^2$. Upon excitation, the electron in $4f^1$ ground state is photo-excited to the $5d^1$ levels leaving the 4f shell empty. Emission of light occurs as the system relaxes and returns to the $4f^1$ state and this light photon covers a broad band [140] as a result of electronic transitions within Ce^{3+} between the $[Xe]4f^05d^16s^0$ to $[Xe]4f^15d^06s^0$ states. This emission transition is an allowed one since the $5d$ to $4f$ transition is parity allowed, spin allowed and electric dipole allowed [140]. However, the broad band emission observed from Cerium differs greatly with the type of host material [140, 141].

6.3 Experimental Details

$Ca_3Y_2(Si_30_9)_2 : x\ Ce^{3+}$ white powder is synthesized with the solution combustion route for $x = 0.01,\ 0.02,\ 0.04,\ 0.08$ and 0.16 using $CaNO_3$, YNO_3, TEOS and Urea as a starting materials. Here, x is measured in mole percentage. First, the starting materials are dissolved in 10 ml de-ionized water and kept under magnetic stirring for one hour. The mixture is then contained in China crucible and quickly put into a muffle furnace pre-heated to 600 ^oC. After few minutes, the solution precursors boiled, swelled, evolved a large amount of gases and are ignited yielding product. After keeping the product for 10 minutes in the furnace, dry foam-like powder of $Ca_3Y_2(Si_30_9)_2$ is then pulled out quickly. It is then grinded into powder using mortar and pestle which are pre-cleaned with water and ethanol. The crystal structure of this material is studied by x-ray diffraction (XRD) using a Bruker D8 advance x-ray diffractometer operating at 40 kV and 40 mA using $Cu\ K_\alpha = 0.15406\ nm$. Its optical properties is studied using UV-VIS spectrometer in the wavelength range of 250 - 800 nm. The excitation and emission spectra are measured at room temperature using Cary Eclipse fluorescence spectrometer model: LS-55 with a built-in 150 W Xenon flash lamp. The values of the chromaticity coordinates of the phosphor have been estimated from the 1931 Commission Internationale de l'Eclairage (CIE) system using the excitation wavelength of 365 nm. For TL measurements, the samples are prepared into discs of 5 mm in diameter and 1 mm thick. A UV source is used for TL excitation prior to heating. The TL is detected using TL reader type TL1009I offered by Nucleonix systems Pvt. Ltd., India interfaced to a PC where the TL signals were analyzed. Samples are heated from 0 to 400 ^oC for different UV doses. Measurements of the TL fading are done after keeping the sample for different storage times before

heating.

6.4 Results and Discussion

6.4.1 XRD analysis

Fig. 6.2 shows the XRD pattern of the synthesized $Ca_3Y_2(Si_30_9)_2 : x\ Ce^{3+}$ nanophosphor. It shows monoclinic phase of the powder and the diffraction peaks match well

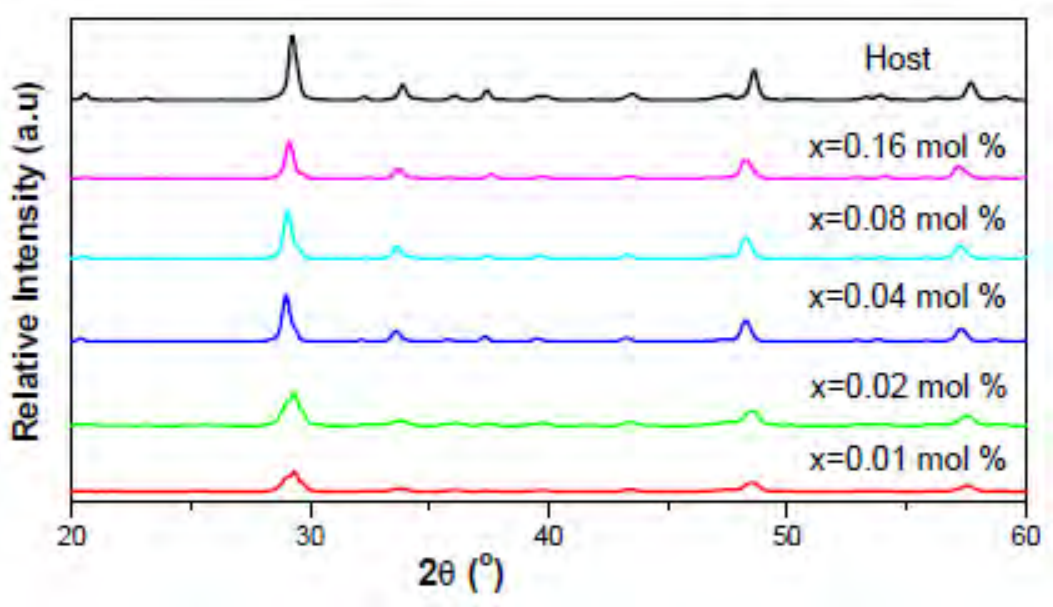

Figure 6.2: XRD pattern of the synthesized $Ca_3Y_2(Si_30_9)_2 : x\ Ce^{3+}$ samples.

with the standard JCPDS card number 87-0459 except for the relative intensity. This shows that Ce^{3+} ions entered into the sample without changing the crystalline structure of the samples. It is worth noting that the relative intensity of the diffraction peaks increased when doped with relatively large concentration of Ce^{3+} for up to $x = 0.08$ and then decreased at $x = 0.16$ as shown in Fig. 6.3 using the dominant

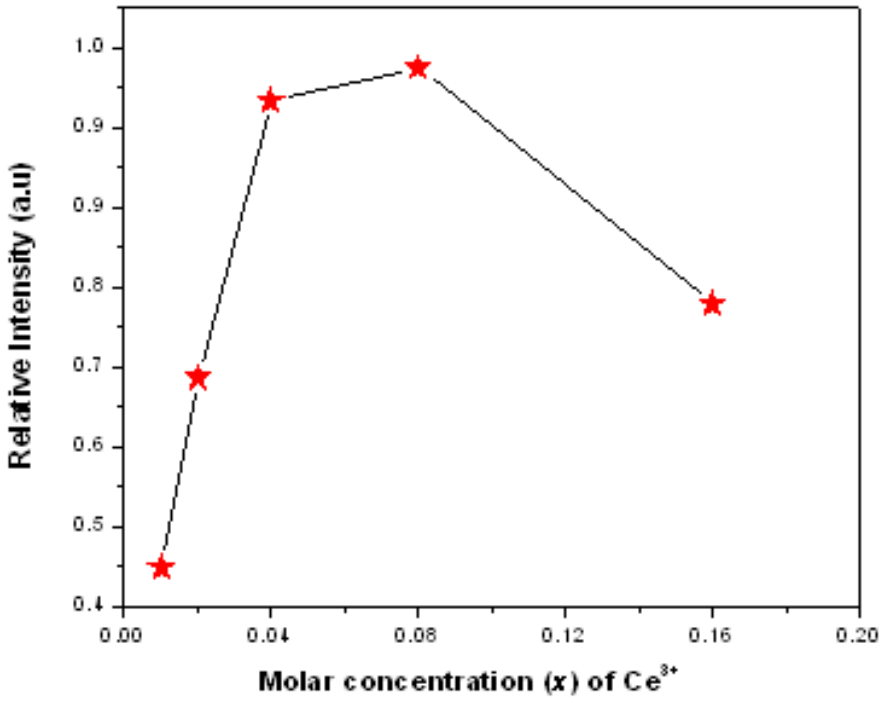

Figure 6.3: The variation of the dominant diffraction peak around $2\theta = 29\ ^0$ with the concentration x. The values are normalized with respect to the highest diffraction peak at $x = 0.08$.

peak around $2\theta = 29^0$. The increment in the intensity of the diffraction peaks up to $x = 0.08$ could be attributed to the improved crystallinity of the samples with increase in Ce^{3+} concentration. However, at higher doping concentration ($x = 0.16$) of Ce^{3+}, the decrease in the intensity of diffraction peaks could be ascribed to the degradation in the crystalline quality due to crystal distortion. Similar results have been reported in literature [143]. The strain (ε)induced in the samples due to crystal imperfection and distortion is calculated from Eq. 5.3.2 using the dominant diffraction peak around $2\theta = 29^o$ and is shown in Table 6.1.

It can be seen that there is a decrease in the lattice strain with increasing doping concentration of Ce^{3+} $Ca_3Y_2(Si_30_9)_2$ and this could be because of the reduction

x in mole percentage	Strain
0.01	0.65561
0.02	0.65534
0.04	0.34305
0.08	0.33153
0.16	0.33092

Table 6.1: Strain developed in the synthesized $Ca_3Y_2(Si_30_9)_2 : x\ Ce^{3+}$ samples.

(minimization) of bonding defects. It has been reported that lattice strain can either increase [142] or decrease [143] with rise in doping concentration.

6.4.2 Photoluminescence properties

Fig. 6.4(a) shows the room temperature PL emission spectra of $Ca_3Y_2(Si_30_9)_2 : x\ Ce^{3+}$ at excitation of 365 nm. The spectra show a broad band extending from about 350 to 600 nm. This band can be ascribed to the allowed $[Xe]5d^1$ to $[Xe]4f^1$ transition of Ce^{3+} [140]. It is interesting to note that the emission spectra correspond to three different emission wavelengths and hence energies. It can be seen that the curves obtained for $x = 0.04$ and $x = 0.08$ correspond to emission wavelength of 390 nm, the curve obtained for $x = 0.02$ corresponds to 396 nm and those obtained for $x = 0.01$ and $x = 0.16$ correspond to emission wavelength of about 425 nm. The three different emission energies of the PL spectra are explained in terms of the fact that $Ca_3Y_2(Si_30_9)_2$ exhibits three different crystallographic Y sites [111, 140]. These sites are Y_1 (CN 8), Y_2 (CN 7) and Y_3 (CN 6) and they can be randomly occupied by Ce^{3+}. Matthias Mller and Thomas Jstel reported that due to increasing crystal field splitting of the d-orbitals, the emission energy of d-f transitions decreases with decreasing coordination number [140]. Therefore, the observed PL emission spectra confirmed

the occupation of three different sites. Curves obtained for $x = 0.04$ and $x = 0.08$ are assigned to Ce^{3+} occupying Y_1 site, the curve obtained for $x = 0.02$ is assigned to Ce^{3+} occupying Y_2 site and curves obtained for $x = 0.01$ and $x = 0.16$ are assigned to Ce^{3+} occupying Y_3 site. The PL emission intensity of $Ca_3Y_2(Si_30_9)_2 : x\ Ce^{3+}$ is enhanced

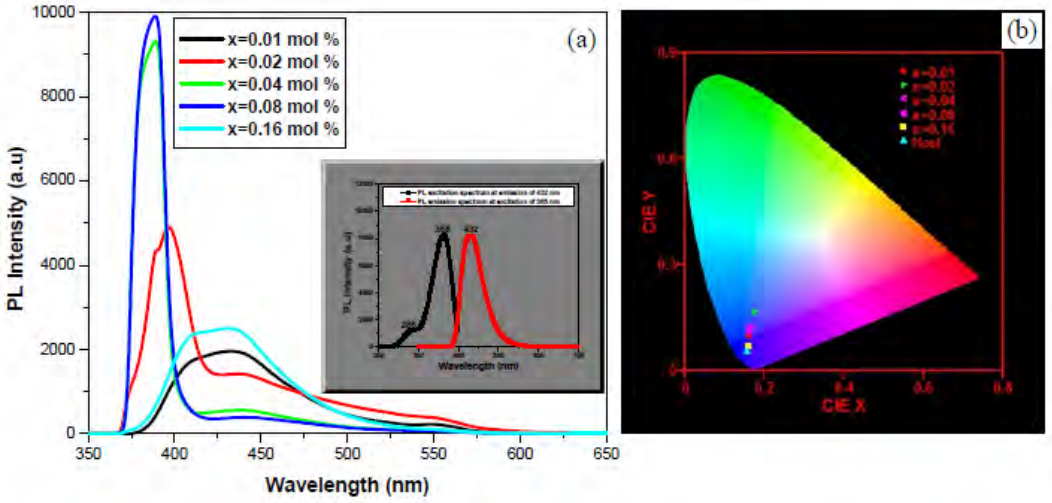

Figure 6.4: (a) Room temperature PL emission spectra of $Ca_3Y_2(Si_30_9)_2 : x\ Ce^{3+}$. The inset shows the PL excitation of the host material at emission of 432 nm and its PL emission at excitation of 365 nm, and (b) CIE chromaticity coordinates.

gradually with increasing x value from 0.01 to 0.08 and then decreases for $x = 0.16$. Thus, $x = 0.08$ is taken as the critical concentration. For $x = 0.16$, the concentration of Ce^{3+} is excessive leading to concentration quenching. It is reported that the decrease in PL intensity for activator concentration beyond a critical concentration shows the occurrence of energy transfer among the activator ions (Ce^{3+} in this case) at different sites in the lattice, resulting in concentration quenching [144, 145]. The probability of energy transfer increase with increase in Ce^{3+} concentration as the distance between the Ce^{3+} becomes small. The critical energy transfer distance (R_C)

can be approximated using Blasse formula [144, 145, 146] which is given by,

$$R_C \approx 2\left(\frac{3V}{4\pi X_C Z}\right)^{\frac{1}{3}}, \tag{6.4.1}$$

where V is the unit cell volume, X_C is the critical concentration of Ce^{3+}, and Z is the number of formula units coupled in the unit cell. Here $V = 1.5221\ nm^3$, $X_C = 0.08$, and $Z = 4$, as a result the calculated value of R_C is 2.087 nm. Thus, as Ce^{3+}-Ce^{3+} distance is greater than 0.5 nm, multi-polar interaction is more effective as compared to exchange interaction. This situation was explained by Dexter's theory. The type of the multi-polar interaction is determined from the following equation [144, 145],

$$\frac{I}{x} = k\left[1 + \beta\ x^{\frac{\theta}{3}}\right]^{-1}, \tag{6.4.2}$$

where k and β are constants for the same excitation condition for a given matrix crystal, θ=6, 8 and 10 is corresponding to electric dipole-diploe (d-d), electric dipole-electric quadrapole (d-q) and electric quadrapole-electric quadrapole (q-q) interactions, respectively and I is the PL intensity corresponding to the dopant concentration x.

Eq.6.4.2 can be written as,

$$\log\left(\frac{I}{x}\right) = C - \frac{\theta}{3}\log(x), \tag{6.4.3}$$

where C is constant. The variable θ has the electric multipolar character and it can be obtained from the slope $(-\theta/3)$ of the plot of $\log(I/x)$ versus $\log(x)$ as shown in Fig. 6.5. The slope of the linear fit of the graph $\log(I/x)$ versus $\log(x)$ is found to be -1.827. Therefore, the calculated value of θ is 5.481 which is close to 6 indicating that the energy transfer mechanism for $Ca_3Y_2(Si_30_9)_2 : x\ Ce^{3+}$ phosphor is electric dipole- dipole interaction.

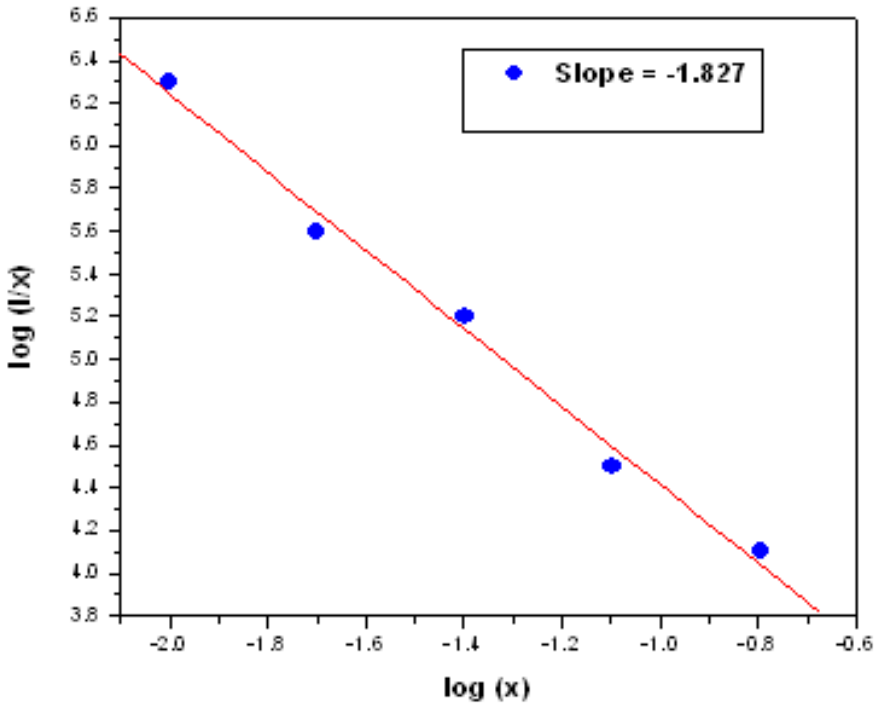

Figure 6.5: The graph of $\log(I/x)$ versus $\log(x)$ of Ce^{3+} for $Ca_3Y_2(Si_30_9)_2 : x\ Ce^{3+}$.

The inset of Fig. 6.4(a) shows the room temperature photoluminescence excitation and emission spectra of $Ca_3Y_2(Si_30_9)_2$ host material. The excitation spectrum consists of two absorption peaks at 286 and 365 nm. The emission spectrum shows an intense blue emission band with peak at 432 nm (photon energy of $\sim$ 2.9 eV). This PL emission could be attributed to deep level emission which can be explained in terms of two models as suggested by I. Shalish et al [147]. According to I. Shalish et al., the first model involves electron transitions from conduction band to a deep state in the lower half of the band gap while the second involves transitions from a deep state in the upper half of the gap to the valence band. Though, the intense PL emission at 432 nm could be ascribed to the latter phenomenon in our case, the nature of the transition and the deep level itself requires further study. The values

of the chromaticity coordinates of $Ca_3Y_2(Si_30_9)_2 : x\ Ce^{3+}$ samples have been estimated from the 1931 Commission Internationale de l'Eclairage (CIE) system using the excitation wavelength of 365 nm (see Fig. 6.4(b)). This system helps us visualize the variation in color emitted from the samples and the coordinates are measured as (x, y). When $x = 0.08$, the CIE coordinates are (0.30, 0.31), which is close to the ideal white light (0.33, 0.33).

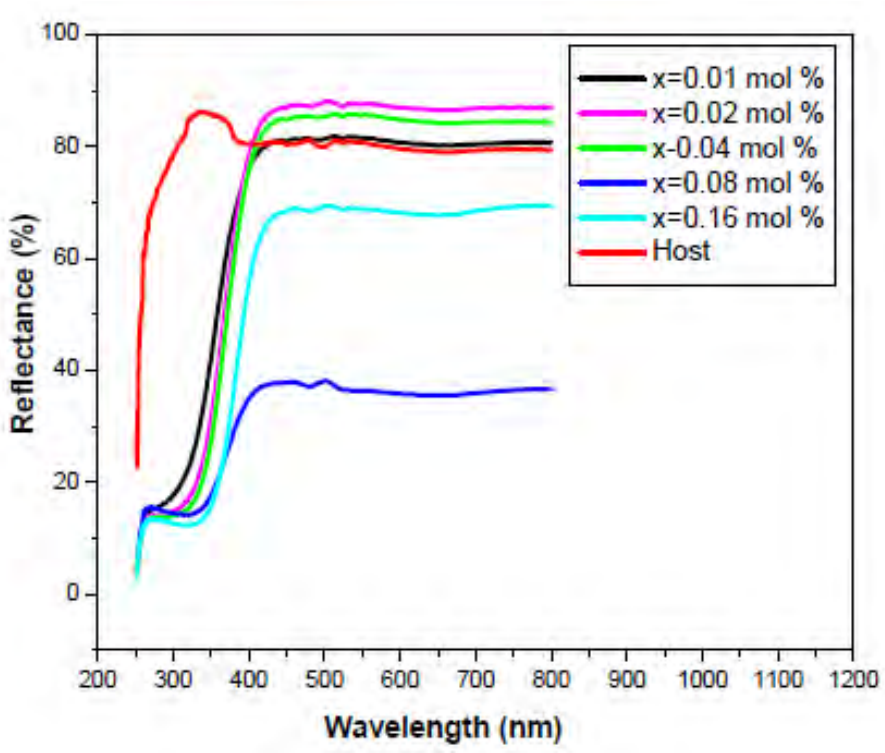

Figure 6.6: Graph of Reflectance as a function of wavelength.

The reflectance spectra of the undoped and Ce^{3+} doped samples are shown in Fig. 6.6. A red shift in the optical band gap of all the doped samples was observed as compared to the host material. Impurity band formation is an obvious consequence of increased doping concentration and the trapping of the Ce^{3+} atoms at the

grain boundary leads to the introduction of the Ce^{3+} defect states within the forbidden band. With increasing Ce^{3+} doping, density of this Ce^{3+} induced defect states increases, leading to the observed decrease of band gap or red shift [148].

6.4.3 Thermoluminescence properties

The TL glow curves of $Ca_3Y_2(Si_30_9)_2$ host material for different UV doses are shown in Fig. 6.7(a). It can be observed that the TL intensity increases with increase in UV dose for all the doses used up to 50 min as shown in Fig. 6.7(b). The glow peaks in general attained their peak maxima at different temperatures upon variation of UV dose indicating that they obey general order kinetics. The TL kinetic parameters

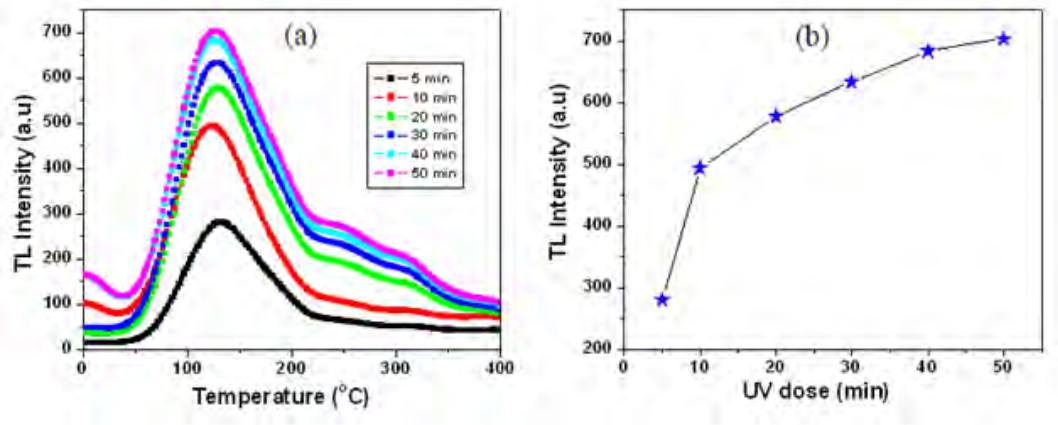

Figure 6.7: (a) TL glow curves for different UV exposure time, and (b) the variation of TL maxima with UV dose.

such as activation energy (E) and order of kinetics (b) are analyzed using Eqs. 3.2.13 to 3.2.18 of peak shape method. The frequency factor (s) can be calculated using Eq. 5.3.3 for general order kinetics [1]. The shape factor (μ), the activation energy (E) and the frequency factor (s) of the glow peaks corresponding to different UV exposure times (t) are summarized in Table 6.2.

t (min)	Peaks	T_1	T_M	T_2	τ	δ	ω	μ	b	E (eV)	s (s^{-1})
5	Peak 1	89	125	162	36	37	73	0.51	1.96	0.56	4.6×10^6
	Peak 2	140	176	212	36	36	72	0.50	1.90	0.70	2.7×10^7
	Peak 3	162	242	314	80	72	152	0.47	1.81	0.85	6.8×10^7
20	Peak 1	82	118	157	36	39	75	0.52	2	0.54	3.4×10^6
	Peak 2	128	173	212	45	39	84	0.46	1.77	0.69	2×10^7
	Peak 3	219	256	292	37	36	73	0.49	1.88	0.99	1.2×10^9
30	Peak 1	80	118	155	38	37	75	0.49	1.88	0.53	2.2×10^6
	Peak 2	126	165	207	39	42	81	0.52	2	0.67	2.1×10^7
	Peak 3	173	250	328	77	78	155	0.50	1.90	0.87	8.7×10^7

Table 6.2: Shape factor, activation energy and frequency factor of the glow peaks corresponding to different UV exposure times (t). T_1, T_M, and T_2 are measured in ^oC.

The introduction of Ce^{3+} in to the host material resulted in completely different TL properties of the samples in such away that the shape and peak positions of the glow curves are changed. Moreover, they are broad over a wide temperature range. Fig. 6.8 shows the observed TL intensity of the prepared samples for different concentration of Ce^{3+}.

The incorporation of Ce^{3+} have a strong effect on charge trapping processes taking place in the phosphor material during and after irradiation and on the TL kinetics as well. This could be the reason for the change in the TL properties following the addition of Ce^{3+} into the host material. Finally, the TL fading profile of the $Ca_3Y_2(Si_30_9)_2 : x\ Ce^{3+}$ was studied. During storage of a TL material after irradiation, there is a probability that charge carriers escape from the trapping centers within the material even at low temperature, resulting in the so-called fading of the TL signal. Moreover, during the time between irradiation and heating, the defect structures acting as trapping and recombination centers, may undergo some transformations

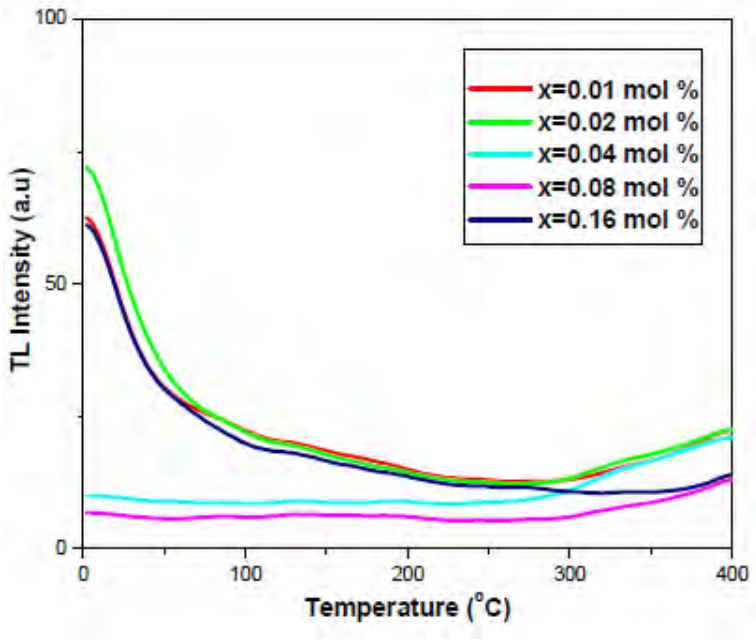

Figure 6.8: The TL glow curves of $Ca_3Y_2(Si_30_9)_2 : x\ Ce^{3+}$.

leading to change of sensitivity. The main external factors affecting fading are temperature and time of the storage. Fig. 6.9(a) shows the TL fading of $Ca_3Y_2(Si_30_9)_2$ host material. It is worth noting that the glow curve with quick measurement shows initial room temperature intensity that is likely to be TL from traps with peak temperatures at or below 25 ^0C. But after storage time of 20 minutes, this initial room temperature intensity was greatly reduced and there is smooth initial rise. This is because of room temperature activation of electrons initially trapped in these shallow traps and recombination with holes during the storage time. Relatively deeper traps populated by electrons were activated at higher temperatures during the heating stage. The variation of the maximum of the TL peaks with storage time and the corresponding exponential fit are depicted in Fig. 6.9(b). The obtained TL fading in Fig. 6.9(b) can be well fitted with a second order exponential decay function using

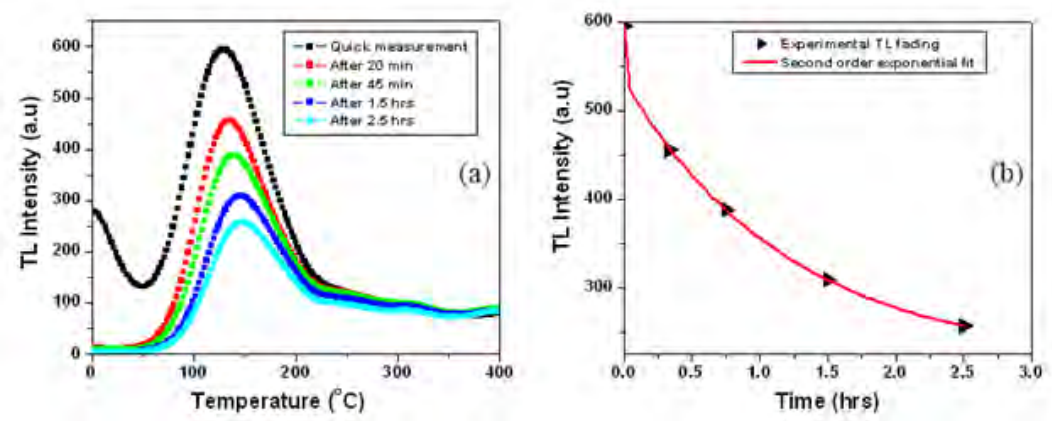

Figure 6.9: TL fading of $Ca_3Y_2(Si_30_9)_2$ host material, and (b) the variation of TL peak maxima with storage time.

the following equation:

$$I(T) = C + A_1 \ \exp\left(-\frac{t}{\tau_1}\right) + A_2 \ \exp\left(-\frac{t}{\tau_2}\right), \tag{6.4.4}$$

where I is the TL intensity, A_1 and A_2 are constants t is the time and τ_1 and τ_2 are the partial lifetimes for the exponential components. Using Origin software, Eq. 6.4.4 is found to be,

$$I(T) = 216.4 + 61.4 \ \exp\left(-\frac{t}{0.012}\right) + 317.5 \ \exp\left(-\frac{t}{1.216}\right). \tag{6.4.5}$$

In general, the observed good TL behavior of $Ca_3Y_2(Si_30_9)_2$ host material is the increase in its TL intensity for all the UV-doses applied up to 50 minutes. Though this is particularly important for dosimetric application of this material, the fact that it undergoes fast TL fading puts this possible application in question. In addition to linear dose response, a material to be used for TL dosimetry purposes is required to have low or no fading. For example, dosimeters with TL fading of the order of only 10 percent at the end of the third month are reported in literature [149, 150, 151]. Thus, fading can be regarded as a quality indicator for a dosimeter.

6.5 Conclusion

The structural and luminescence properties of $Ca_3Y_2(Si_30_9)_2 : x\ Ce^{3+}$ synthesized by using the solution combustion method are investigated. For the $Ca_3Y_2(Si_30_9)_2$ host material, an intense emission band with peak at 432 nm (photon energy of $\sim 2.9\ eV$) is observed from PL spectrum. This PL emission could be ascribed to electron transitions from conduction band to a deep state in the lower half of the band gap or transitions from a deep state in the upper half of the gap to valence band. The photoluminescence (PL) emission spectra of the doped samples monitored at excitation of 365 nm show a broad band extending from about 350 to 600 nm which could be attributed to the allowed $[Xe]5d^1$-$[Xe]4f^1$ transition of Ce^{3+}. The PL intensity increased for up to critical concentration of $x = 0.08$ and then decreased because of energy transfer among Ce^{3+} ions through electric dipole-dipole interaction resulting in concentration quenching. Important TL kinetic parameters such as activation energy (E), the frequency factor (s) and the order of kinetics (b) of the undoped samples are determined by employing peak shape method. Moreover, increment in the intensity of the TL glow peaks is observed with increasing UV dose within the range of the dose used (5-50 min) indicating that it is a promising candidate for the application of UV dosimetry. However, this material suffers from fast TL fading. The TL glow curves of the Ce^{3+} doped samples show the tendency of having peak maxima at temperature greater than 400 ^oC.

Chapter 7

Summary

7.1 Summary

In this thesis, the analytical, numerical and experimental results of the glow curves from nanomaterials are studied and compared. TL glow curves of doped and undoped $Ca_3Y_2(Si_30_9)_2$ nanophosphor synthesized by solution combustion technique are investigated for possible applications in dosimetry. The TL results of this host material are also compared with theoretical results of that of nomaterials, particularly, silicon quantum dots. The reason for selecting silicon quantum dot is that the data of radiative recombination probability is reported in literature for the size of this material ranging between 2-8 nm. Therefore, the TL glow curves can easily be generated by using this data in the rate equations governing the TL process for a given number of traps. The similarity in theoretical and experimental glow curves of the materials studied indeed show that different nanomaterials may have comparable radiative recombination probabilities. The TL properties of $Ca_3Y_2(Si_30_9)_2$ host material approximately show linear response to the UV dose applied and hence it is

a suitable candidate for UV-dosimetry. However, the incorporation of Ce^{3+} into this host material modified the TL glow curves in such away that they are broad over a wide temperature range. Moreover, its band gap is red shifted following doping with Ce^{3+}. The PL intensity increased for up to critical concentration of $x = 0.08$ and then decreased because of energy transfer among Ce^{3+} ions through electric dipole-dipole interaction resulting in concentration quenching.

7.2 Limitation of the Study

Solution combustion technique is a well known method for synthesizing nanometerials and the average crystallite size of the synthesized $Ca_3Y_2(Si_30_9)_2$ nanophosphor deduced from XRD result using Scherer equation is 28 nm. However, this size is significantly larger than the largest silicon quantum dot whose TL properties are studied in this work for theoretical comparison. This could be the reason for the slight difference in the experimental and theoretical results of the TL glow curves though the results are strongly similar.

7.3 Recommendation for Future Work

Future work, particularly on $Ca_3Y_2(Si_30_9)_2$ nanophosphor includes exploration of its structural and luminescence properties using various approaches such as post-synthesis annealing and reducing the average crystallite size through different techniques. The reason for the change in the TL properties of this material after incorporation of Ce^{3+} should also be clearly identified. Further investigation of this material can also follow through synthesis of its thin films.

Publications

- Nebiyu Gemechu, Teshome Senbeta, Belayneh Mesfin, Francis Dejene, Synthesis and luminescence properties of $Ca_3Y_2(Si_30_9)_2 : x\ Ce^{3+}$ nanophosphor, Journal of Materials Science: Materials in Electronics, DOI: 10.1007/s10854-0177105-1.

- Nebiyu Gemechu, Francis Dejene, Vadim Mal'nev, Teshome Senbeta, Belayneh Mesfin, Kittessa Roro, Effect of Retrapping on Thermoluminescence Peak Intensities of Small Amorphous Silicon Quantum dots, Acta Physica Polonica A, **129**, 362 (2016).

- Nebiyu Gemechu, Teshome Senbeta, Belayneh Mesfin, Thermoluminescence from Silicon quantum dots in two traps one recombination center model Ukrainian Journal of Physics, **62**, 140 (2017).

- Nebiyu Gemechu, Teshome Senbeta, Belayneh Mesfin, Structural characterization and determination of Thermoluminescence kinetic parameters of $Ca_3Y_2(Si_30_9)_2$ host material (Submitted to African Review of Physics).

Conference participations

- Ethiopian Physical Society, Mekelle, 2014.

- South African Institute of Physics, Port-Elizabeth, 2015.

- Egypt-South Africa Collaboration, University of the Free State, 2015.

Bibliography

[1] S.W.S. McKeever, *Thermoluminescence of solids*, Cambridge Solid State Science Series, Oklahoma State University, (1988).

[2] M. Karmakar, Indian J. Phys. **84**, 529 (2010).

[3] X. Qin, Y. Ju, S. Bernhard, N. Yao, Mater. Res. Bull. **42**, 1440 (2007).

[4] Y. Parganiha, J. Kaur, V. Dubey, D. Chandrakar, N. Suryanarayana, Research Chem. Intermed. **42**, 2267 (2015).

[5] A. Meijerink, W. Schipper, G. Blasse, J. Phys. D: Appl. Phys. **24**, 997 (1991).

[6] E. Pekpak,, A. Ylmaz, G. Ozbayoglu, J. Alloy. Compds. **509**, 2466 (2011).

[7] Y. Parganiha, J. Kaur, V. Dubey D. Chadrakar, Superlattice. Microst. **77**, 152 (2015).

[8] K. Watanabe, M.K. Slattery, J. Opt. Soc. Amer. **16**, 398 (1928).

[9] T. Lyman, Phys. Rev. **48**, 149 (1935).

[10] [R. Tousey, K. Watanabe, D. Purcell, Phys. Rev. **83**, 792 (1951).

[11] K. Becker, *Solid State Dosimetry*, CRC Press Cleveland, Ohio, (1973).

[12] J.H. Schulman, W. Shurcliff, R.J. Ginther, F.H. Attix, Nucleonics **11**, 52 (1953).

[13] J.R. Cameron, N. Suntharalingam, G.N. Kenny, *Thermoluminescence Dosimetry*, University of Wisconsin Press, Madison, (1968).

[14] R.J. Ginther, R.D. Kirk, J. Electrochem. Soc. **104**, 365 (1957).

[15] M.J. Aitken, *Thermoluminescence Dating*, Academic Press, London, (1984).

[16] M.J. Aitken, Archaeological involvements of physics. Phys. Lett. **40**, 279 (1978).

[17] P Kumari, P K Baitha, J Manam, Indian J Phys **89**, 1297 (2015).

[18] B. Choudhury, A. Choudhury, J. Lumin. **136**, 339 (2013).

[19] T. S. Atabbaev, H. H. Thi Vu, Z. Piao, Y. H. Hwang, H. K. Kim, J. Alloys Coumpd. **541**, 263 (2012).

[20] L. R. Singh, S. D. Singh, Journal of Nanomaterials, 2012 (2012).

[21] L. Jiang, Y.L. Zhang, C.Y. Li, J.Q. Haq, Q. Su, J. Lumin. **128**, 1904 (2008).

[22] M. Akselrod, V.S. Kortov, D.J. Kravetsky, V.I. Gotlib, Radiat. Prot. Dosim. **33**, 119 (1990).

[23] M. Akselrod, N.A. Larsen, V. Whitley, S.W.S. McKeever, J. Appl. Phys. **84**, 3364 (1998).

[24] M. Akselrod, V.S. Kortov, D.J. Kravetsky, V.I. Gotlib, Radiat. Prot. Dosim. **32**, 15 (1990).

[25] C.M. Sunta, E. Okuno, J.F. Lima, E.M. Yoshimura, J. Phys. D Appl. Phys. **27**, 2636 (1994).

[26] R. Chen, D. Lo, J. L. Lawless, Radiat. Prot. Dosim. **119**, 33 (2006).

[27] A. M. Sadek, H. M. Eissa1, A. M. Basha, and G. Kitis, Phys. Status Solidi B **252**, 721 (2014).

[28] V. Pagonis, G. Kitis and C. Furetta, *Numerical and Practical Exercises in Thermoluminecsnce*, USA, Springer, (2006).

[29] C. Furetta, S.Guzman, B.Ruiz, E.Cruz-Zaragoza, Applied Radiation and Isotopes **69**, 346 (2011).

[30] Miho Hatanaka and Satoshi Yabushita J. Phys. Chem. A, **113**, 12615 (2009).

[31] Hikaru Unesaki et al, Inorg. Chem. **53**, 8270 (2014).

[32] Yury P. Rakovich, John F. Donegan, *Semiconductor Nanocrystal Quantum Dots Synthesis, Assembly, Spectroscopy and Applications*, Austria, Springer, 2008.

[33] S. Tripathy, R. K. Soni, S. K. Ghoshal and K. P. Jain, Bull. Mater. Sci. **24**, 285, (2005).

[34] Zhiyong Zhou, Michael L. Steigeward, Richard A. Frienser, and Louis Brus, Phys. Rev. B **71**, 1, (2005).

[35] S. Bhushan, Nucl. Tracks **10**, 215 (1985).

[36] Ullrich Mitschke and Peter Bauerle, J. Mater. Chem. **10**, 147 (2000).

[37] Anatoly P. Pushkarev J. Mater. Chem. C **2**, 1532 (2014).

[38] M.T. Jose, S.R. Anishia, O. Annalakshmi, V. Ramasamy, Radiation Measurements **46**.

[39] K. T. Hillie and H. C. Swart, Appl. Surf. Sci **183**, 304 (2001).

[40] L. Oosthuizen, H. C. Swart, P. E. Viljoen, P. H. Holloway and G. L. P. Berning, Appl. Surf. Sci **120**, 9 (1997).

[41] S. H. Shin, J. H. Kang, D. Y. Jeon and D. S. Zang, J. Solid State Chem **178**, 2205 (2005).

[42] Fernando Heering Bartoloni, et al, J. Org. Chem. **60**, 374 (2015).

[43] Biebele Abel, et al, Nano Biomed Eng. **7**, 92 (2015).

[44] R. S. Chandok, etal, Indian Journal of Pure and Applied Physics **44**, 519 (2006).

[45] H. H. Seliger, et al, The Journal of General Physiology **45**, 1003 (1962).

[46] H.D. Haddock, Mark A. Moline, and James F. Case, Annu. Rev. Mar. Sci. 443 (2010).

[47] B. V. Bukvetskii, N. V. Petrochenkova, and A. G. Mirochnik, Russian Chemical Bulletin, International Edition **64**, 2427 (2015).

[48] B.P. Chandra, Nucl. Tracks **10**, 225 (1985).

[49] Weijie Zhou et al, J. Mater. Chem. C **3**, 9161 (2015).

[50] S. Stellmer, M. Schreitl, T. Schumm, Scientific Reports **5**, 15580 (2015).

[51] T. Calderon, REVISTA MEXICANA DE FISICA S **54** , 21 (2008).

[52] V. Veligura et al, J. Lumin. **157**, 321 (2015).

[53] Shigeo Shionoya and William M. Yen, Phosphor Handbook, CRC Press LLC, Boca Raton, (1999).

[54] A. M. Srivastava and C. R. Ronda, Phosphors, Electrochem. Soc. Inter **49**, 1 (2003).

[55] G. H. Dieke, H. M. Crosswhite, Appl. Optics **2**, 675 (1963).

[56] A. Charlesby, Radiat. Phys. Chem. **17**, 399 (1981).

[57] Y. Hama, Y. Kimura, M. Tsumura, N. Omi, J. Chem. Phys. **53**, 115 (1980).

[58] R. Visocekas, T. Ceva, C. Marti, F. Lefaucheux, M. C. Robert, Phys. Stat. Sol. (A) **35**, 315 (1976).

[59] F. Urbach, Wein. Ber. IIa, 363 (1930).

[60] J.T. Randall, M.H.F. Wilkins, Proc. Roy. Soc. (London) ser. A **184**, 365 (1945).

[61] G.F.J. Garlick, A.F. Gibson, Proc. Phys. Soc (London) **60**, 574 (1948).

[62] Yogita Parganiha et al, Res Chem Intermed, (2015).

[63] J. G Alves. et al, Radiation Protection Dosimetry **111**, 21 (2004).

[64] J. R. Rieke, F. Daniels, J. Phys. Chem. **61**, 629 (1957).

[65] L. M. Atlas, R. F. Firestone, Journal of the Americal Ceramic Society **43**, 476 (1960).

[66] M. R. Mayhugh, J. Appl. Phys. **41**, 4776 (1970).

[67] Raffaele Liuzzi, et al, PLOS ONE — DOI:10.1371/journal.pone.0139287, (2015).

[68] F. Daniels, C. A. Boyd, D. F. Saunders, Science **117**, 343 (1953).

[69] N.A. Larsen, L. Botter-Jensen, S.W.S. McKeever, Radiat. Prot. Dosim. 84, 87 (1999)

[70] C.M. Sunta, Radiat. Effects 79, 149 (1983)

[71] A.R. Lakshmanan, K.G. Vohra, Nucl. Instrum. Methods 159, 585 (1979)

[72] Reuven Chen, J. Phys. D: Appl. Phys. **16**, 107 (1983).

[73] C.E. May, J.A. Partridge, J. Chem. Phys. **40**, 1401 (1964).

[74] R. Chen, J. Electrochem. Soc. (Solid State Sci.) **116**, 1254 (1969).

[75] R. Visocekas, La Luminescence de la calcite aprs irradiation cathodique. TL et luminescence par effettunel, Ph.D. Thesis, UniversitePiere et Marie Curie, Paris, (1978).

[76] R. Chen, N. Kristianpoller, Z. Davidson, R. Visocekas, J. Lum. **23**, 293 (1981).

[77] C.M. Sunta, W.E.F. Ayta, J.F.D. Chubaci, S. Watanabe, J. Phys. D Appl. Phys. **38**, 95 (2005).

[78] J. M. Gomez Ros and G. Kitis, Radiation Protection Dosimetry, **101**, 47 (2002).

[79] D. Curie, *Luminescence in crystals*, John Wiley Sons Inc. New York, (1963).

[80] G.F.J. Garlick and A.F. Gibson, Proc. Phys. Soc. **60**, 574 (1948).

[81] Furetta C., Guzman S., Ruiz B. Cruz-Zaragoza E., Appl. Radiat. Isot.**69**, 346 (2011).

[82] B.M. Ilich, Sov. Phys. Solid State **21**, 1880 (1979).

[83] C. Furetta, S.Guzman b, B.Ruiz, E.Cruz-Zaragoza, Applied Radiation and Isotopes **69**, 346 (2011).

[84] C.E. May and J.A. Partridge, J. Chem. Soc. **40**, 1401 (1964).

[85] C. Muntoni, A. Rucci, and A. Serpi, Ricerca Scient. **38**, 762 (1968).

[86] Adrie J.J. Bos et al, Radiation Measurements **46**, 1410 (2011).

[87] M. Topaksu, V.Correcher, J.Garcia-Guinea, M.Yksel, Applied Radiation and Isotopes **95**, 222 (2015).

[88] W. Hoogenstraaten, Philips Res. Rep. **13**, 515 (1958).

[89] Neha Tiwari, R.K. Kuraria, Raunak Kumar Tamrakar, Journal of Radiation Research and Applied Sciences **7**, 542 (2014).

[90] R. Chen, J. ElectrochemSoc. Solid State Sci. **116**, 1254 (1969).

[91] R. Chen, S. W. S. McKeever, *Theory of Thermoluminescence and Related Phenomena*, World Scientific, Singapore, (1997).

[92] G.F.J. Garlick and A.F. Gibson, Proc. Phys. Soc. **60**, 574 (1948).

[93] C.E. May and J.A. Partridge, J. Chem. Soc. **40**, 1401 (1964).

[94] N. Takeuchi, K. Inabe, and H. Nanto, J. Mater. Sci. **10**, 159 (1975).

[95] G. Cao, *Nanostructures and Nanomaterials, Synthesis, properties and applications*, 6th edition, Imperial college press, London UK, (2004).

[96] B. D. Culity, *Elements of x-ray diffraction*, Addison-Wesley, (1956).

[97] Charles Kittle, *Introduction to Solid State Physics*, Eighth edition, USA, (2005).

[98] J. N. Reddy and K.V.R. Murthy, Defect and Diffusion Forum, **357**, 261 (2014).

[99] J. G. Sol'e. L E Baus'a, and D. Jaque, *An Introduction to the Optical Spectroscopy of Inorganic Solids*, 33, (2005).

[100] Jianwei Wang, PhD Dissertation, University of Georgia, (2002).

[101] Yu. A. Skryshevskii, and V. A. Skryshevskii, J. Appl. Phys. **2711**, 1 (2001).

[102] C. Furetta, *Handbook of Thermoluminescence*, Cambridge University Press, London, (1988).

[103] N. M. Abdul-Ameer, M. C. Abdulrida, Journal of Modern Physics **2**, 1530 (2011).

[104] K. Dohnalova,T. Gregorkiewicz and K. Kusova, J. Phys.: Condens. Matter **26**, 1 (2014).

[105] S. Martini, L. K. Teles, M. Marques, E. B. Angelo, A. A. Quivy, World Journal of Condensed Matter Physics **1**, 161 (2011).

[106] Eun-Chel Cho et al., Advances in Opto-Electronics, Hindawi Publishing Corporation, 1 (2007).

[107] D Mendoza-Anaya, C Angeles, P Salas, R Rodriguez and V M Castano, Nanotechnology **14**, 12, (2003).

[108] N. G. Debelo, Lat. Am. J. Phys. Educ. **6**, 327 (2012).

[109] V. Pagonis, G. Kitis, Phys. Status Solidi B, 1 (2012).

[110] A. M. Sadek, H. M. Eissa, A. M. Basha, G. Kitis, Phys. Status Solidi B **252**, 721 (2015).

[111] Anna Dobrowolska, J. Solid State Chem. **184**, 1707 (2011).

[112] Matthias Mller,Thomas Jstel, J. Lumin. **155**, 398 (2014).

[113] Zhiping Yang, Hongyan Dong, Xiaoshuang Liang, Chuncai Hou, Lipeng Liu, and Fachun Lu, Dalton Trans. **43**, 11474 (2014).

[114] V.B. Mikhailik, Materials Letters **63**, 803 (2009).

[115] K. Madhukumar et al., Bull. Mater. Sci. **30**, 527 (2007).

[116] K C Patil, S T Aruna, and T. Mimani, Sol.State and Mate. Sci. **6**, 507 (2002).

[117] J. J.kim, J. H. Kang, D. C. Lee and D. Y. Jeon, Am. Vac.Soc. (2003).

[118] S. S. Manoharan and K. C Patil. J. Am. Cer. Soc. **141**, 1012 (1992).

[119] M. A Sekar and K C Patil, J. Mater. Chem. **2**, 739 (1992).

[120] R. G. Chandran and K C Patil, Mater. Res. Bull. **27**, 147 (1992).

[121] P Ravindranathan, S Komameni and R Roy, J. Mater. Sci. Lett. **12**, 369 (1993).

[122] N A Dhas and K C Patil, Ceram. Inter. **20**, 57 (1994).

[123] Y Zhang and G. C Stangle, J. Mater. Res. **9**, 1997 (1994).

[124] D A Furnor, M R More and A M SegadHes, Mater. Res. Bull. **31**, 243 (1996).

[125] N. Suriyamurthy and B S Panigrahi, J. Lumin. **128**, 1809 (2008).

[126] G A Hirata, F. Raamos, R Garcia, E J Bosze, J M Kittrick, J. Phys. Stat. Sol(a) **188**, 179 (2001).

[127] Z Qui, Y. Zhou, M Lu, A Zhang and Q Ma, Acta Mat. A **55**, 2615 (2007).

[128] B. M. Mothudi, PhD Thesis, University of the Free State, (2009).

[129] B. Cullity, *Elements of X-ray Diffraction*, Addison-Wesley publishing, USA, (1956).

[130] Shao-Ying Ting et al, J. Nanomat. **2012**, 1 (2012).

[131] R. A. Zargar et al, Optic **127**, 6997 (2016).

[132] A. B. Murphy, Sol. Energ. Mat. Sol. C. **91**, 1326 (2007).

[133] YI-Chin Chu et al, J. Electrochem. Soc. **156**, 221 (2009).

[134] D. Cooke et al., Appl. Phys. Lett. **88**, 103 (2006).

[135] H. Huang, B. Yan, Solid State Commun. **132**, 773 (2004).

[136] T. Bottger, C. Thiel, R. Cone, Y. Sun, Phys. Rev. B **79**, 115104 (2009).

[137] B. Comaskey et al., Opt. Lett. **18**, 2029 (1993).

[138] B. Lauritzen et al., Phys. Rev. Lett. **104**, 080502(2010).

[139] Z. Cole et al., Appl. Phys. Lett. **81**, 3525 (2002).

[140] Matthias Mller,Thomas Jstel, J. Lumin. **155**, 398 (2014).

[141] Zhiping Yang, Hongyan Dong, Xiaoshuang Liang, Chuncai Hou, Lipeng Liu, and Fachun Lu, Dalton Trans. **43**, 11474 (2014).

[142] Yong Gao et al., Journal of Electronic Materials, **46**, 911 (2017).

[143] B. Rajesh Kumara, B. Hymavathi, J. Asian Ceram. Soc. (2017), http://dx.doi.org/10.1016/j.jascer.2017.02.001.

[144] Zhang Xin et al., Chin. Phys. B **22**, 097801 (2013).

[145] Yi Zhang et al., Optical Materials Express **2**, 92 (2012).

[146] J. Zhou, Z. Xia, J. Lumin. **146**, 22 (2014).

[147] I. Shalish, et al., Phys. Rev. B **59**, 9748 (1999).

[148] K. C. Yung, H. Liem, H. S. Choy, Journal of Physics D: Applied Physics **42**, 185002 (2009).

[149] C.P. Furetta, Nuclear Instruments and Methods in Physics Research **411**, 417 (2000).

[150] M. Prokic, Radiation Protection Dosimetry **100**, 265 (2002).

[151] N.E.-K.-A. El-Faramawy, Radiation Physics and Chemistry **58**, 9 (2000).